THESIS

ANALYSIS OF SIMULATED DILUTE ANODE TAIL-GAS COMBUSTION CHARACTERISTICS ON A CFR ENGINE

Submitted by

Alexander Balu

Department of Mechanical Engineering

In partial fulfillment of the requirements

For the Degree of Master of Science

Colorado State University

Fort Collins, Colorado

Spring 2020

Master's Committee:

Advisor: Daniel Olsen

Bret Windom
Daniel Baker

ABSTRACT

ANALYSIS OF SIMULATED DILUTE ANODE TAIL-GAS COMBUSTION CHARACTERISTICS ON A CFR ENGINE

Recent innovations in metal-supported solid oxide fuel cells (MS-SOFC) have increased the longevity and reliability of fuel cells. These innovations drive the desire to create power generating systems that combine different ways of extracting power from a fuel to increase overall fuel conversion efficiency. This investigation assesses the feasibility of operating an internal combustion engine (ICE) with the anode tail-gas, which is a blend of H_2, CO, CO_2, H_2O, and CH_4, exhausted by a MS-SOFC. This engine would be used to support the fuel cell balance of plant equipment, including a compressor and expander, and produce excess electrical power.

Seven variations of the expected anode tail-gas blends were determined by varying the dewpoint temperature of the fuel. In three of the test blends, CO_2 replaced the water content of the fuel to allow for initial feasibility testing without the capital investment required to simulate the tail-gas with steam injection. Gas blends are tested by combining separate flows of each constituent, and combustion is tested using a Cooperative Fuel Research (CFR) engine. Compression ratio (CR), spark timing, intake manifold temperature (IMT), and boost pressure were manipulated to obtain optimal operating conditions. All test blends produced power and reached stable engine operation. Response surface method (RSM) optimization was used to experimentally optimize operating parameters and determine the maximum achievable efficiency utilizing the CFR engine.

Initial feasibility testing performed on test blends with CO_2 in place of water showed that all combinations successfully produced power in the engine. The mixture with the highest levels of CO_2 was problematic and required an increased CR of 14.4:1, advanced timing of 40° before top dead center (BTDC), and an increased IMT of 70°C. All CO_2 test blends operated at brake efficiencies ranging from 12-17% during initial testing. After the feasibility of this project was determined, a steam generator and steam flow meter were installed and used to fully simulate the anode tail-gas blends with steam injection. All fully simulated anode tail-gas blends produced power in the engine, although the blend with the most water content caused operational problems with the CFR engine test stand. These problems were caused by large amounts of water entering the engine lube oil system. RSM optimization was performed on the most viable test blends which had steam injection to 40°C and 90°C fuel dewpoint temperatures. During optimization, the 40°C and 90°C dewpoint temperature blend brake efficiency increased from 20% to 22.2%, and 17% to 22.3%, respectively.

This study determined that ICE operation on dilute anode tail-gas is possible. Anode tail-gas combustion data was collected and used to inform engine and combustion models to facilitate prototype engine development for further testing.

ACKNOWLEDGMENTS

As always, I would like to start with my family who have given me incredible memories and helped me to relax when I needed a break from school or work. My wife, Lieu, who has been by my side and empowered me to work to the best of my ability through everything for almost 14 years. My son, Oliver, and my daughter, Quynh, who have kept me grounded through all of this, but have also had to give up meaningful time with me while I accomplish this task. My mother, Kathy, and father, Dale, who supported me and my family while I completed my MSME and my wife completed her DVM. I could not have asked for better grandparents for my children.

The support I have received at CSU has been phenomenal, my advisor, Dr. Daniel Olsen, provided me with this amazing opportunity and guided and supported my work throughout the entire process. My committee members, Dr. Bret Windom and Dr. Daniel Baker, took time out of their busy schedules to support this project and provide the feedback that helped make this thesis what it is today. I would also like to thank all of the CSU Powerhouse personnel who helped me in this endeavor, specifically the Control Room staff, Kirk Evans, Mark James, and James Tillotson, and also people from Dr. Olsen's research group, namely, Chris Van Roekel, who provided guidance as I learned more about internal combustion engines and performing research, and Scott Baylif, who was at my side as we performed a massive amount of work to prepare the CFR engine test stand for this research. This work would not have been possible without the support I received from all these people.

TABLE OF CONTENTS

LIST OF FIGURES

CHAPTER 1: INTRODUCTION

1.1. Background and Motivation

Recent innovations in metal-supported solid oxide fuel cells (MS-SOFC) have increased their longevity and reliability. An MS-SOFC has been developed that operates at an intermediate temperature of 600°C, has increased power density due to its ability to operate at elevated pressures, and possesses a high internal reforming capability, which allows it to operate using pipeline natural gas (NG) [1]. The reduction of operating temperatures for this MS-SOFC decreases preheater duty more than 60% which reduces the energy penalty required to raise system pressures. The increase in cell power density offsets the increased cost of the pressure vessel required to operate at elevated pressures, helping to maintain a low overall $/kW system cost. There are still significant barriers to the widespread adoption of MS-SOFC power generation systems. These barriers include decreased overall system efficiency due to the high balance of plant (BOP) equipment power requirements, a reduction to 40-45% from a SOFC fuel utilization of 80%, and relatively high BOP equipment costs of ~760 $/kW [2]. MS-SOFC technology developments drive the desire to create power generating systems that combine different ways of extracting power from a fuel to increase overall fuel conversion efficiency while decreasing cost. The exhaust gas from the anode side of an MS-SOFC carries substantial thermal energy, with temperatures of 600°C, and, although it is highly diluted (~80% CO_2 and H_2O), it also contains a significant amount of chemical potential energy, ~2600 kJ/kg LHV. The highly dilute nature of the anode tail-gas would cause extremely low flame speeds, but this effect is offset by the relatively high levels of H_2 (~17%) which will increase the tail-gas laminar flame speed. When an MS-SOFC releases this exhaust gas into the atmosphere, it represents a loss of potential energy for beneficial uses like power generation and heating.

The purpose of this project is to determine if the dilute tail-gas exhausted by the anode side of the MS-SOFC can fuel an internal combustion engine (ICE). If feasible, this could lead to the development of a hybrid power generation system that operates at an overall system efficiency >70%-LHV, at a rated power of 125 kW with a cost of <850 $/kW [2]. Figure 1 shows a simplified schematic of the proposed hybrid system. On the left side of the figure NG fuel is shown entering the anode side of the MS-SOFC while the air supply is preheated and compressed prior to entering the cathode side of the MS-SOFC. Spent fuel exhausted from the anode side of the fuel cell is used to fuel an ICE. Both the ICE and the MS-SOFC supply power to a DC/AC inverter to provide 120V AC electric power. A low-cost system of this size could lead to increased adoption of distributed electricity generation systems that would relieve strain on the electric grid, reduce the dependence on lower efficiency fossil-fuel generation systems and eliminate losses from transmission and distribution [2]. Distributed electricity generation of this kind also provides the ability to convert waste heat to useful thermal energy.

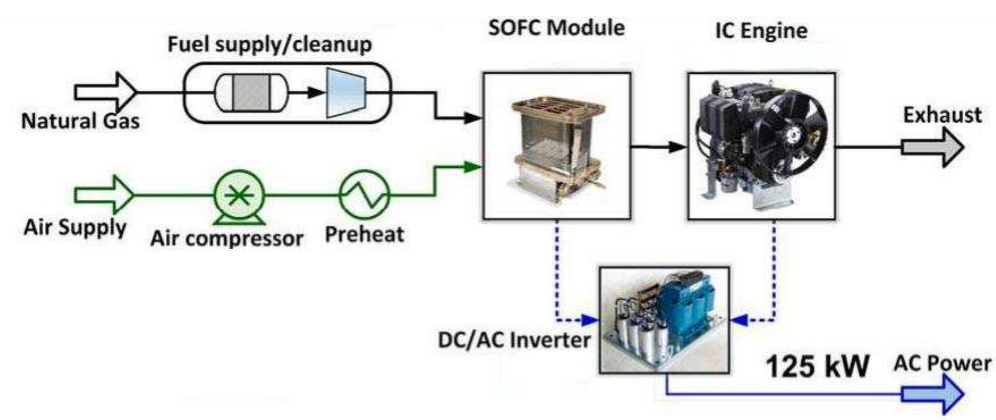

Figure 1: Hybrid SOFC/Internal combustion engine schematic [2].

The development of this hybrid system requires a detailed investigation into the dilute anode tail-gas fuel properties, including understanding the requirements to achieve combustion and the ability to determine where the limits of misfire and knock onset are for the fuel [3].

Combustion testing is performed using the Cooperative Fuel Research (CFR) engine located at the Colorado State University (CSU) Powerhouse. This testing provides the data to inform Converge and GT-Power simulations, which in turn assists in the development of a prototype engine designed to burn this fuel.

1.2. Literature review

1.2.1. Alternative Gaseous Fuels

Research involving alternative gaseous fuels is well documented and readily available. This research is valuable to this project as these fuels usually are much more dilute than NG. Although the expected composition of the anode tail-gas for this project is much more dilute than the standard alternative gaseous fuel, challenges encountered in the use of alternative gaseous fuels should provide insight into expected engine operation.

Producer gas is an alternative gaseous fuel that comes from the gasification of solid organic matter, usually agricultural waste in the form of rice husk, sugarcane trash, or bagasse [4]. Biomass gasification technology has existed for more than 70 years. The need for reduced greenhouse gas emissions has driven advancements in the gasification technology used today. Producer gas generated by this technology is of much higher quality than what has been used in the past, making it a more viable fuel. Typical producer gas contains 18-20% each of H_2 and CO, about 2% CH_4, and the rest made up of inert gases like CO_2 and N_2 [4]. The use of producer gas in a spark-ignited (SI) engine requires derating of the engine. Derating is required due to the reduced LHV of a mixture of producer gas and air at an equivalence ratio phi (ϕ) = 1 when compared with NG. Producer gas also has less knock resistance than NG and requires adjustments to spark timing to reach maximum brake torque. Mixtures with higher H_2 content have faster flame speeds, which need more delayed spark timing to achieve maximum brake torque and ideal locations of peak pressure.

Babu investigated the effects of converting a spark ignited NG engine to run on producer gas [5]. High diluent concentrations cause a decrease in engine knock propensity, and a decrease in volumetric efficiency. The typical level of CO_2 and N_2 diluents is 60% for producer gas. The diluents found in anode tail-gas are comprised of H_2O and CO_2 and add up to almost 80% of the fuel composition. Fuel conditioning is required to lower diluent levels in anode tail-gas to the levels found in producer gas. Babu states that increasing CR is one way to limit required engine de-rating when utilizing dilute fuels [5]. Observations regarding producer gas fueled engine emissions show a decrease in both CO and NO_x [5]. Babu concludes that the reason for this is that the generally basic constituents present in producer gas are easier to burn and that the high levels of diluents lead to reduced burning temperatures which tend to decrease NO_x production [5].

Digester gas and landfill gas come from the anaerobic digestion of biodegradable materials by microorganisms. This gas is typically about 60% CH_4 and 40% CO_2 [6]. Digester gas requires that the CR be increased to achieve the same power levels seen in an ICE using methane fuel [7]. This increase in CR is possible because of the relatively high level of diluents contained in digester gas. These diluents act as a knock suppressant. Anode tail-gas and digester gas should share some of the same considerations required when fueling an ICE due to their similarly dilute nature.

1.2.2. H_2O Effect on Combustion

The effects of varying amounts of H_2O concentration in ICE fuel were investigated. Singh studied the effects of H_2O addition up to 40% on laminar flame speed in H_2/CO fuels with initial

H_2/CO ratios of 5/95 and 50/50 [8]. H_2O addition to the 5/95 fuel showed increases in flame speed up to 20% H_2O but flame speed decreased with further H_2O addition. H_2O addition to the fuel blend with more H_2 content, the 50/50 blend, caused flame speed to decrease as H_2O concentration increased for all levels of H_2O addition. Further analysis of the chemical effect of H_2O addition on H_2/CO fuels is provided by Singh to explain the different effects under different H_2 concentrations [8].

1.2.3. Steam/Water Injection

The composition of the anode tail-gas is expected to have large amounts of H_2O. To adequately simulate the anode tail-gas, a reliable method of H_2O injection must be developed. Two studies were referenced to assess the design considerations involved with developing an H_2O injection system. The process for water injection, in the case of Arruga [9], or steam injection, in the case of Cesur [10], both had simple approaches. Arruga tested the differences between one port fuel injector (PFI) and two different gasoline direct injectors (GDI). Arruga found it essential to find a balance between using a lower spray angle injector to reduce wall wetting while still having an angle large enough to maximize the coverage of volume of intake airflow. Arruga determined that both GDI had better spray pattern characteristics to disperse water than the PFI injector. Ultimately, the injector with the widest spray angle, the Bosch GDI, was chosen for its clean spray pattern and lower mass flow rate for the same duty cycle when compared with a Denso GDI [9]. Cesur utilized an electronically controlled steam injection system that used a boiler, heated with exhaust waste heat, operating at 3 bar, 133.5°C, and saturation conditions. The injectors used for the steam were solenoid valves that were placed at the back of the intake manifold [10].

1.3. Research Objectives

The objectives of this research are as follows:

(1) Determine the composition of anode tail-gas expected and develop multiple test blends to determine the ideal conditioning of the fuel.

(2) Determine the feasibility of utilizing MS-SOFC exhausted dilute anode tail-gas to fuel an ICE.

(3) Perform an analysis of engine operating conditions required for maximum efficiency operation of the most ideal anode tail-gas blends and submit operational data to inform GT-Power and Converge models to assist with prototype engine development.

CHAPTER 2: METHODS

2.1. Test Blend Determination

The anticipated composition of the anode tail-gas has been determined to be nominally 18% H_2, 5% CO, 28% CO_2, and 49% H_2O [2]. Seven variations of the expected anode tail-gas blend were determined and used for engine testing. Test blends were based on expected tail-gas composition with no H_2O dropout, full H_2O dropout and with H_2O dropout to 40°C and 90°C dewpoint temperatures. As shown in Table 1, blend 1 is the expected tail-gas composition with all H_2O removed and blends 2-4 represent the anode tail-gas with H_2O content replaced with CO_2 directly by mole fraction for preliminary testing. Test Blends 5-7 repeat the same H_2O dropout conditions but with steam injection to fully simulate the anticipated anode tail-gas composition. Test blend composition and energy content are shown graphically in Figure 2 which shows the effect of water dropout and CO_2 replacement on fuel blend composition. Figure 2 also shows an order of magnitude difference between the LHV of anode tail-gas blends and NG. There is also a comparison between the test blends and NG for an air/fuel mixture with $\phi = 1$. The difference in energy content for stoichiometric air/fuel ratios between test blends and NG comes from the large difference in air-fuel ratio for each. The air-fuel ratio for each test blend 0.47 – 1.17 while the air-fuel ratio for NG is ~16.15. More fuel flow rate is required to attain the same total energy flow (LHV$\cdot\dot{m}_{fuel}$) of NG.

Table 1: List of Test Blends and their Characteristics

Test Blend #	Test Blend	H_2O Dropout	H_2O replaced with CO_2?
1	Full Water Dropout	100%	N/A
2	40°C (CO_2)	Dewpoint = 40°C	Yes
3	90°C (CO_2)	Dewpoint = 90°C	Yes
4	No Water Dropout (CO_2)	0%	Yes
5	40°C (Steam)	Dewpoint = 40°C	No
6	90°C (Steam)	Dewpoint = 90°C	No
7	No Water Dropout (Steam)	0%	No

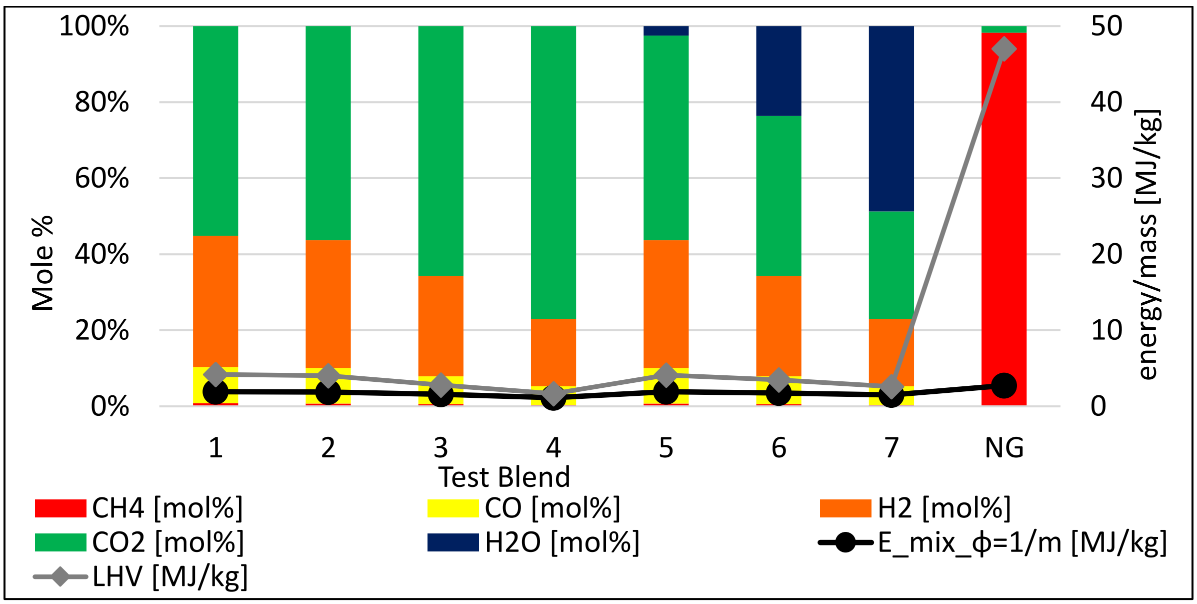

Figure 2: Anode tail-gas blends to be simulated. These blends, their lower heating value (LHV) and the amount of energy contained in an air-fuel mixture with phi (ϕ) = 1 are compared to a standard blend of natural gas (NG).

2.2. CFR Test Stand Gas-Blending System

A gas blending system capable of combining all expected constituents at their required flow rates was needed to perform this testing. CSU's CFR test stand was equipped with a gas blending system, but this system required several major modifications to satisfy testing requirements. First, the gas-blending system's Omega FMA 1700 flow meters were calibrated using a high-flow secondary reference flow meter and a more accurate low flow wet-gas meter.

Additional modifications were performed to optimize flow, fix leaks, and reduce potential leak paths so that the CH_4, CO, H_2, and air flow meters could meet the specifications required to fully simulate all test blends. The extremely low LHVs of the test blends necessitated higher fuel flow rates than what the gas-blending system was originally designed to supply. All required flow rates, except CO_2, were within acceptable ranges for the available flow meters. In the most extreme case, the No Water Dropout (CO_2) blend, a flow rate >250 standard liters per minute (SLPM) of CO_2 was required. This high flow rate required the design of a separate CO_2 injection system. Also, the fuel blending system was not designed for blending steam/water into the fuel, which mandated the design and implementation of a steam injection system.

2.3. CO_2 Flow Meter and Injection System Design

Because of the extremely low LHVs of the test blends, higher flow rates of fuel were required. A new CO_2 injection system was needed to accurately simulate CO_2 replacement test blends. The design requirements for this system included a flow meter, a method to extend overall testing time, and that any potential safety concerns were addressed. The final system design is shown in Figure 3.

The flow of CO_2 was measured by utilizing choked flow measurement across a Swagelok SS-6L-MH metering valve. This required metering valve inlet temperature and pressure measurement. The metering valve flow coefficients (C_v) were also measured at every quarter turn using a secondary reference flow meter. Equation (1) was used to calculate mass flow rate q from measured parameters and also to determine the flow coefficient of the valve at its different positions [11].

$$q = 3273.45 C_v P_1 \sqrt{1/G_g T_1} \tag{1}$$

The valve inlet pressure is P_1, G_g is the specific gravity of the gas, and T_1 is the valve inlet temperature. Choked flow was maintained throughout testing by ensuring that the metering valve inlet pressure was at least twice its outlet pressure. Four liquid CO_2 dewars were installed in parallel to extend available testing time. This arrangement provided much more total CO_2 mass than compressed gas cylinders could provide. The use of liquid CO_2, along with large system pressure drops, resulted in the sublimation of CO_2 before injection into the engine. This sublimation caused issues with maintaining required CO_2 flow to sufficiently dilute the H_2 in the fuel blend, which resulted in autoignition of the fuel mixture in the engine inlet and exhaust piping. A heated regulator and several lengths of silicone heat tape were sized and installed to account for the Joule-Thompson cooling experienced across the pressure drops in the system.

A normally-shut safety valve was installed in the system to prevent the possibility of uncontrolled flow of CO_2 into the building interior. LabVIEW controlled the position of this valve and operated the heated regulator. In the event of a loss of power or high CO_2 alarm, the heated regulator would de-energize, and the cutout valve would fail shut.

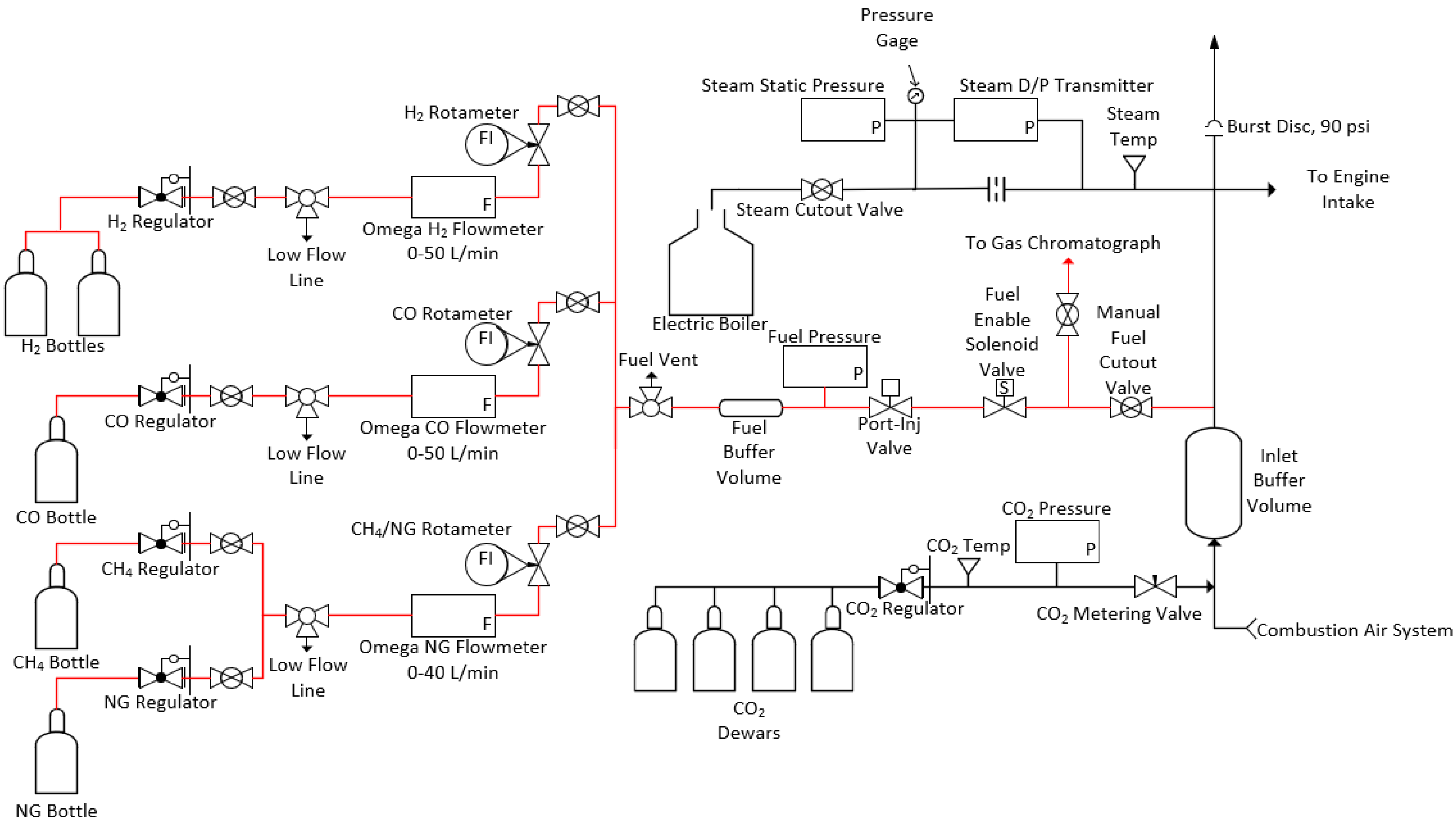

Figure 3: CFR test stand fuel blending system including new designs for CO_2 and steam injection systems.

2.4. Steam Flow Meter and Injection System

The steam injection system required to fully simulate the anode tail-gas consisted of a 10kW Reimers RB10 dry steam boiler, and a custom-made orifice plate with tapped flanges based on ISO 5167. Silicone heat tape and exhaust header wrap were installed around intake piping between the steam injection point and intake air heater to maintain wall temperatures above the air-fuel mixture dewpoint temperature. The orifice piping was installed with a downward slope to allow any condensed water to drain downstream. A drain valve was installed on the upstream orifice flange tap to remove condensation upstream of the orifice plate during startup and intermittently during operation. Upstream static pressure was measured using an Omega PX319-100A5V transducer, and differential pressure (D/P) was measured using an Omega PX409-015DWU5V transducer. A water bucket with volume measurement was installed as the water source for the boiler. The water bucket allowed flow rate verification by measuring total water usage while steam was flowing. The CFR test stand and boiler setup are shown in Figure 4.

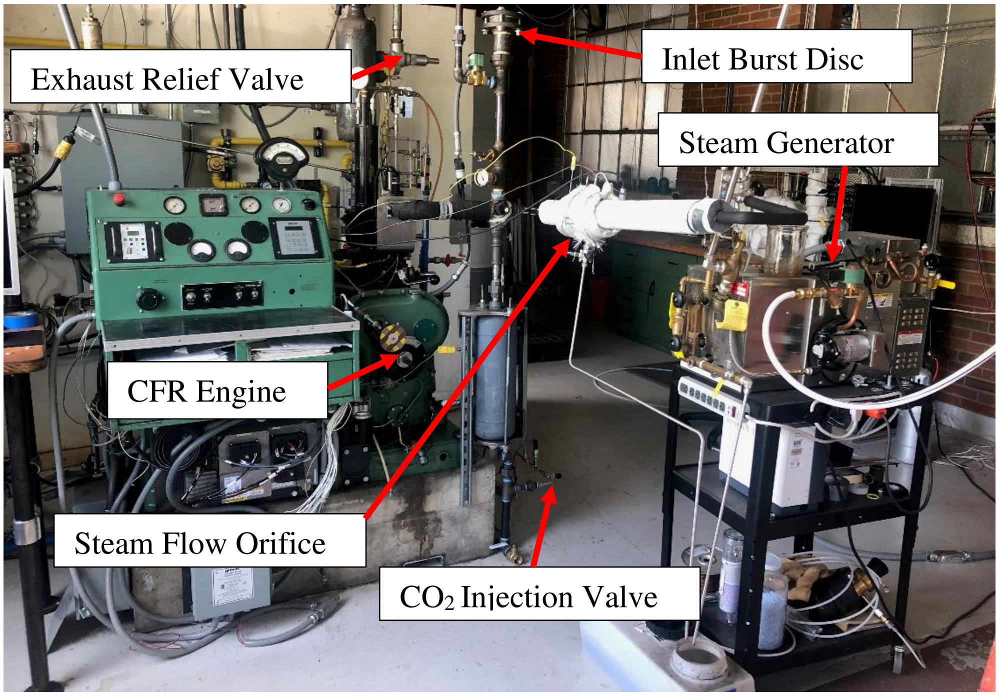

Figure 4: CSU CFR Test Stand with Steam Generator and Steam Flow Orifice.

2.5. CFR Test Stand

The CFR engine test stand is uniquely suited to the testing required for this project. Table 2 highlights the capabilities and attributes of the CFR engine test stand.

Table 2: CFR engine technical specifications

Specification	Description
Crankcase Type	Model CFR-48D, Cast Iron
Cylinder Type	Cast Iron, Flat Combustion Surface, Integral Coolant Jacket
Compression Ratio	Adjustable 4:1 to 18:1
Cylinder Bore (Diameter)	82.55 mm
Stroke	114.3 mm
Displacement	611.73 cc

Some of the critical CFR attributes are as follows:

- Single-cylinder research engine with movable cylinder head to allow online adjustment of engine CR.
- Yaskawa U1000 Regenerative Variable Frequency Drive (VFD) to allow engine testing at different engine speeds.
- Inlet mixture heater to set and maintain intake manifold temperature (IMT).

- A Woodward Large Engine Control Module (LECM) enables fixed and dynamic spark timing control. Spark timing can be set to a fixed value or can be adjusted dynamically to maintain different combustion parameters cycle to cycle.
- Digital encoder and magnetic pickups used on the flywheel. Magnetic pickups offer cylinder, intake, and exhaust pressure measurements at every 10^{th} crank angle degree.

Data Acquisition Capabilities

- High-frequency intake (Kistler 4007D), exhaust (Kistler 4049B), and in-cylinder (Kistler 6061B) pressure transducers.
- Live feed of combustion statistics, including values and coefficient of variance (COV) of Indicated Mean Effective Pressure (IMEP), peak pressure, and location of peak pressure.
- Live Fast Fourier Transform (FFT) based knock analysis.
- An ECM Dual-Channel AFRecorder 4800 Series Fast Air-Fuel Ratio Analyzer measures air-fuel ratio.
- A Rosemount 5-gas analyzer rack with Siemens instrumentation measures CO, CO_2, total hydrocarbons (THC), O_2, and oxides of nitrogen (NO_x).
- A Fourier Transform InfraRed Spectrometer used to measure CH_4, formaldehyde, and ammonia.

The engine also has several control parameters including fixed and dynamic spark timing, CR, engine boost and exhaust pressure, IMT, engine speed, ϕ, and engine power. The engine attributes listed above were crucial to testing and characterization of the test blends in this project. Figure 3 shows a simplified schematic of the CFR test stand gas-blending system. More information about this CFR test stand can be found by referencing Wise [3].

2.6. Test Methods

Four phases of testing were performed to determine the characteristics of each test blend. The equivalence ratio is held at 1.0 for all trials to enable the use of a 3-way catalyst for emissions control in future prototype engines. The first phase of testing, Initial Feasibility Testing, focused on Full Water Dropout and CO_2 replacement fuel blends 1-4. This testing was focused on determining the combustibility of each fuel blend. Once combustion was achieved, spark timing would be swept at several compression ratios to provide data for combustion modeling. Testing was performed using CO_2 replacement to provide proof of concept data and to ensure that fuel with this high level of diluents could be used in an ICE. Testing began by starting up and preheating the CFR engine using NG. Once the engine was warm, NG flow to the engine was isolated, and CO_2 flow was initiated to ensure that enough diluent was present to prevent the combustion of H_2 outside of the engine cylinder. After baseline CO_2 flow was established, fuel supplies for CH_4, CO, and H_2 were opened, and their regulator pressures were balanced to 100 psi. Each flow was slowly admitted to the engine through a needle valve while monitoring constituent flow rates until the desired gas-blend composition was achieved.

Each test blend was tested with a starting CR of 10.7:1, with IMT at 45°C, and spark timing at 15⁰ before top dead center (BTDC). The test plan began by increasing CR, then spark timing would be advanced, and, finally, the inlet mixture temperature would be increased until steady combustion was achieved. The maximum CR was limited to 14.4:1, spark timing was limited to 40° BTDC, and IMT was limited to 80°C. Once combustion was achieved, data would be recorded. After recording the initial combustion data, the CR was increased until the critical CR (CCR) was obtained at low levels of audible knock. A data point would then be taken, CR would be lowered slightly to prevent engine knock, and then spark timing would be advanced to achieve maximum brake torque timing. Maximum brake torque timing is the spark timing at which maximum engine power is produced while operating at a constant speed. For reference, maximum brake torque timing occurs when the location of peak pressure for the cycle equals about 18⁰ after top dead center (ATDC) when running on NG.

The second phase of testing, Steam Injection Fuel Blend Testing, was focused on the 40°C, 90°C and No Water Dropout steam injection test blends 5-7. Testing was performed by following the procedure used for the CO_2 replacement fuel blends without the use of excess CO_2 to simulate water content. During this testing IMT was held at 80°C, for the 40°C (Steam) and

90°C (Steam) blends, and at 90°C for the No Water Dropout (Steam) blend to prevent condensation in the engine intake. Although 80°C and 90°C are below the dewpoint temperatures for the 90°C (Steam) and No Water Dropout (Steam) blends, which are ~90°C and ~100°C respectively, the combined air-fuel dewpoint temperatures of these blends are ~60°C and ~86°C respectively.

The third phase of testing, Constant IMEP Testing, was performed on all fuel blends except the No Water Dropout blends 4 and 7 due to their unsatisfactory performance. This phase of testing involved a sweep of CR with indicated mean effective pressure (IMEP) held at 870±15 kPa, and spark timing at maximum brake torque timing, determined during Initial Feasibility and Steam Injection Blend Testing. This testing was performed to allow direct comparison of blend combustion characteristics and was intended to allow for ideal fuel blend selection for the next phase of testing.

The final phase of testing, Response Surface Method (RSM) Optimization, involved testing based on the design of experiment fundamentals. “The core idea of the RSM is the match of mathematical models to experimental results and the verification of the model by statistical techniques” [12]. A simplified version of the RSM is used for this testing, which involves three steps: determine the type of RSM suitable for this testing, develop the objective function, and determine the optimization variables. Figure 5 shows several options for RSM. For this testing, a modified Box-Behnken Design was used. After testing and determining the center point, the optimization variables are incremented or decremented to define each corner of the hyperspace shape. After the center point, no optimization variable is held at a step size of zero. For this testing, the objective function was determined to be measured engine brake efficiency as this is the parameter of interest when comparing the 40°C (Steam) and 90°C (Steam) blends.

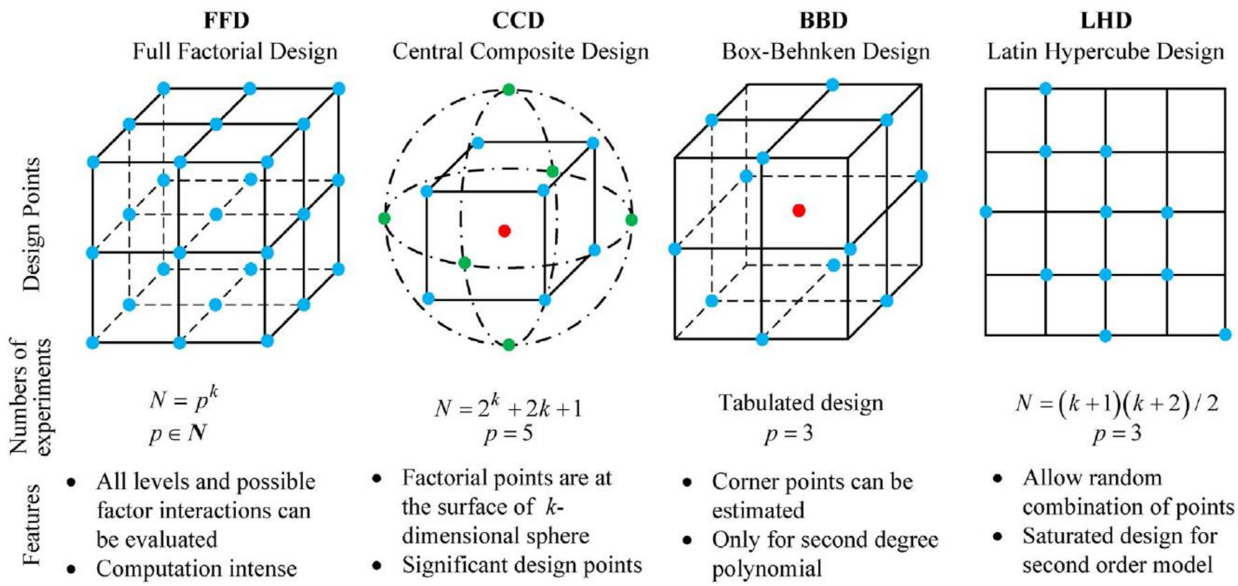

Figure 5: Experimental strategies for RSM [12].

The variables used for this optimization were IMT, engine RPM, the crank angle where 50% of fuel has been burned (CA50), IMEP, and CR. Various step sizes were determined for each variable to ensure that testing was performed at a high enough resolution to find the maximum brake efficiency without an excessive number of testing steps. With five optimization variables, the modified Box-Behnken Design required 32 data points to locate all corners of the hyperspace shape. Brake efficiency was measured at each corner. Using the center point as a reference, a field of vectors was developed to compare corner brake efficiencies to the center brake efficiency. The gradient of this vector field was calculated for each variable to provide unit vectors that indicate the direction of the fastest increase of brake efficiency. Optimization variable step sizes are then multiplied with their respective unit vectors to determine data points required to follow the path of the steepest efficiency increase. This optimization vector is followed until a new maximum brake efficiency is determined. The maximum of this optimization vector is set as the new center point for a new Box-Behnken Design shape, and the process is repeated until increases in brake efficiency are negligible.

Figure 6 depicts a flow chart created to visualize the testing sequence planned for this research. Test blend determination is shown starting with the No Water Dropout (Steam) and Full Water Dropout blends followed by the fuel conditioning and CO_2 replacement steps taken determine the other five test blends. Each row represents a step in the test blend selection process or a phase of testing.

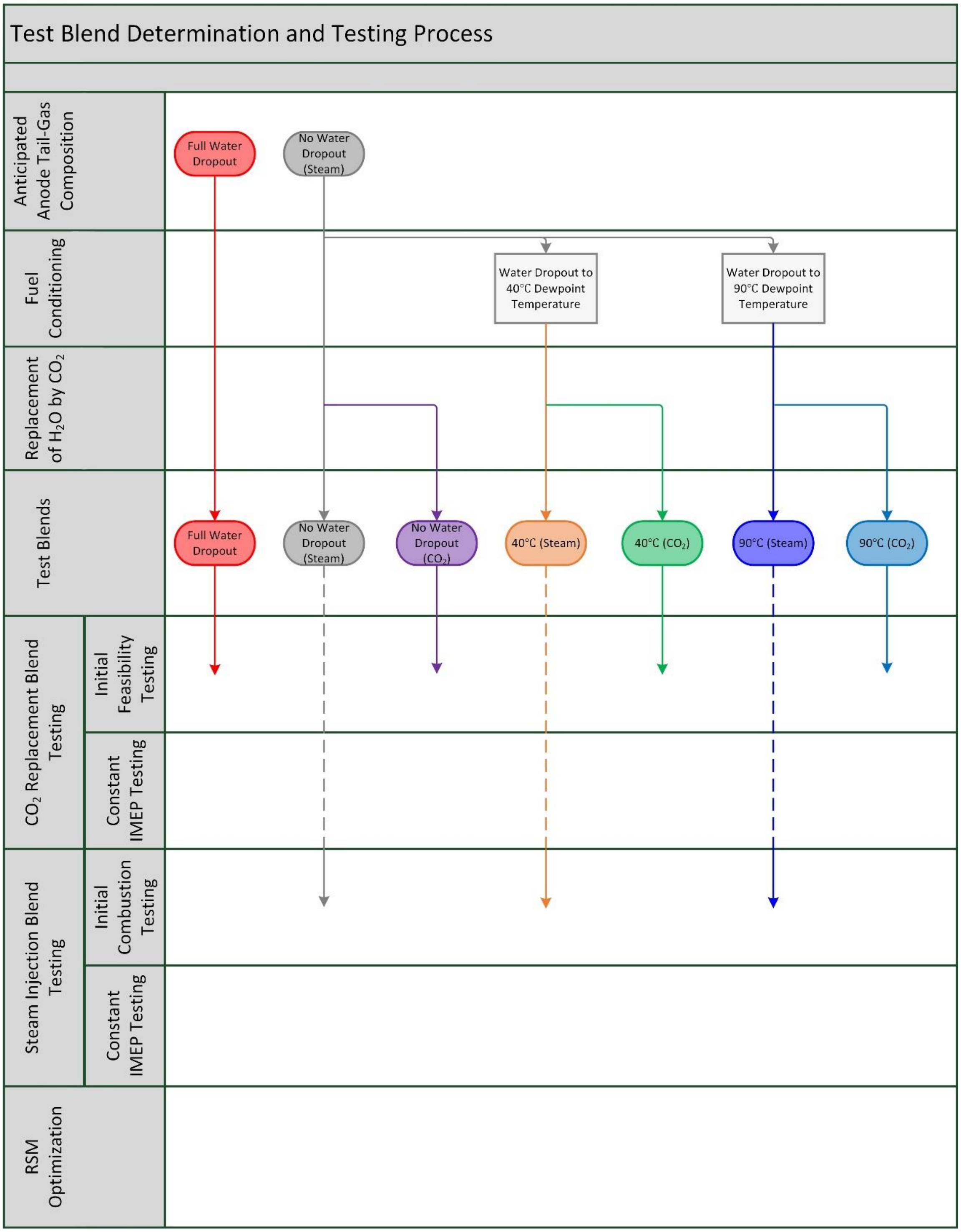

Figure 6: Flowchart representing test blend determination, selection and testing sequence planned for this research. The final and completed flowchart is presented in the Conclusions in Figure 89.

2.7. Uncertainty Analysis

Uncertainty analysis was required for this research to ensure that brake efficiency comparisons between fuels were statistically different. As this research was performed on the same engine test stand during a relatively short time, it was decided that systematic or "fixed" errors were irrelevant to the direct comparison of test blends. Random errors are relevant to these experiments and were measured by taking the same data point at the beginning of each day of testing. The standard deviation of each parameter at these data points was calculated to determine the repeatability of those parameters. The parameters of interest were electrical power generated in kW ($\dot{W}_e$), the flow of each combustible gas in kg/s ($\dot{m}_{CH4}$, $\dot{m}_{CO}$, and $\dot{m}_{H2}$). These parameters, combined with the generator efficiency (η_{gen}) and the lower heating value of each fuel (LHV_{CH4}, LHV_{CO}, and LHV_{H2}), were used to calculate the brake efficiency at each data point. Equation (2) is used to calculate the engine brake efficiency (η_{brake}).

$$\eta_{brake} = \frac{\dot{W}_e / \eta_{gen}}{\dot{m}_{CH4} LHV_{CH4} + \dot{m}_{CO} LHV_{CO} + \dot{m}_{H2} LHV_{H2}} \tag{2}$$

The root-sum-square (RSS) method was used to calculate the propagation of random error from each parameter to the calculated η_{brake} [13]. Equation (3) shows the RSS technique with the result, R, and a parameter, $\hat{X}_i$ [13].

$$\delta R_{X_i} = \left[\sum_{i=1}^{M} \left(\frac{\partial R}{\partial \hat{X}_i} \delta \hat{X}_i\right)^2\right]^{1/2} \tag{3}$$

Equation (4) shows the RSS technique applied to Equation (2) with a term for each measured parameter, $\dot{W}_e$, $\dot{m}_{CH4}$, $\dot{m}_{CO}$, and $\dot{m}_{H2}$. Each δ term represents the standard deviation (SD) of all daily points collected for that parameter added to the SD of the current data point. All other variables represent the mean value of each parameter for the current data point. $\delta\eta_{brake}$ represents the +/- random error uncertainty applied to each brake efficiency data point.

$$\delta\eta_{brake} = \left[\left(-\frac{LHV_{CH4}\dot{W}_e \big/ \eta_{gen}}{(LHV_{CH4}\dot{m}_{CH4} + LHV_{CO}\dot{m}_{CO} + LHV_{H2}\dot{m}_{H2})^2}\delta CH_4\right)^2 + \left(-\frac{LHV_{CO}\dot{W}_e \big/ \eta_{gen}}{(LHV_{CH4}\dot{m}_{CH4} + LHV_{CO}\dot{m}_{CO} + LHV_{H2}\dot{m}_{H2})^2}\delta CO\right)^2 + \left(-\frac{LHV_{H2}\dot{W}_e \big/ \eta_{gen}}{(LHV_{CH4}\dot{m}_{CH4} + LHV_{CO}\dot{m}_{CO} + LHV_{H2}\dot{m}_{H2})^2}\delta H_2\right)^2 + \left(-\frac{1 \big/ \eta_{gen}}{(LHV_{CH4}\dot{m}_{CH4} + LHV_{CO}\dot{m}_{CO} + LHV_{H2}\dot{m}_{H2})^2}\delta \dot{W}_e\right)^2\right]^{1/2} \quad (4)$$

CHAPTER 3: CO_2 REPLACEMENT BLEND TESTING

3.1. CO_2 Replacement Blend Initial Feasibility Testing

Initial feasibility testing was performed using the methods described in Chapter 2. Data was collected at several compression ratios, and a timing sweep was performed for each compression ratio to provide more data to inform combustion models. The Full Water Dropout, 40°C (CO_2), and 90°C (CO_2) test blends attained combustion and produced engine power at the initial testing conditions with a CR of 10.7:1, 45°C IMT, and 15° BTDC. The Full Water Dropout and 40°C (CO_2) test blends maximum brake torque timing for a CR of 10.7:1 was close to these initial conditions, so those blends produced steady power with no misfires. The 90°C (CO_2) blend did combust and produce power at the initial testing conditions but had a misfire fraction of 18%. The 90°C (CO_2) test blend required advanced timing to achieve steady combustion. The No Water Dropout (CO_2) test blend did not combust or produce power until CR was increased to 14.4:1, and timing was advanced to 40° BTDC. At those conditions, the No Water Dropout (CO_2) test blend had a misfire fraction of 65%. The IMT was increased to 70°C, and the misfire fraction decreased to 0.2%. Table 3 shows the conditions for each fuel blend when combustion was first achieved. The No Water Dropout (CO_2) test blend shows a negative brake efficiency due to the CFR wattmeter showing a negative power during these conditions. Since the CFR motor can be used as a motor and as a generator, the power meter measures negative power generation as the motor is drawing power to turn the engine. During the initial combustion conditions for the No Water Dropout (CO_2) test blend, too little power was produced to turn the engine on its own, but the power drawn to turn the electric motor was reduced. Table 3 also shows that the IMEP COV was 173.3% for this data set. This COV is due to the high misfire fraction of 65%, which caused the standard deviation of IMEP to be 1.733 times the average IMEP.

Table 3: Initial combustion conditions for each test blend.

Parameter	Full Water Dropout	40°C (CO_2)	90°C (CO_2)	No Water Dropout (CO_2)
CR	10.7:1	10.7:1	10.7:1	14.4:1
Ignition Timing [° ATDC]	-15	-15	-15	-40
Speed [RPM]	936	937	935	913
Inlet Temperature [°C]	45	45	45	45
Boost Pressure [kPa]	128	130	177	264
Total Fuel Flow [g/min]	147	152	248	417
Brake Efficiency [%]	13.90	13.21	10.28	-5.2
Average Peak Pressure [kPa]	4018.7	3837.7	4269.7	8505.3
Peak Pressure COV [%]	4.27	5.14	5.36	6.41
Average IMEP [kPa]	669.5	650.7	614.0	154.3
IMEP COV [%]	1.11	9.58	50.6	173.3
Misfire Fraction [%]	0	0.8	18	65

Figure 7 shows the average cylinder pressure vs. crank angle during a timing sweep for the Full Water Dropout test blend performed at a CR of 12.9:1. Several distinct trends can be observed as timing is advanced. The average peak pressure increases, the location of peak pressure advances toward TDC, and the shape of the average cylinder pressure trace becomes sharper. The sharpness of the pressure trace is associated with a higher location of peak pressure COV at -15 ATDC timing (29.6%) and -17 ATDC timing (18.3%) compared to the location of peak pressure COV at timings of -19 to -25 ATDC (~11.8%).

Figure 8 shows the average cylinder pressure vs. crank angle during a timing sweep for the 40°C (CO_2) test blend performed at a CR of 10.7:1, a CR of 12.9:1, and shows the same timing sweep conducted at CR 12.9:1 at an increased IMEP. The same trends observed over the timing sweep in Figure 7 are present in Figure 8. Figure 8 also shows an increase in peak pressure for the same ignition timing due to increased CR and a similar trend with increased IMEP.

Figure 9 shows the average cylinder pressure vs. crank angle during a timing sweep for the 90°C (CO_2) test blend performed at a CR of 10.7:1 and 12.9:1. Similar trends are observed across each timing sweep and at each CR to those seen in Figure 7 and Figure 8.

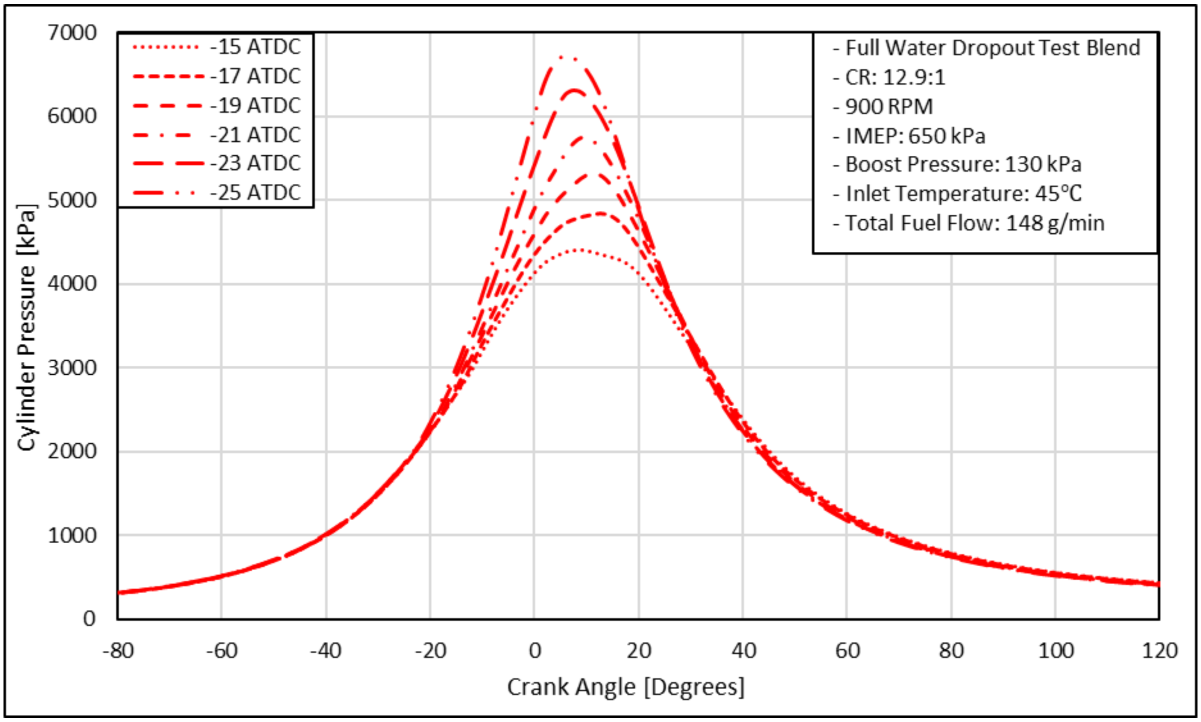

Figure 7: Cylinder pressure vs. crank angle for Full Water Dropout test blend with a sweep of ignition timing at CR 12.9:1. The legend lists the ignition timing for each test point.

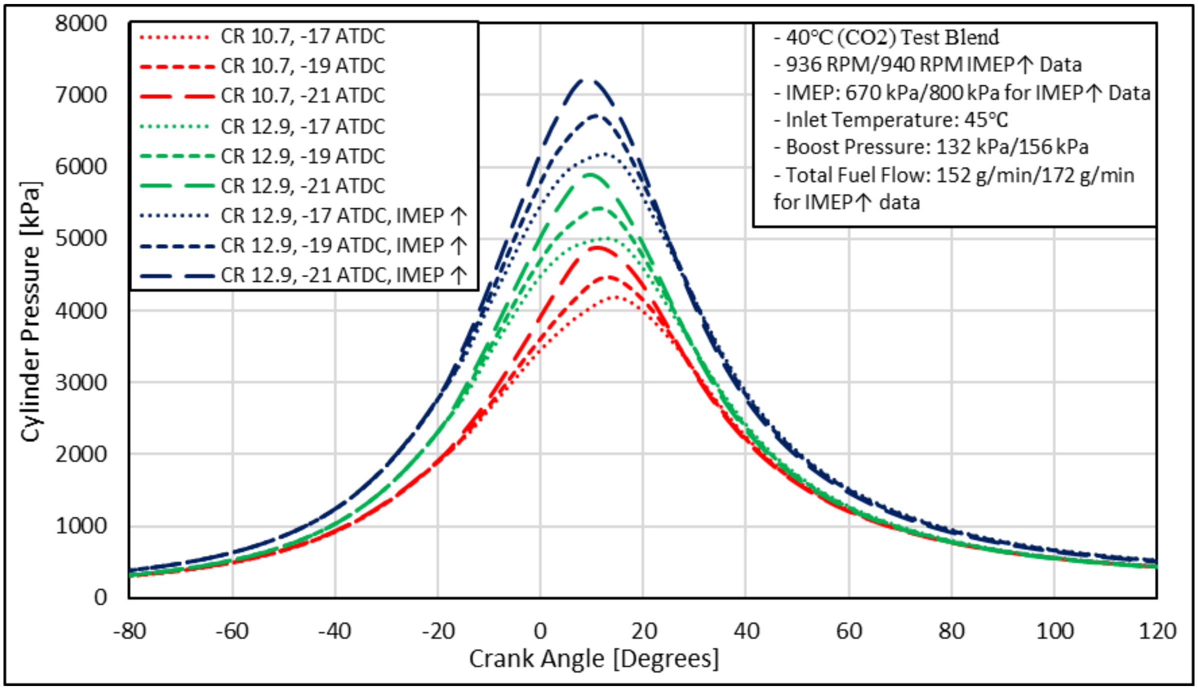

Figure 8: Cylinder pressure vs. crank angle for 40°C (CO_2) test blend with a sweep of ignition timing at CR 10.7:1, 12.9:1, and 12.9:1 with increased IMEP. The legend lists ignition timing and CR conditions.

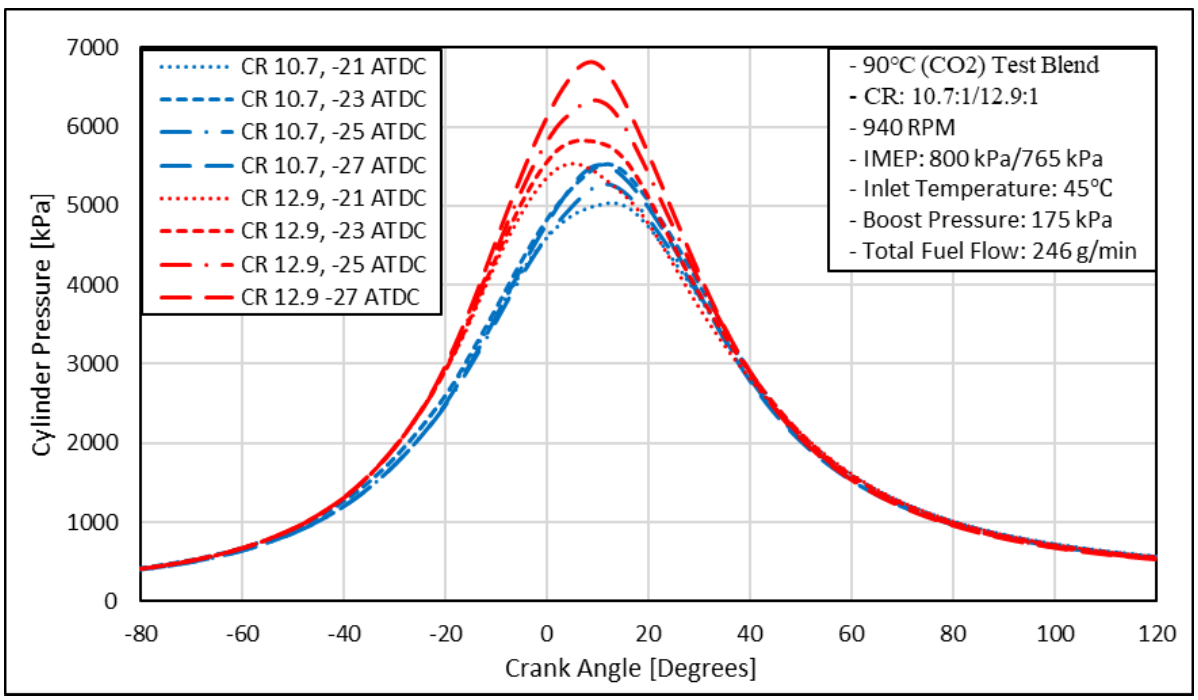

Figure 9: Cylinder pressure vs. crank angle for 90°C (CO_2) test blend with a sweep of ignition timing at CR 10.7:1, and 12.9:1. The legend lists ignition timing and CR conditions.

Figure 10 reveals the average cylinder pressure vs. crank angle for the most efficient test points for each fuel tested during initial feasibility testing with NG data added for comparison. Table 4 lists the conditions for each data set shown in Figure 10. The more dilute test blends required more advanced timing and higher boost pressure to maintain IMEP and $\phi = 1$, resulting in higher peak cylinder pressure for the more dilute fuel blends. Figure 10 shows that the No Water Dropout (CO_2) blend experienced extreme peak pressure values when compared to the other fuel blends. The extreme conditions required for steady combustion of the No Water Dropout (CO_2) fuel blend show that this blend is not ideal for use in an ICE. The other fuel blends have much more acceptable conditions at this compression ratio when compared to NG. The peaks of the test blends are not as sharp as the peak for natural gas, due to the reduced combustion rates of the simulated tail-gas.

Table 4: Parameters of most efficient data points gathered for initial feasibility testing with NG for comparison.

Parameter	Full Water Dropout	40°C (CO_2)	90°C (CO_2)	No Water Dropout (CO_2)	NG
CR	12.9:1	12.9:1	12.9:1	14.4:1	10.5:1
Ignition Timing [° ATDC]	-17	-19	-27	-40	-13
Speed [RPM]	936	937	940	939	900
Inlet Temperature [°C]	45	45	45	45	61
Boost Pressure [kPa]	130	131	167	267	104
Total Fuel Flow [g/min]	148	154	248	419	14.8
Energy Flow (LHV$\cdot\dot{m}_{fuel}$) [kW]	11.3	11.4	13.0	13.3	11.55
Electric Power [kW]	1.37	1.44	1.86	1.77	1.92
Maximum Brake Efficiency [%]	13.54	14.17	16.15	14.81	18.58
Average Peak Pressure [kPa]	4201.1	5439.0	6836.4	10627.8	5374.8
Peak Pressure COV [%]	4.59	4.15	4.72	4.42	4.92
Average IMEP [kPa]	658.7	681.3	785.0	763.9	823.9
IMEP COV [%]	4.93	1.09	1.05	9.57	0.93
Misfire Fraction [%]	0	0	0	0.2	0

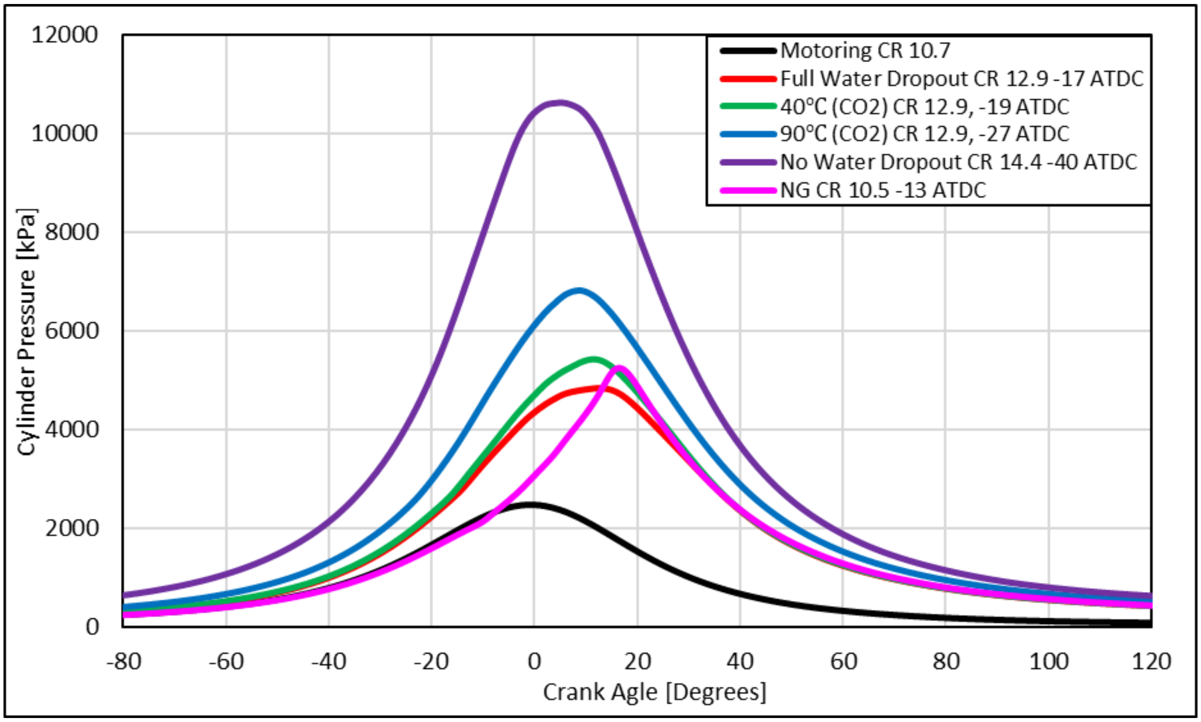

Figure 10: Cylinder pressure vs. crank angle for each test blend's most efficient data point from initial combustion testing. NG and motoring data included for comparison. Refer to Table 4 for specific testing parameters. The legend lists ignition timing and CR values.

Figure 11 and 11 show the apparent heat release rate (AHRR) vs. crank angle for the 40°C (CO_2) blend across the same sweep of ignition timing at two CRs and with increased IMEP for comparison. Figure 11 demonstrates that increasing CR lowers peak AHRR, except in the case of 17° BTDC spark timing. The 19° and 21° BTDC spark timings also show a slower decrease of AHRR during cylinder expansion. In Figure 12, the increase in IMEP from 670 kPa to 800 kPa results in higher peak AHRRs with ignition timing held constant. This higher IMEP is achieved through increasing fuel flow to increase energy flow into the cylinder and increasing boost pressure to maintain $\phi = 1$.

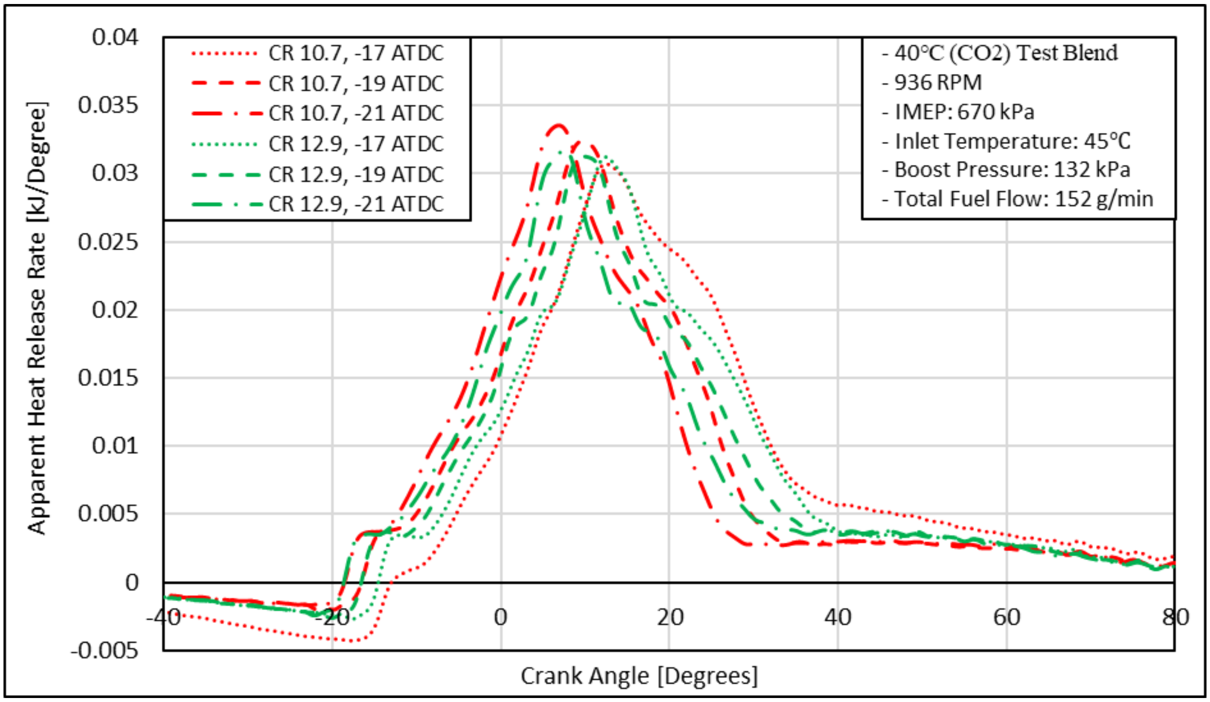

Figure 11: AHRR vs. crank angle for 40°C (CO_2) test blend with a sweep of ignition timing at CR 10.7:1, and 12.9:1. The legend lists ignition timing and CR values.

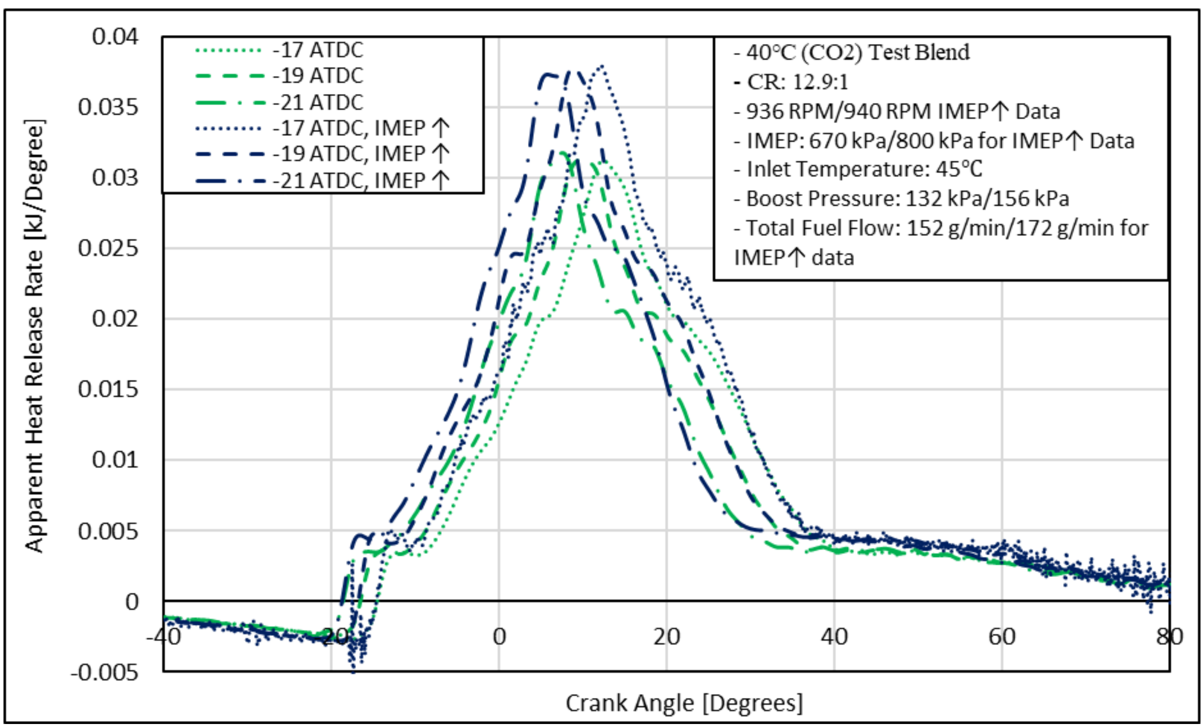

Figure 12: AHRR vs. crank angle for 40°C (CO_2) test blend with a sweep of ignition timing at CR 12.9:1 with IMEP = 670 kPa and 800 kPa. The legend lists ignition timing values.

In Figure 13, the AHRR vs. crank angle is shown for the most efficient test points of each fuel tested during initial feasibility testing with NG data added for comparison. Table 4 lists the conditions for each data set shown in Figure 13. This figure illustrates that the peak AHRR for NG is much higher than the simulated tail-gas blends. The large amounts of diluents contained in the simulated tail-gas blends cause the peak AHRRs to be much lower. The figure also displays similar peak AHRRs for the Full Water Dropout, 40°C (CO_2), and 90°C (CO_2) test blends at each test blend's maximum brake torque timing. As the diluents increase across each of these blends, maximum brake torque timing advances away from TDC, which causes the location of peak AHRR for each of these blends to advance closer to TDC. The No Water Dropout (CO_2) test blend does not fit this trend since this test blend is not operating at maximum brake torque timing as only one data point with steady combustion was able to be collected due to issues with engine operation, extreme peak pressure and unfavorable operating conditions. Figure 13 also shows that AHRR for simulated tail-gas blends remains relatively high much further into the expansion stroke of the engine when compared with NG. This slow burn rate causes reduced engine efficiency.

Figure 14 shows the mass fraction burned vs. crank angle for the most efficient test points for each fuel tested during initial feasibility testing with NG for comparison. Table 4 lists the conditions for each data set shown in Figure 14. The dip below zero for the No Water Dropout (CO_2) blend represents heat loss to cylinder walls due to the highly advanced timing and long ignition delay. NG shows the highest burn rate and shortest burn duration as it reaches 90% mass fraction burned before 20° ATDC. The simulated tail-gas blends show much slower burn rates, and each reaches 90% mass fraction burned at close to 50° ATDC. This slow combustion is inefficient as it continues late into the expansion stroke, causing much its energy to be lost.

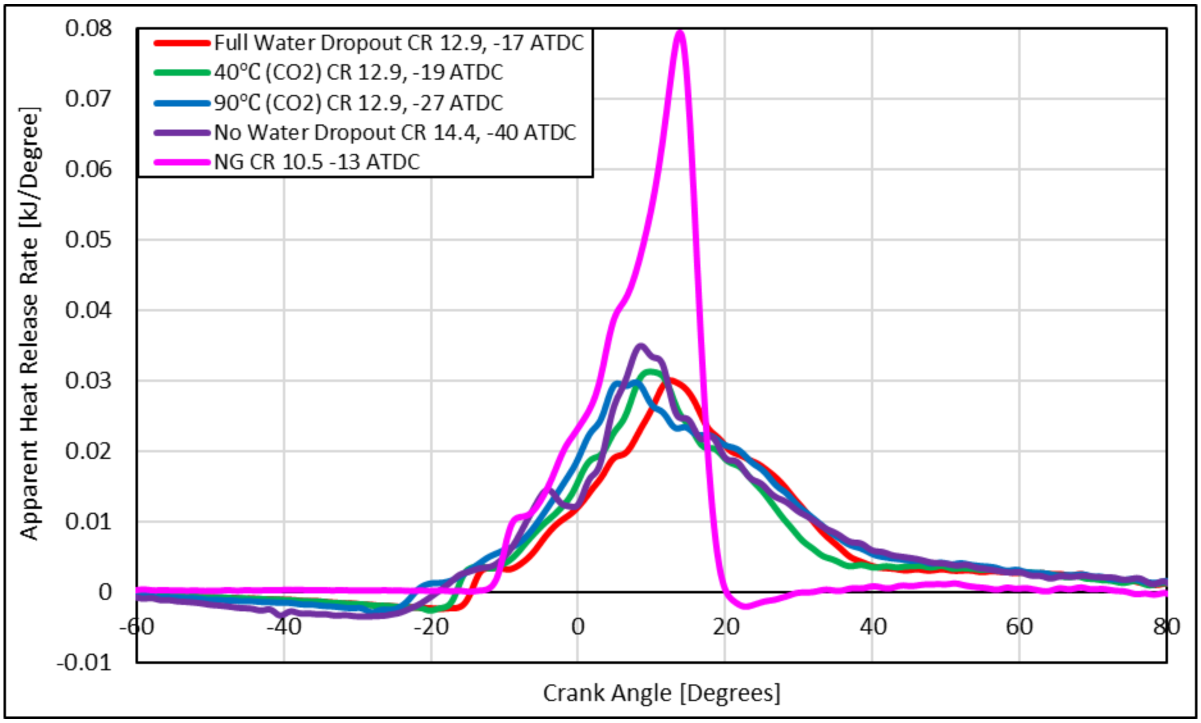

Figure 13: AHRR vs. crank angle for each test blend's most efficient data point from initial combustion testing. NG data included for comparison. Refer to Table 4 for specific testing parameters. The legend lists ignition timing and CR values.

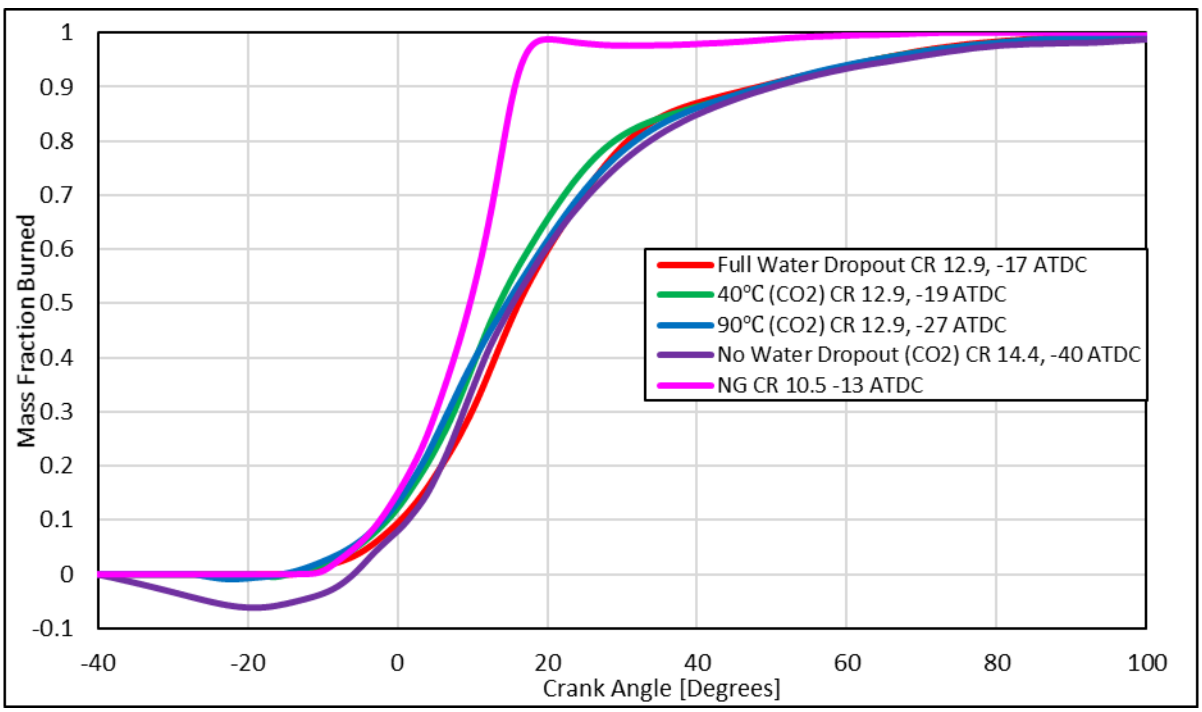

Figure 14: Mass fraction burned vs. crank angle for each test blend's most efficient data point from initial combustion testing. NG data included for comparison. Refer to Table 4 for specific testing parameters. The legend lists ignition timing and CR values.

Figure 15 displays the brake efficiency vs. ignition timing for the Full Water Dropout, 40°C (CO_2), and 90°C (CO_2) test blends. The Full Water Dropout test blend maximum brake torque timing was 17° BTDC, the 40°C (CO_2) test blend was 19° BTDC, and the 90°C (CO_2) test blend was 27° BTDC. The 90°C (CO_2) test blend demonstrated a sizable increase in brake efficiency as the timing was advanced, due to fuel and air flows being increased to reach ~1.5kW of engine power while large amounts of misfires were occurring at less advanced timing. As the 90°C (CO_2) timing was advanced and misfire fraction decreased the engine power level increased to a maximum of 1.86 kW, causing an increase in brake efficiency far above what was seen with other test blends. Uncertainty bars are included in Figure 15 and were calculated using the method described in Section 2.7. The levels of uncertainty were low enough during these tests to show that the efficiency differences measured between each blend and the rise in efficiency seen in the 90°C (CO_2) blend were statistically significant. Although the brake efficiency measured at maximum brake torque timing is higher for the 90°C (CO_2) blend than the Full Water Dropout and 40°C (CO_2) blends, the 90°C (CO_2) blend is not necessarily a better fuel. The increased efficiency measured for the 90°C (CO_2) blend can be attributed to higher boost pressure, more energy flow, and higher engine power. Further testing is required to determine the ideal fuel blend.

In Figure 16 the IMEP COV vs. ignition timing for each test blend except for the No Water Dropout (CO_2) blend is shown. The IMEP COV is lowest at the most efficient test points for each blend. A low IMEP COV means a low cycle to cycle variance of IMEP, which is the result of more steady combustion. This decrease in the IMEP COV as timing is advanced for the 90°C (CO_2) test blend is a direct result of a lowering misfire fraction which is displayed in Figure 17.

Figure 17 can be compared to Figure 15 and Figure 16 to see how steady combustion, measured here as a low IMEP COV and low misfire fraction, results in higher brake efficiency.

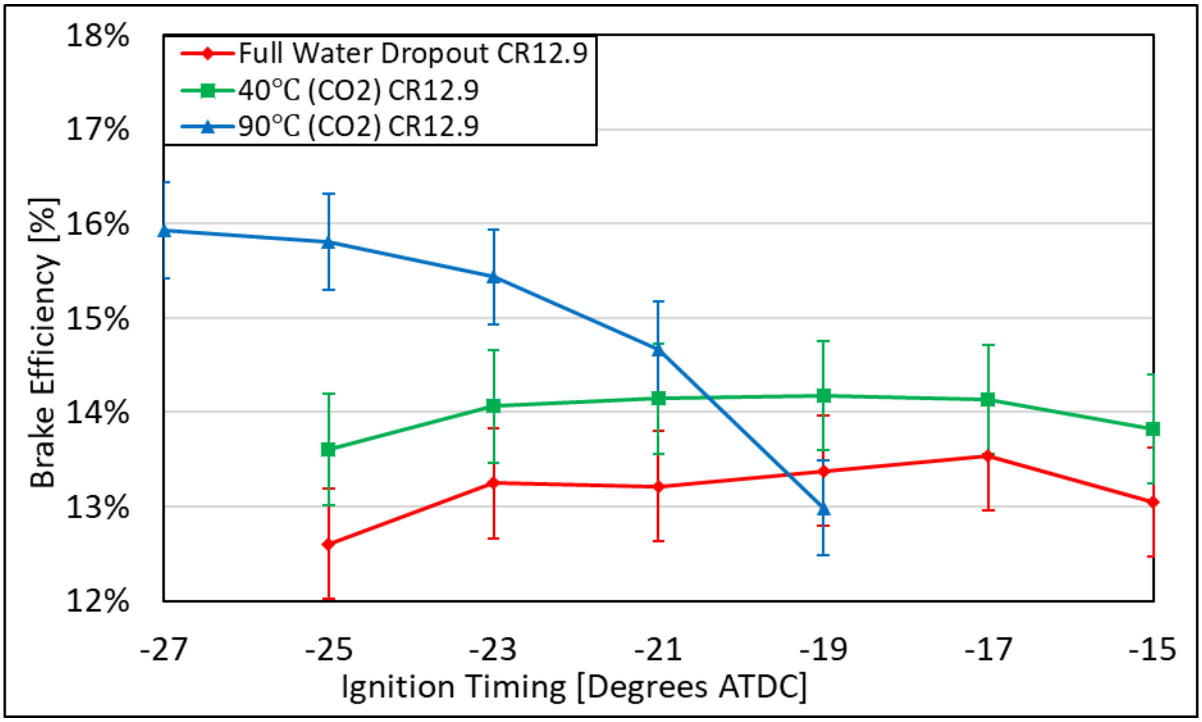

Figure 15: Brake efficiency vs. ignition timing for all test blends, except the No Water Dropout (CO_2) blend, at CR 12.9:1. Refer to Table 4 for specific testing parameters and No Water Dropout (CO_2) blend parameters.

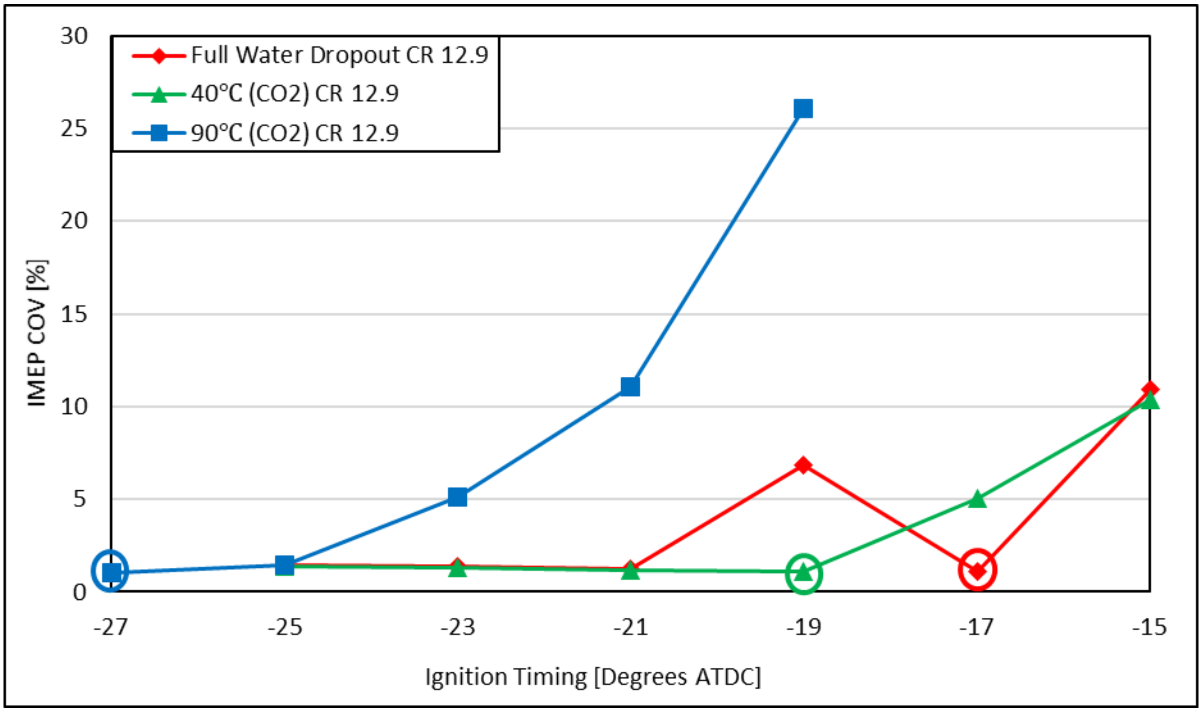

Figure 16: IMEP COV vs. ignition timing for all test blends, except the No Water Dropout (CO_2) blend, at CR 12.9:1 with the most efficient test points for each blend circled. Refer to Table 4 for specific testing parameters and No Water Dropout (CO_2) blend parameters.

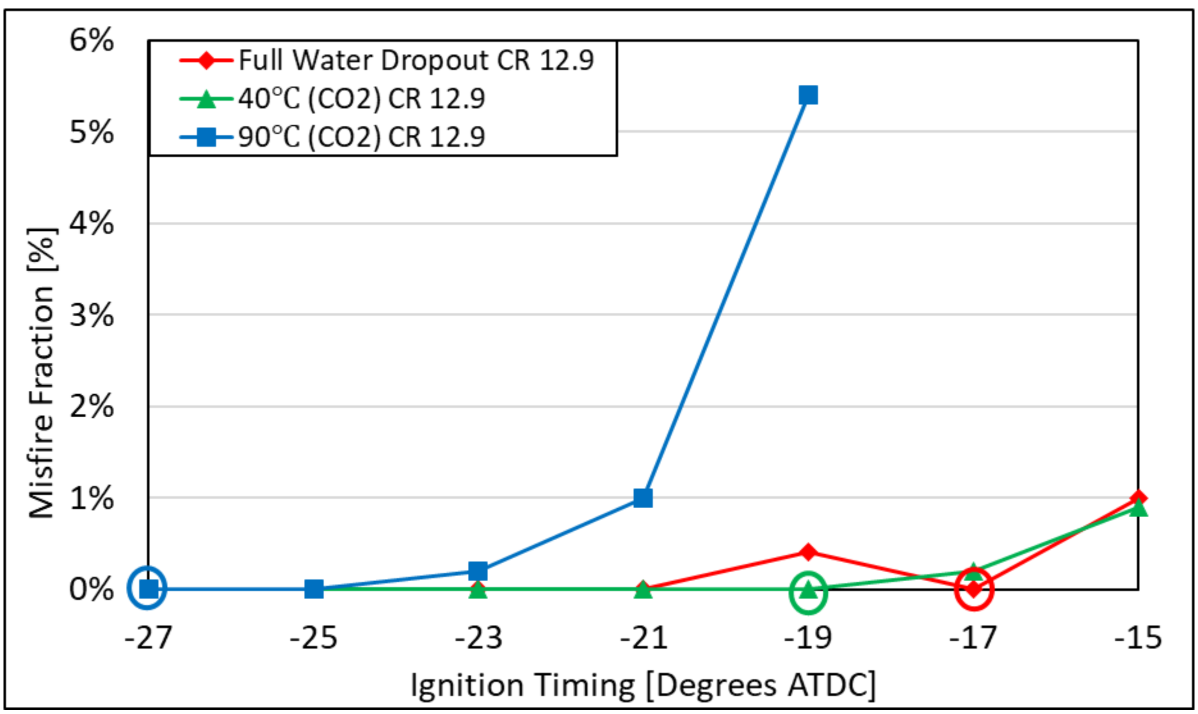

Figure 17: Misfire fraction vs. ignition timing for all test blends, except the No Water Dropout (CO_2) blend, at CR 12.9:1 with the most efficient test points for each blend circled. Refer to Table 4 for specific testing parameters and No Water Dropout (CO_2) blend parameters.

3.2. Constant IMEP CO_2 Blend Testing

Constant IMEP testing was performed to allow a more direct comparison of combustion characteristics between each test blend. During initial feasibility testing fuel flow rates were set and held constant after initial combustion was achieved. Afterwards, the fuel flow would be increased with boost pressure to produce 1.3-1.5 kW of electrical power at $\phi = 1$. This method allowed an accurate comparison between the Full Water Dropout and 40°C (CO_2) blends as the maximum brake torque timing for each blend was close to the initial conditions. For the 90°C (CO_2) blend, this power level was set while brake efficiency was at its lowest, and the misfire fraction was 18%. As timing was advanced, the 90°C (CO_2) blend saw a substantial increase in brake efficiency and engine power, which made it difficult to directly compare this blend to the Full Water Dropout and 40°C (CO_2) test blends.

During the constant IMEP testing, the maximum brake torque timing from initial feasibility testing was used as a reference to find and adjust for maximum brake torque timing at current conditions. As this testing was also used to compare these blends to the steam injection test blends, IMT was held at 70°C, and pipe walls were heated to prevent condensation. Although the 90°C (Steam) test blend has a dewpoint temperature of 90°C, once this blend is mixed with air at $\phi = 1$, the dewpoint temperature is reduced to 55°C. For this testing, IMEP was maintained at 870±15 kPa. This testing also excludes the No Water Dropout (CO_2) and No Water Dropout (Steam) test blends as they were deemed unsuitable for engine operation due to complications with extreme engine operating conditions and issues with water contamination of the engine lube oil system.

Figure 18 shows the cylinder pressure vs. crank angle across a sweep of CR for the Full Water Dropout test blend at maximum brake torque timing. As CR is increased, cylinder peak pressure increases and, the location of peak pressure advances towards TDC for CRs up to 12.2:1. The data recorded for a CR of 12.9:1 shows a slight inflection point just before reaching peak pressure, which indicates the occurrence of light knock. Indication of heavier knock is shown for a CR of 13.6:1 with a more distinct inflection point before reaching peak pressure. These inflection points indicate the moment of autoignition in the cylinder.

Figure 19 shows the cylinder pressure vs. crank angle across a sweep of CR for the 40°C (CO_2) test blend at maximum brake torque timing. Trends similar to those seen in Figure 18 are observed for the 40°C (CO_2) test blend except that indications of engine knock are only seen once the CR is increased to 13.6:1.

Figure 20 displays the cylinder pressure vs. crank angle across a sweep of CR for the 90°C (CO_2) test blend at maximum brake torque timing. Trends similar to those seen in Figure 18 and Figure 19 are observed for the 90°C (CO_2) test blend except that indications of engine knock are not seen in any data set. The CR was only increased to 12.9:1 as increasing CR further caused significant decreases in engine efficiency and intermittent loss of combustion. One possible cause for this is that the squish region at higher compression ratios was too small to allow the flame front to advance without being quenched for this more dilute test blend.

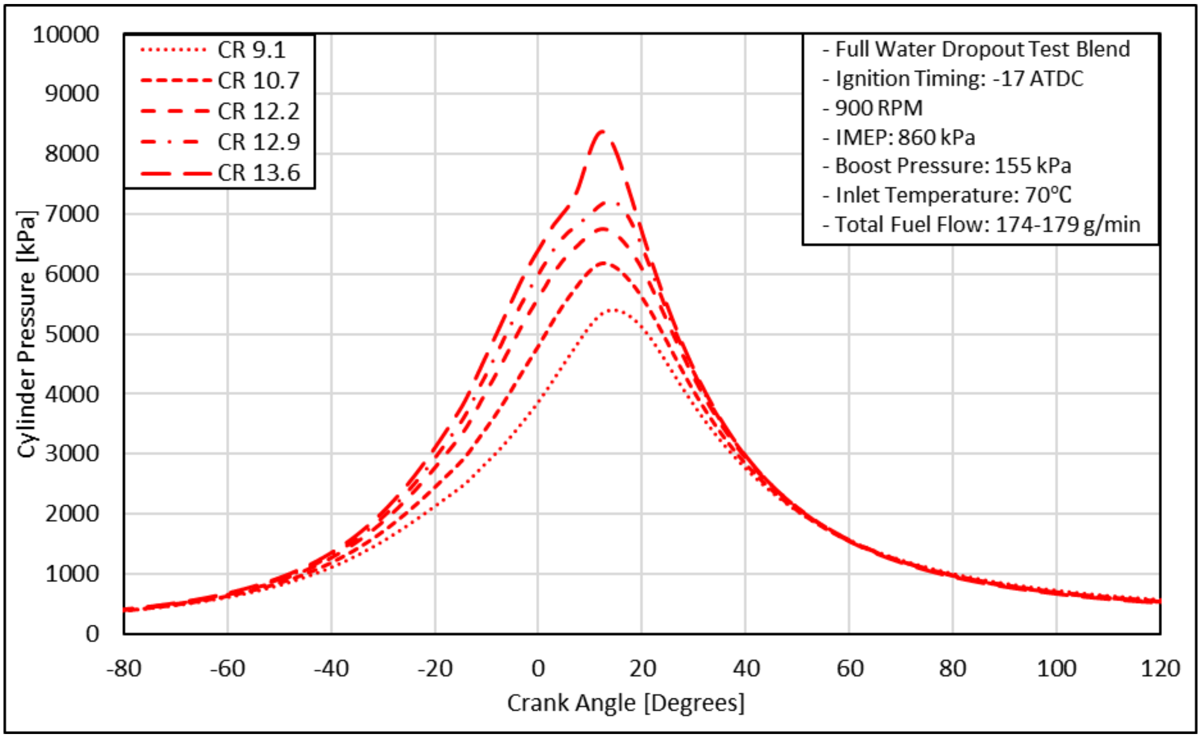

Figure 18: Cylinder pressure vs. crank angle for Full Water Dropout test blend at maximum break torque timing of -17° ATDC with a sweep of CR from 9.1:1 - 13.6:1.

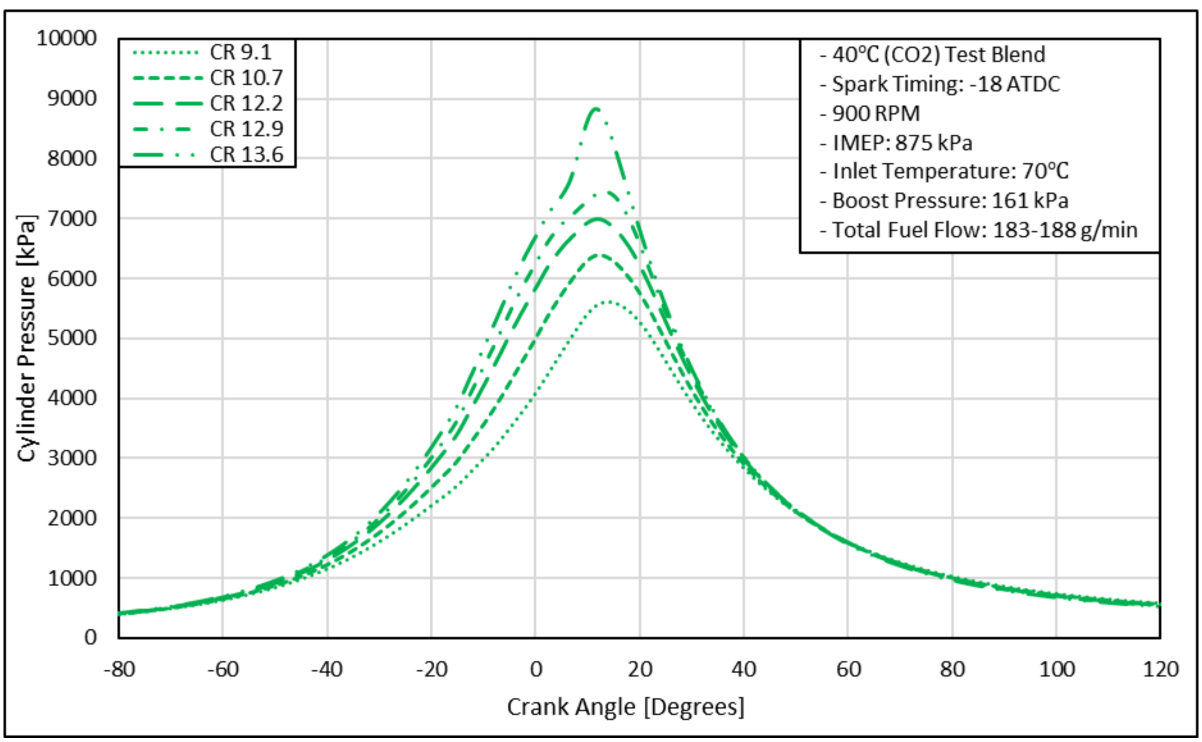

Figure 19: Cylinder pressure vs. crank angle for 40°C (CO_2) test blend at maximum break torque timing of -18° ATDC with a sweep of CR from 9.1:1 - 13.6:1.

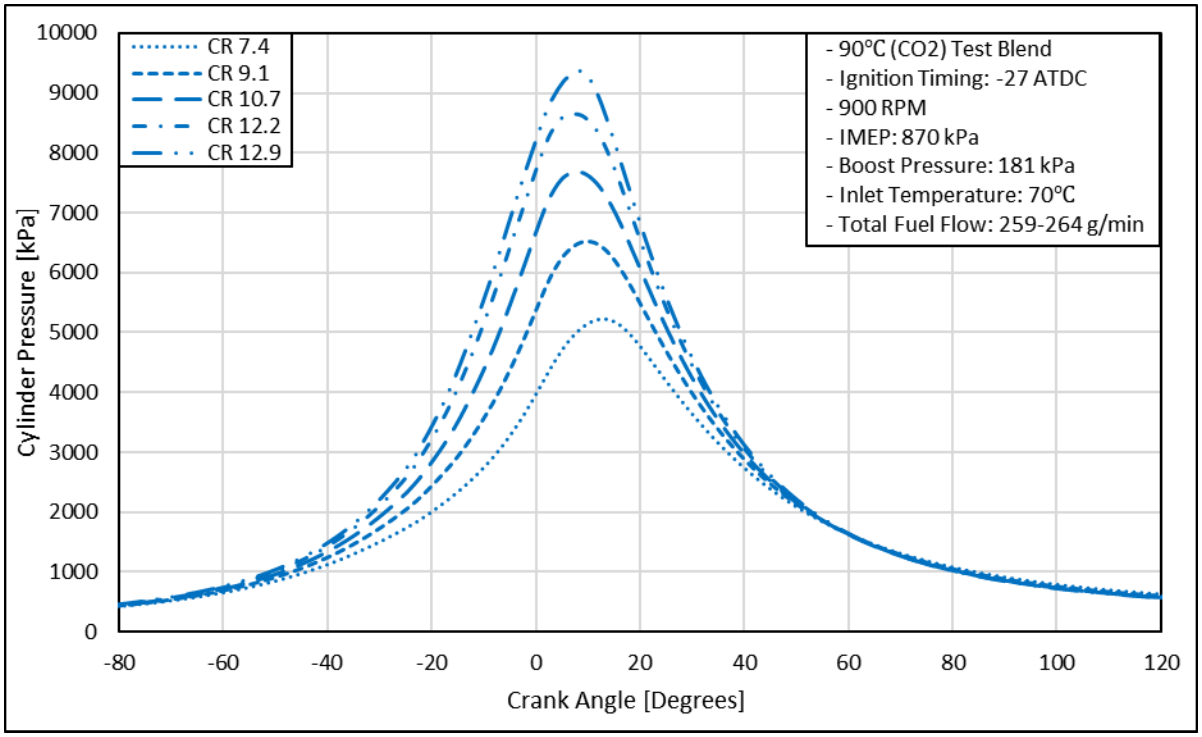

Figure 20: Cylinder pressure vs. crank angle for 90°C (CO_2) test blend at maximum break torque timing of -27° ATDC with a sweep of CR from 7.4:1 - 12.9:1.

Figure 21 shows the average cylinder pressure vs. crank angle for the most efficient test points for each fuel tested during constant IMEP testing with No Water Dropout (CO_2), NG, and motoring data added for comparison. Table 5Table 4 lists the conditions for each data set displayed in Figure 21. The more dilute test blends required more advanced timing and higher boost pressure to maintain IMEP and $\phi = 1$, resulting in higher peak cylinder pressure for the more dilute fuel blends except for the Full Water Dropout blend. The Full Water Dropout blend was able to maintain its brake efficiency at higher compression ratios causing peak cylinder pressure to be higher at the most efficient test point for the Full Water Dropout blend than it was in the 40°C (CO_2) blend. Finding the optimal CR during this testing brought peak cylinder pressures of other blends closer to those seen in the No Water Dropout (CO_2) blend.

Table 5: Parameters of most efficient data points gathered for constant IMEP testing with No Water Dropout (CO_2) blend and NG for comparison. IMEP was maintained at 870±15 kPa.

Parameter	Full Water Dropout	40°C (CO_2)	90°C (CO_2)	No Water Dropout (CO_2)	NG
CR	12.9	10.7	12.2	14.4:1	10.5:1
Ignition Timing [° ATDC]	-17	-18	-27	-40	-13
Speed [RPM]	901	901	901	939	900
Inlet Temperature [°C]	69.7	69.8	69.6	45	61
Boost Pressure [kPa]	156	159	181	267	104
Total Fuel Flow [g/min]	175	183	258	419	14.8
Energy Flow (LHV·$\dot{m}_{fuel}$) [kW]	13.5	13.7	13.6	13.3	11.55
Electric Power [kW]	2.06	2.12	2.08	1.77	1.92
Maximum Brake Efficiency [%]	17.09	17.32	17.12	14.81	18.58
Average Peak Pressure [kPa]	7249.0	6412.3	8671.5	10627.8	5374.8
Peak Pressure COV [%]	5.35	3.39	3.47	4.42	4.92
Average IMEP [kPa]	861.8	877.6	868.1	763.9	823.9
IMEP COV [%]	0.98	1.03	1.39	9.57	0.93
Misfire Fraction [%]	0	0	0	0.2	0
Ignition Delay [Degrees]	11.2	11.8	13.9	41.4	14.8
Burn Duration [Degrees]	25.5	26.6	49.2	48.8	29.1

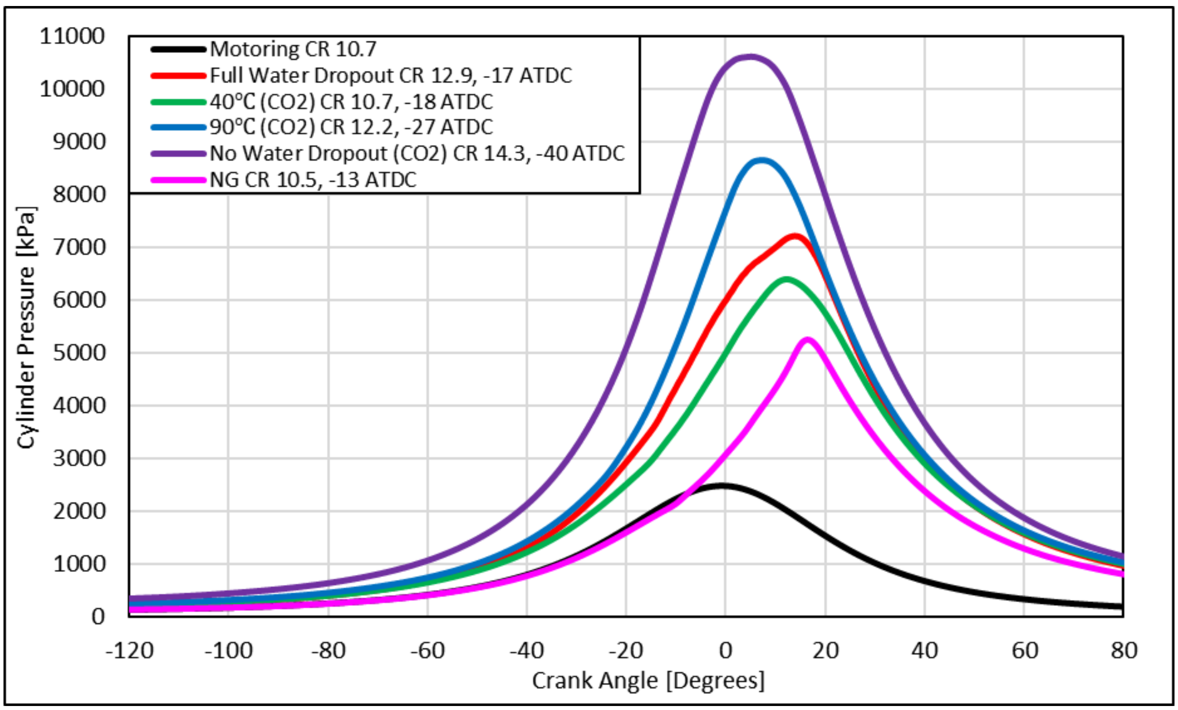

Figure 21: Cylinder pressure vs. crank angle for each test blend's most efficient data point from constant IMEP testing. No Water Dropout (CO_2), NG and motoring data included for comparison. Refer to Table 5 for specific testing parameters. The legend lists ignition timing and CR conditions.

Figure 22 shows the AHRR vs. crank angle across a sweep of CR for the 40°C (CO_2) test blend at maximum brake torque timing. This data shows a decrease in peak AHRR as CR is increased from 10.7:1 to 12.2:1. The effect of engine knock can be seen at a CR of 13.6:1 which causes a large and fast increase in AHRR.

Figure 23 shows the AHRR vs. crank angle for the most efficient test points for each fuel tested during constant IMEP testing with No Water Dropout (CO_2) and NG data added for comparison. Table 5Table 4 lists the conditions for each data set shown in Figure 23. Increasing IMEP and CR during constant IMEP testing has caused the peak AHRR for each test blend to be much higher than what was found during initial feasibility testing. The peak AHRR for each test blend is now higher than the No Water Dropout (CO_2) blend peak AHRR. Figure 23 also shows that, for similar energy flows and IMEP, the peak AHRR lowers as the fuel blend is more diluted. The location of peak AHRR moves towards TDC due to the more advanced timing required for efficient combustion of the more dilute test blends.

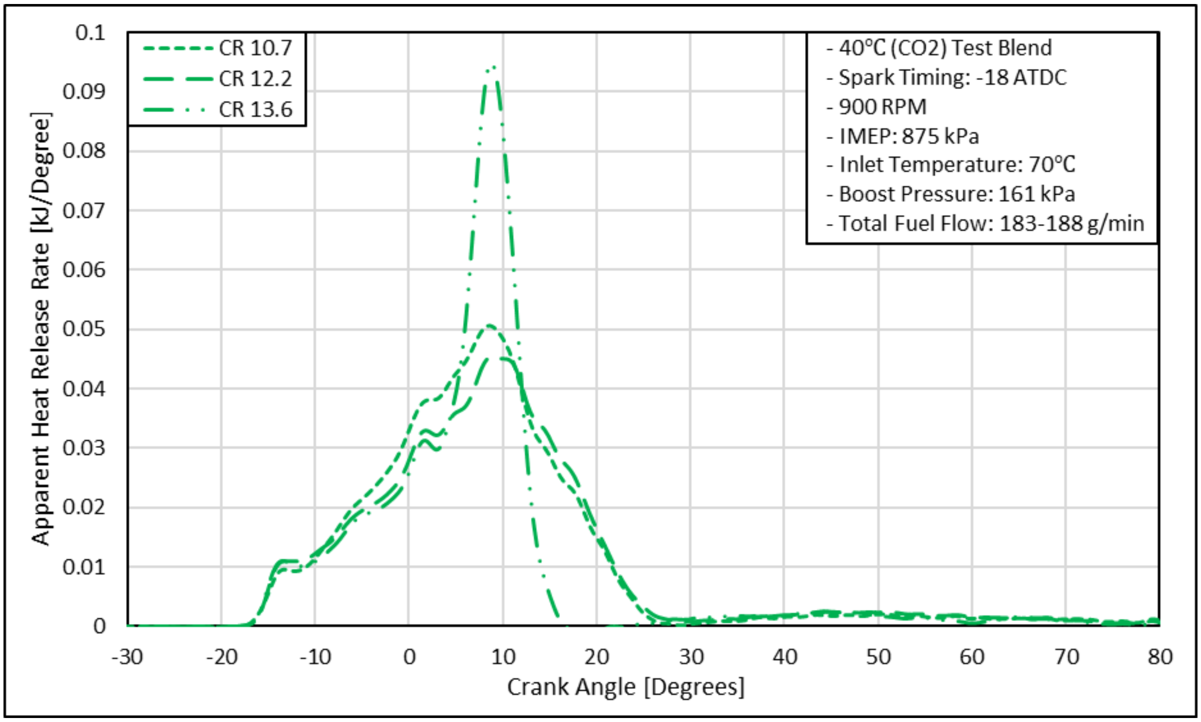

Figure 22: AHRR vs. crank angle for 40°C (CO_2) test blend at maximum break torque timing of -18° ATDC with a sweep of CR from 10.7:1 - 13.6:1.

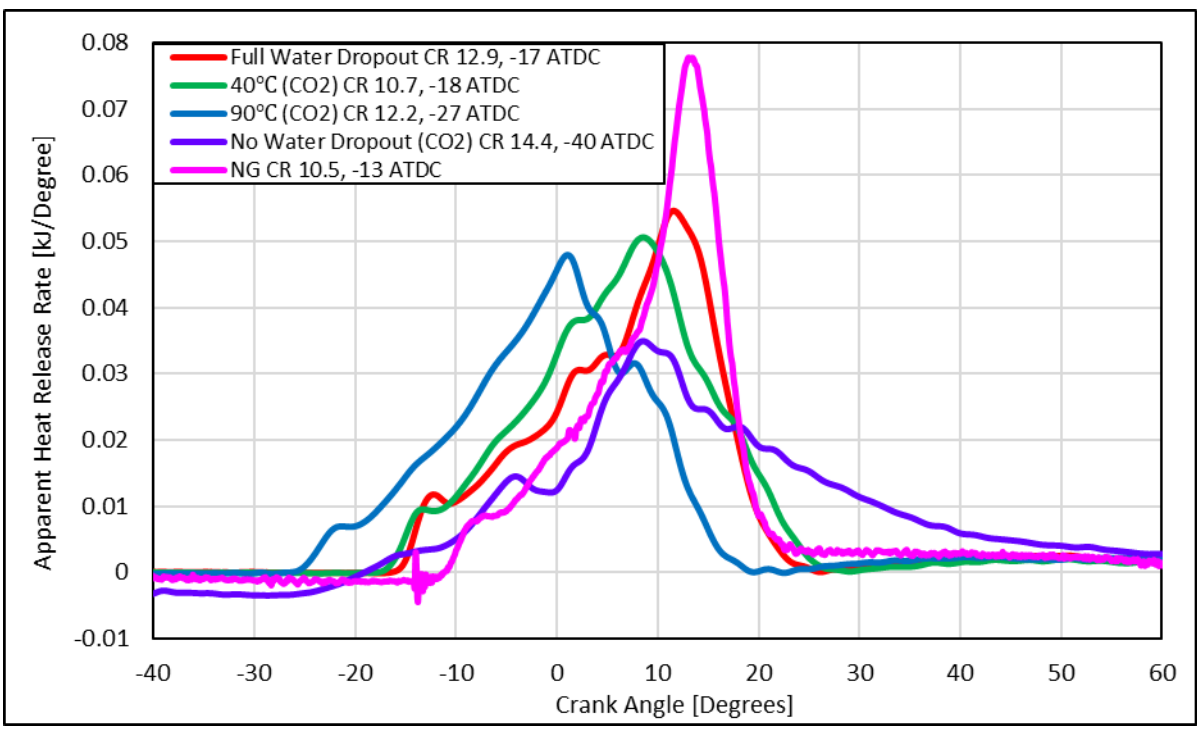

Figure 23: AHRR vs. crank angle for each test blend's most efficient data point from constant IMEP testing. No Water Dropout (CO_2) and NG data included for comparison. Refer to Table 5 for specific testing parameters. The legend lists ignition timing and CR conditions.

The mass fraction burned vs. crank angle across a sweep of CR for the 40°C (CO_2) test blend at maximum brake torque timing can be seen in Figure 24. There is not much change, with an increase in CR from 10.7:1 to 12.2:1. During engine knock at a CR of 13.6:1, the steep slope of mass fraction burned is apparent. Engine knock also causes a decrease in the burn duration as 90% mass fraction burned corresponds to a crank angle of about 13° ATDC.

Figure 25 shows the mass fraction burned vs. crank angle for the most efficient test points for each fuel tested during constant IMEP testing with No Water Dropout (CO_2) and NG data added for comparison. Table 5Table 4 lists the conditions for each data set shown in Figure 25. Operating at maximum brake torque timing and increasing CR caused the Full Water Dropout and 40°C (CO_2) test blends to reach 90% mass fraction burned earlier than the NG test data. The 90°C (CO_2) blend almost reaches 90% mass fraction burned before the NG test data, but its burn rate considerably slows down just before reaching it.

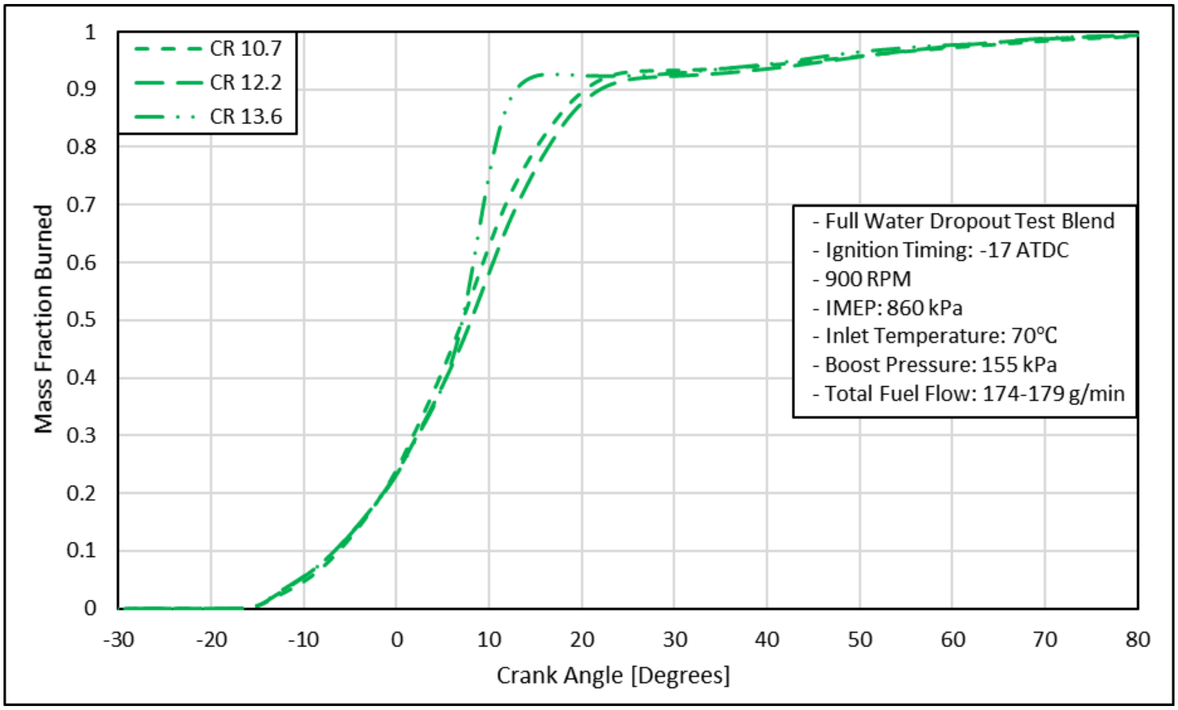

Figure 24: Mass fraction burned vs. crank angle for 40°C (CO_2) test blend at maximum break torque timing of -18° ATDC with a sweep of CR from 10.7:1 - 13.6:1.

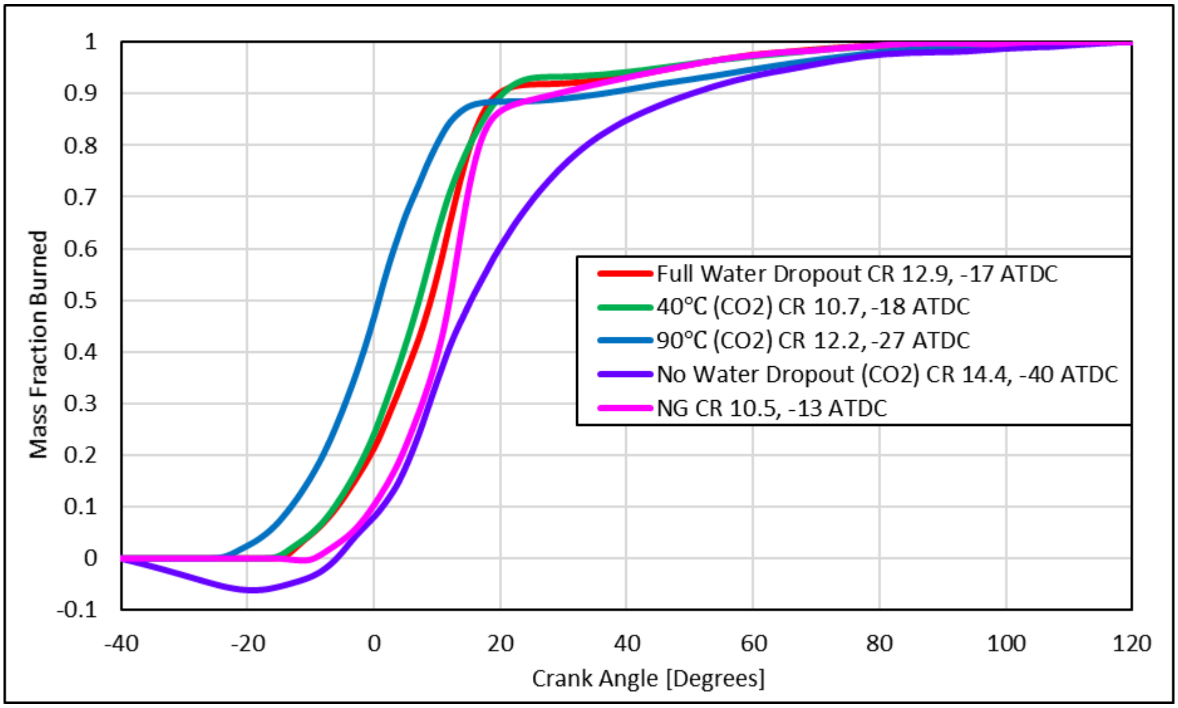

Figure 25: Mass fraction burned vs. crank angle for each test blend's most efficient data point from constant IMEP testing. No Water Dropout (CO_2) and NG data are included for comparison. Refer to Table 5 for specific testing parameters. The legend lists ignition timing and CR conditions.

Figure 26 shows the brake efficiency vs. CR at maximum brake torque timing for the Full Water Dropout, 40°C (CO_2), and 90°C (CO_2) test blends. The levels of uncertainty were similar during these tests to those shown in the initial feasibility testing but, due to holding IMEP relatively constant, the differences in brake efficiency at the most efficient test points for each blend are not statistically significant. The Full Water Dropout and 90°C (CO_2) test blends show that brake efficiency tends to increase as CR increases. The 90°C (CO_2) test blend saw a decrease in brake efficiency above a CR of 12.2:1, possibly due to an increased surface to volume ratio at TDC which leads to flame quenching. 90°C (CO_2) data points above a CR of 12.9:1 could not be gathered due to an inability to maintain combustion. The 40°C (CO_2) blend shows an increase in brake efficiency from 9.1:1 to 10.7:1, and although brake efficiency slightly decreases as CR is increased above 10.7:1, the decrease is minimal.

Figure 27 shows the ignition delay vs. CR at maximum brake torque timing for the Full Water Dropout, 40°C (CO_2), and 90°C (CO_2) test blends. Ignition delay tends to decrease as CR is increased, which is most apparent in the 90°C (CO_2) blend data.

Figure 28 shows the burn duration vs. CR at maximum brake torque timing for the Full Water Dropout, 40°C (CO_2), and 90°C (CO_2) test blends. Burn duration tends to slightly increase as CR is increased from 9.1:1 to 12.2:1 in the Full Water Dropout and 40°C (CO_2) test blends and from 7.4:1 to 10.7:1 for the 90°C (CO_2) blend. For the Full Water Dropout and 40°C (CO_2) test blends, the burn duration decreases above a CR of 12.2:1 due to engine knock. The 90°C (CO_2) blend shows that as CR is increased above 10.7:1, the fuel begins to have a greatly increased burn duration which is an indication of reduced combustion performance and flame quenching, potentially due to the squish volume being too small at TDC for such a dilute fuel.

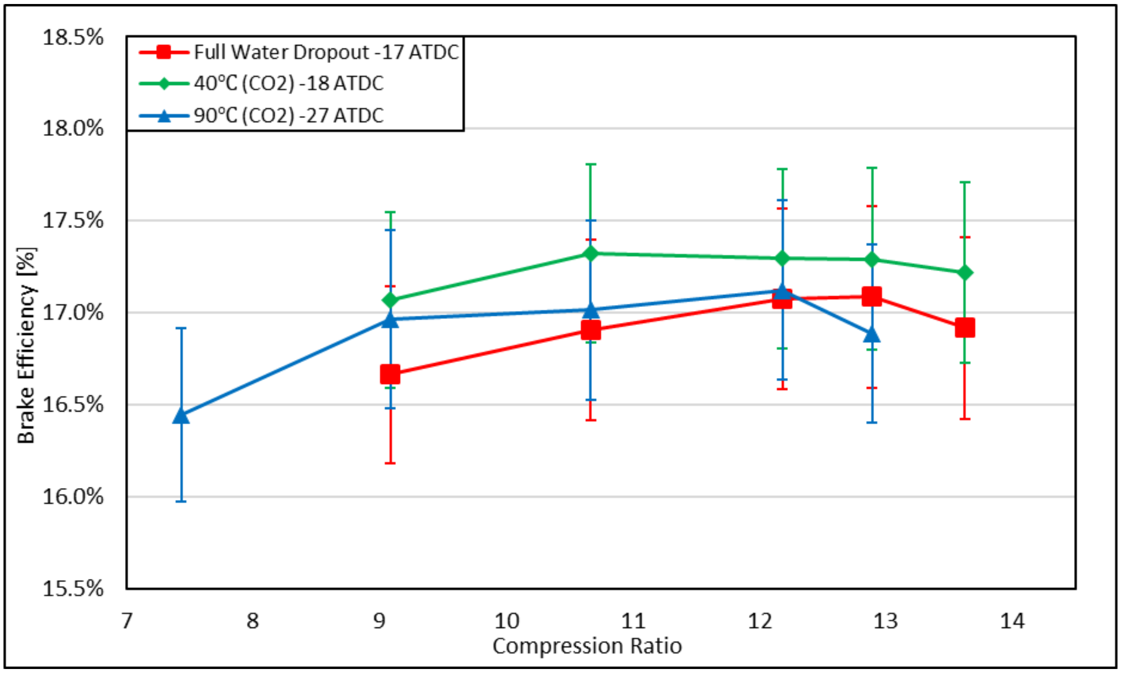

Figure 26: Brake efficiency vs. CR for all test blends, except the No Water Dropout (CO_2) blend, at maximum brake torque timing. Refer to Table 5 for specific testing parameters and No Water Dropout (CO_2) blend parameters. The legend lists the ignition timing for each test point.

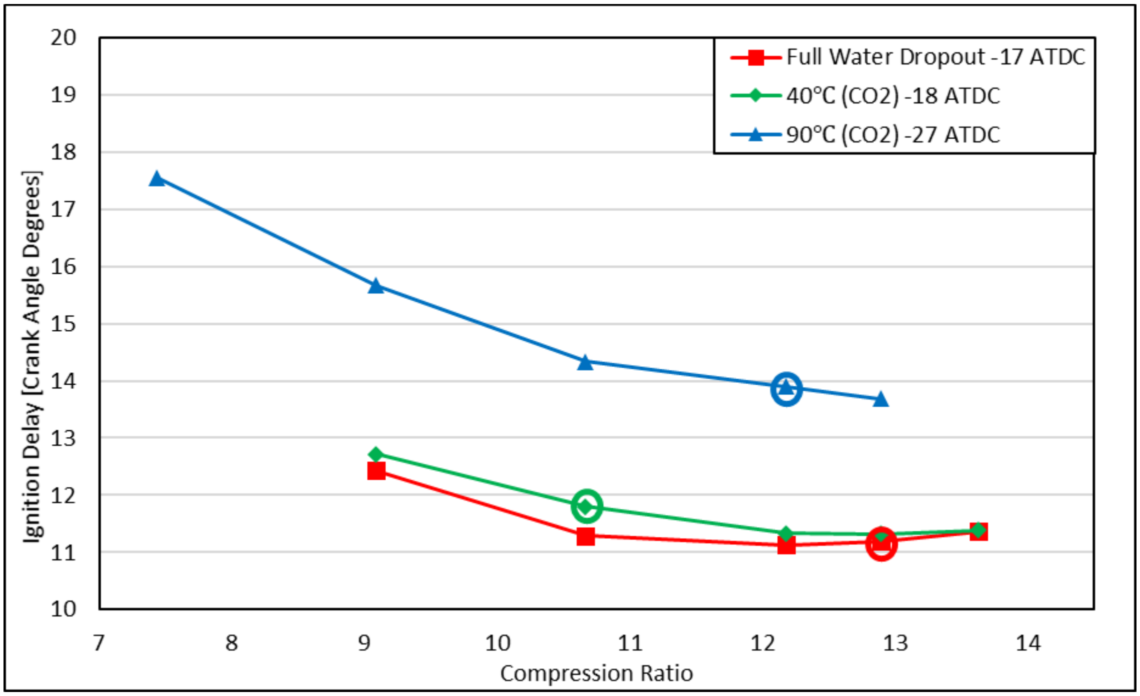

Figure 27: Ignition delay vs. CR at maximum brake torque timing for all test blends, except the No Water Dropout (CO_2) blend, with the most efficient test points for each blend circled. Refer to Table 5 for specific testing parameters and No Water Dropout (CO_2) blend parameters. The legend lists the ignition timing for each test point.

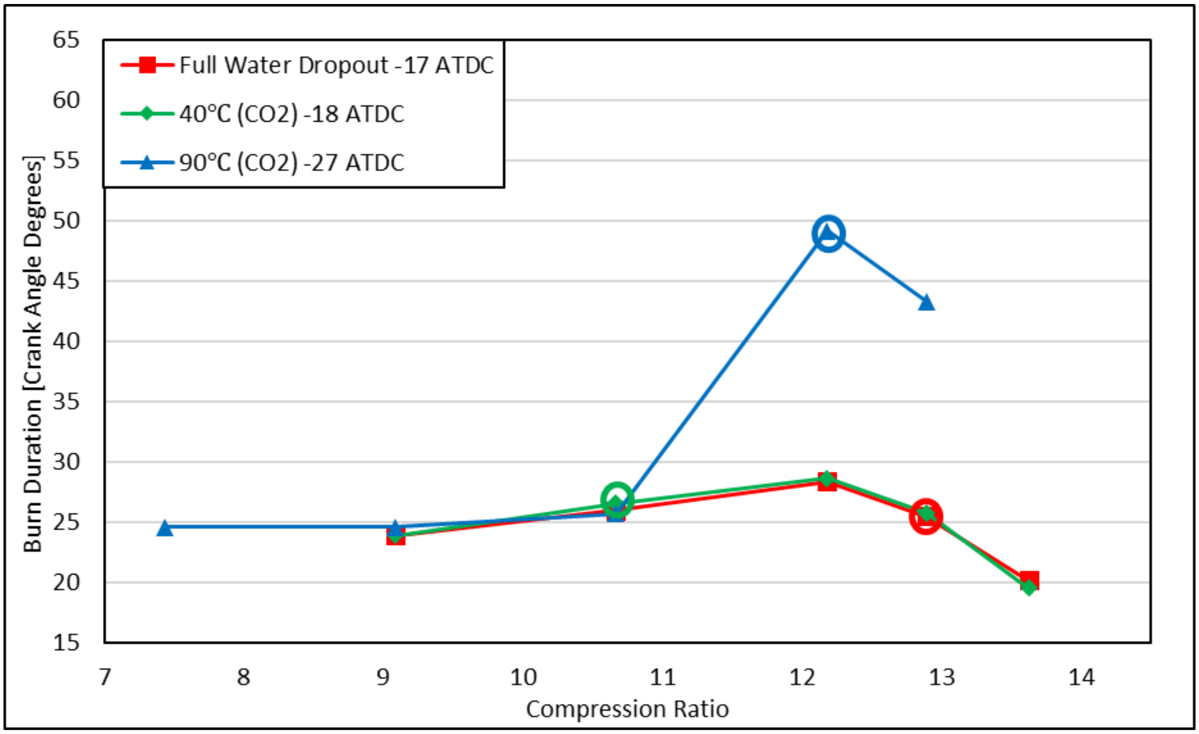

Figure 28: Burn duration vs. CR at maximum brake torque timing for all test blends, except the No Water Dropout (CO_2) blend, with the most efficient test points for each blend circled. Refer to Table 5 for specific testing parameters and No Water Dropout (CO_2) blend parameters. The legend lists the ignition timing for each test point.

Figure 29 shows the IMEP COV vs. CR at maximum brake torque timing for the Full Water Dropout, 40°C (CO_2), and 90°C (CO_2) test blends. IMEP COV remains almost constant as CR is increased. This data shows that steady combustion is possible for each test blend when operated at, or close to, maximum brake torque timing.

Figure 30 shows the peak pressure COV vs. CR at maximum brake torque timing for the Full Water Dropout, 40°C (CO_2), and 90°C (CO_2) test blends. This data is another indication that steady combustion is possible for each test blend as all test points, except for those where engine knock is occurring, show a peak pressure COV below 5%.

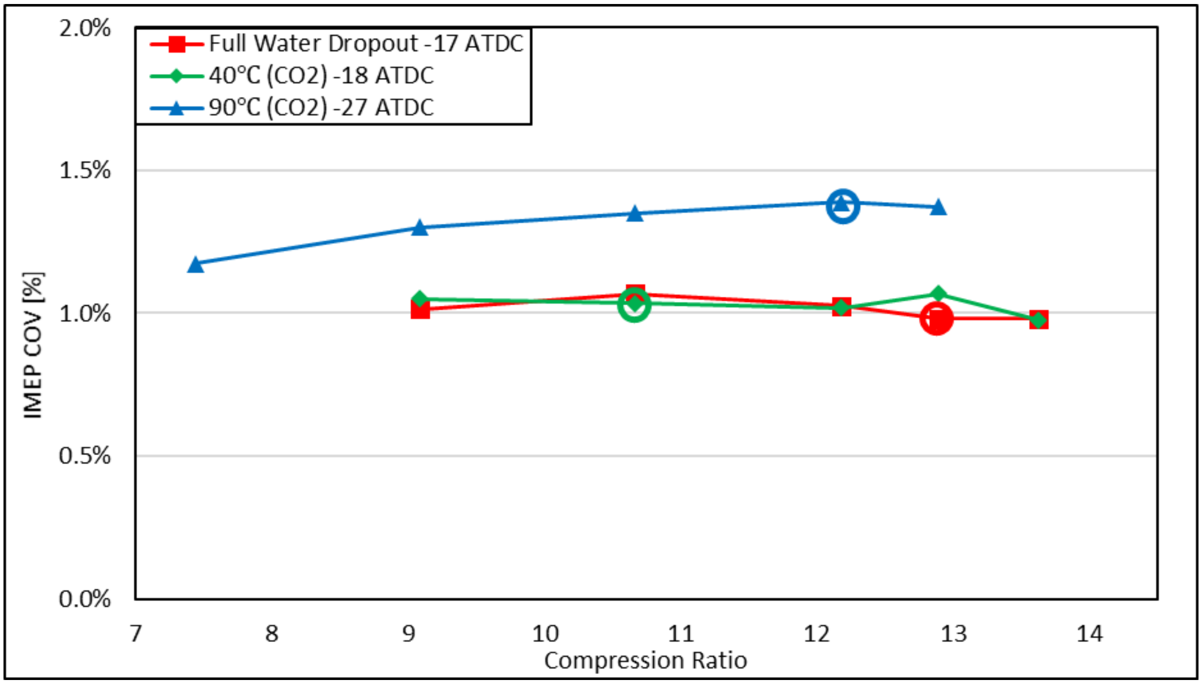

Figure 29: IMEP COV vs. CR at maximum brake torque timing for all test blends, except the No Water Dropout (CO_2) blend, with the most efficient test points for each blend circled in black. Refer to Table 5 for specific testing parameters and No Water Dropout (CO_2) blend parameters. The legend lists the ignition timing for each test point.

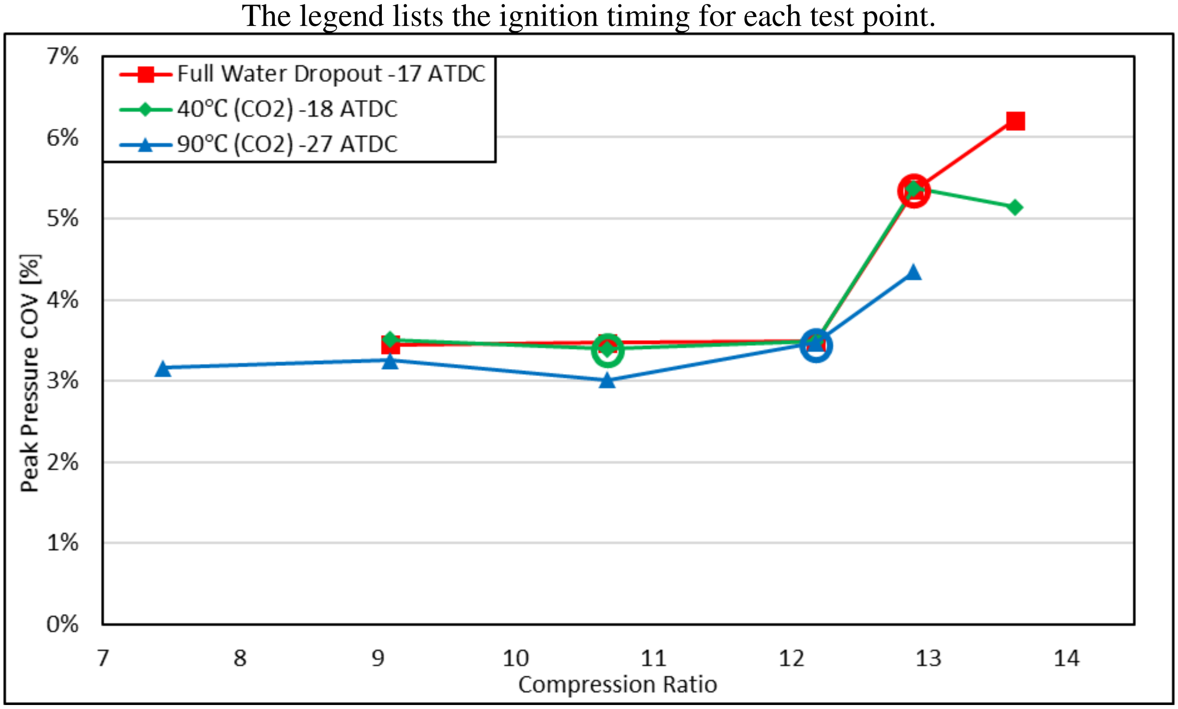

Figure 30: Peak Pressure COV vs. CR at maximum brake torque timing for all test blends, except the No Water Dropout (CO_2) blend, with the most efficient test points for each blend circled in black. Refer to Table 5 for specific testing parameters and No Water Dropout (CO_2) blend parameters. The legend lists the ignition timing for each test point.

3.3. Constant IMEP CO_2 Blend Emissions Data

Emissions data was collected for the Full Water Dropout, 40°C (CO_2) and 90°C (CO_2) test blends during constant IMEP testing. This exhaust flow is sampled before any emission reduction. NG and Methane fuel data points were collected at several operating conditions to provide comparison points for the CFR engine running on gaseous fuels.

Figure 31 shows the brake specific total hydrocarbons (BSTHC) vs. CR for the Full Water Dropout, 40°C (CO_2), and 90°C (CO_2) test blends. NG and Methane fuel data are added for comparison. Figure 31 shows that the number of total hydrocarbons (THC) found in the exhaust gas of the simulated tail-gas blends is much less than what is seen in NG and Methane fuel data. One reason for this is that the simulated tail-gas blends have very low levels of hydrocarbons to begin with. The highest mole fraction of methane (CH_4) is only 0.78% in the Full Water Dropout test blend.

Figure 32 shows the brake specific carbon monoxide (BSCO) vs. CR for the Full Water Dropout, 40°C (CO_2), and 90°C (CO_2) test blends. NG and Methane fuel data are added for comparison. Each fuel shows that BSCO tends to increase as CR is increased. The simulated tail-gas blends show similar or higher levels of CO in their exhaust when compared to methane and NG, most likely due to relatively high mole fractions of CO being present in the simulated tail-gas. The mole fraction of CO in the simulated tail-gas blends ranges from 7.3% to 9.6%.

Figure 33 shows the brake specific NO_x ($BSNO_x$) vs. CR for the Full Water Dropout, 40°C (CO_2), and 90°C (CO_2) test blends. NG and Methane fuel data are added for comparison. Each simulated tail-gas blend shows a much lower level of NO_x when compared to NG and methane fuel. The possible cause of these lower levels of NO_x is decreased combustion temperatures in the highly dilute tail-gas blends.

Overall, the emissions data collected for the simulated tail-gas blends show that emission control system requirements should be lower for engines operating on dilute anode tail-gas than they are for other gaseous fuels.

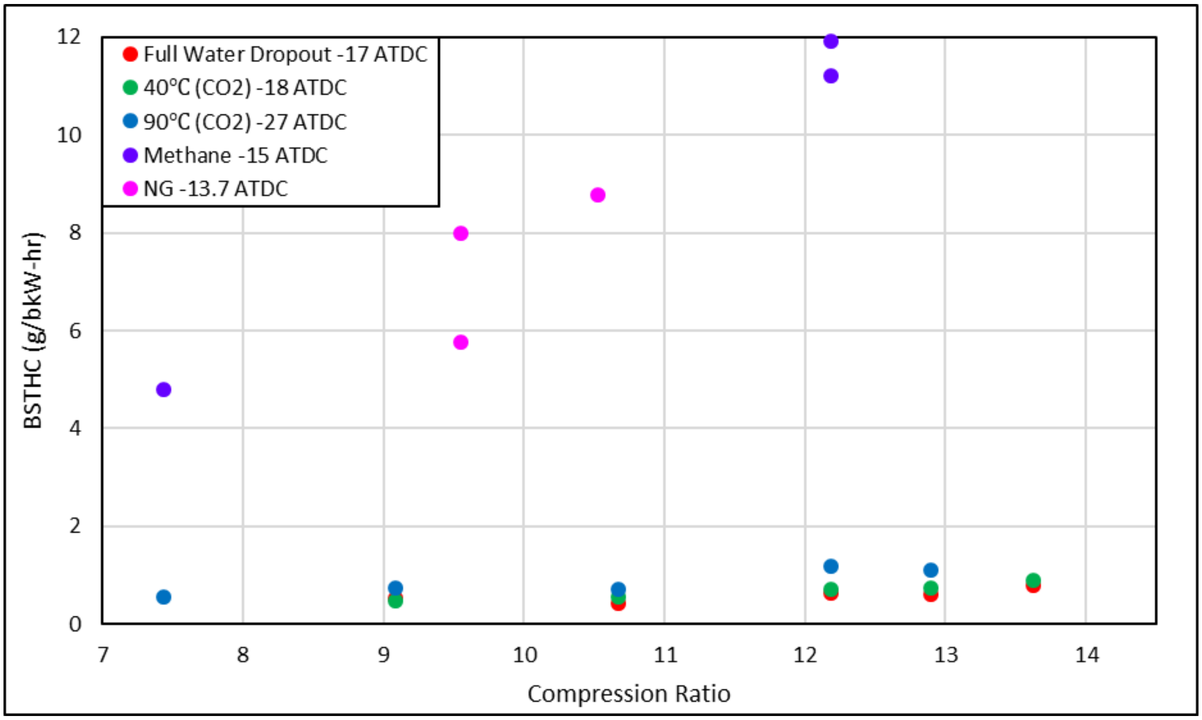

Figure 31: BSTHC vs. CR at maximum brake torque timing for Full Water Dropout, 40°C (CO_2), and 90°C (CO_2) test blends with NG and Methane data for comparison. The legend lists the ignition timing for each test point.

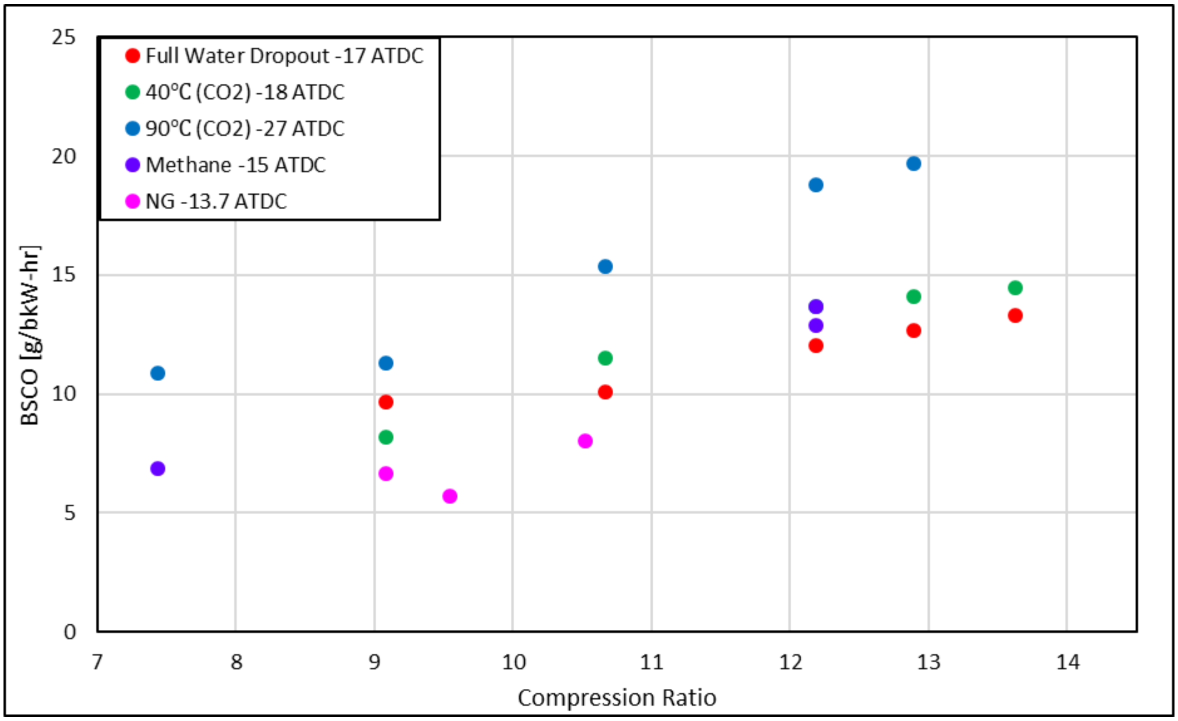

Figure 32: BSCO vs. CR at maximum brake torque timing for Full Water Dropout, 40°C (CO_2), and 90°C (CO_2) test blends with NG and Methane data for comparison. The legend lists the ignition timing for each test point.

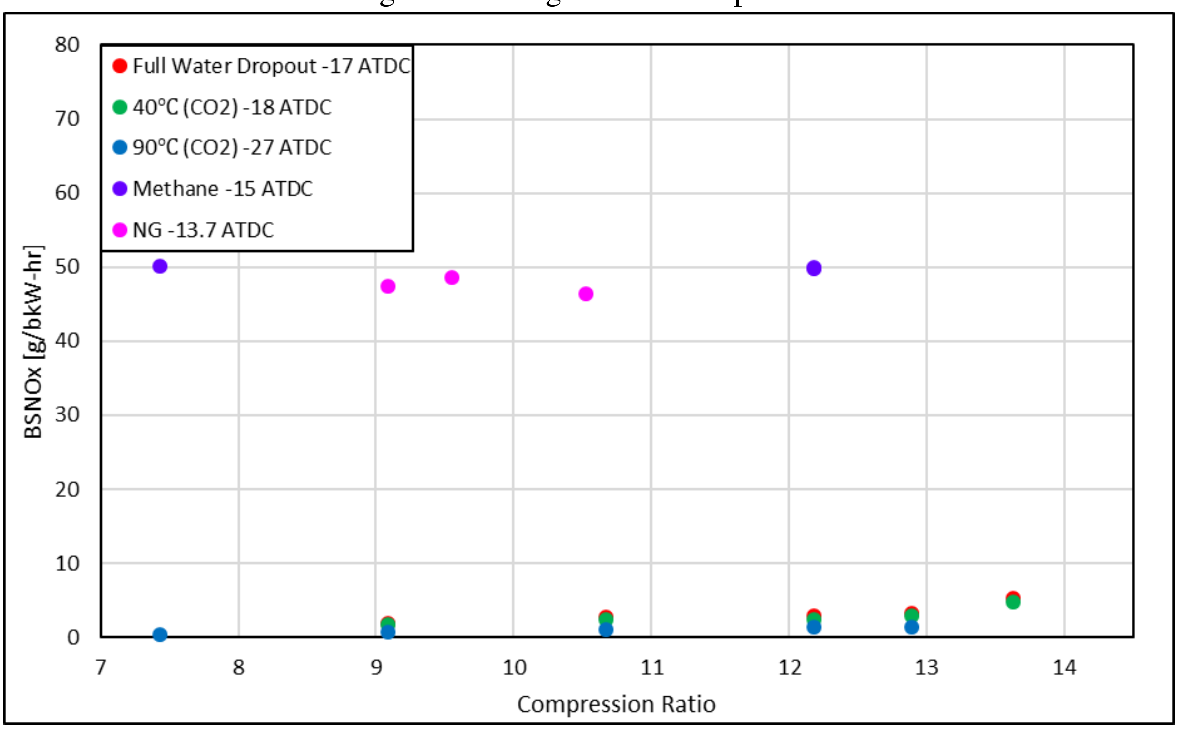

Figure 33: $BSNO_x$ vs. CR at maximum brake torque timing for Full Water Dropout, 40°C (CO_2), and 90°C (CO_2) test blends with NG and Methane data for comparison. The legend lists the ignition timing for each test point.

CHAPTER 4: STEAM INJECTION BLEND TESTING

4.1. Steam Injection Blend Initial Combustion Testing

Steam injection blend initial combustion testing was performed following the procedure used for initial feasibility testing described in Chapter 2. The 40°C (Steam) and 90°C (Steam) blends both produced engine power at initial conditions with a CR of 7.4:1 and ignition timing set to 15° BTDC. Testing for the No Water Dropout (Steam) blend was limited to only a single CR and a timing sweep from 25° to 35° BTDC to protect the engine test stand from operating for long periods with large amounts of water contamination in the lube oil system. The No Water Dropout (Steam) blend produced power beginning at a CR of 10.7:1 with ignition timing at 25° BTDC. Table 6 shows the initial combustion conditions for each steam injection blend with Full Water Dropout blend data added for comparison. This data indicates that the No Water Dropout (Steam) test blend produced power more readily than the No Water Dropout (CO_2) test blend, most likely due to the IMT for this blend was set to 90°C to prevent condensation in the engine intake.

Figure 34 shows the average cylinder pressure vs. crank angle during a timing sweep for the 40°C (Steam) blend at a CR of 10.7:1 and shows the broadest timing sweep performed for any data set. As mentioned in Chapter 3, as timing is advanced, the peak pressure increases, the curve becomes sharper, and the location of peak pressure advances towards TDC.

Figure 35 shows the cylinder pressure vs. crank angle for the 40°C (Steam) test blend at a CR of 10.7:1 and ignition timing at 15° BTDC. IMT and RPM were decreased independently to show their effect (test parameters are listed in Table 7). However, IMT had minimal effect on cylinder pressure and reducing the RPM elevated in-cylinder and peak pressure. One possible cause for this is that the slower engine speed allowed more time for the dilute test blend to combust.

Figure 36 shows the average cylinder pressure vs. crank angle during a timing sweep for the 90°C (Steam) test blend performed at a CR of 12.9:1. Advancing timing for the 90°C (Steam) blend had similar effects to other test blends, but the location of peak pressure was retarded away from TDC between 17° and 23° BTDC.

In Figure 37, the average cylinder pressure vs. crank angle is shown during a timing sweep for the No Water Dropout (Steam) test blend performed at a CR of 10.7:1. This test blend showed a similar trend to the 90°C (Steam) test blend and had the location of peak pressure move away from TDC as the timing was advanced. Peak cylinder pressure at the highest efficiency test point, 35° BTDC, was much lower than what was seen in Figure 10 for the CO_2 replacement version of this test blend. Possible causes for this are a much lower fuel flow rate (266 g/min for the steam injection blend compared to 419 g/min for the CO_2 replacement blend), lower CR for the steam injection blend (10.7:1 vs. 14.4:1), and the less advanced timing used for the steam injection blend (35° BTDC vs. 40° BTDC). Higher cylinder peak pressure and brake efficiency could have been reached through advancing ignition timing but testing at these levels was not performed due to safety concerns.

Table 6: Initial combustion conditions for each test blend with the Full Water Dropout blend for comparison.

Parameter	Full Water Dropout	40°C (Steam)	90°C (Steam)	No Water Dropout (Steam)
CR	10.7:1	7.4:1	7.4:1	10.7:1
Ignition Timing [° ATDC]	-15	-15	-15	-25
Speed [RPM]	936	935	934	934
Inlet Temperature [°C]	45	45	80	90
Boost Pressure [kPa]	128	130	159	197
Total Fuel Flow [g/min]	147	170	199	266
Brake Efficiency [%]	13.90	14.4	12.8	12.1
Average Peak Pressure [kPa]	4018.7	3602.2	2587.2	4978.3
Peak Pressure COV [%]	4.27	3.00	4.86	3.1
Average IMEP [kPa]	669.5	732.6	694.6	670.6
IMEP COV [%]	1.11	1.01	2.89	13.1
Misfire Fraction [%]	0	0	0	0.6

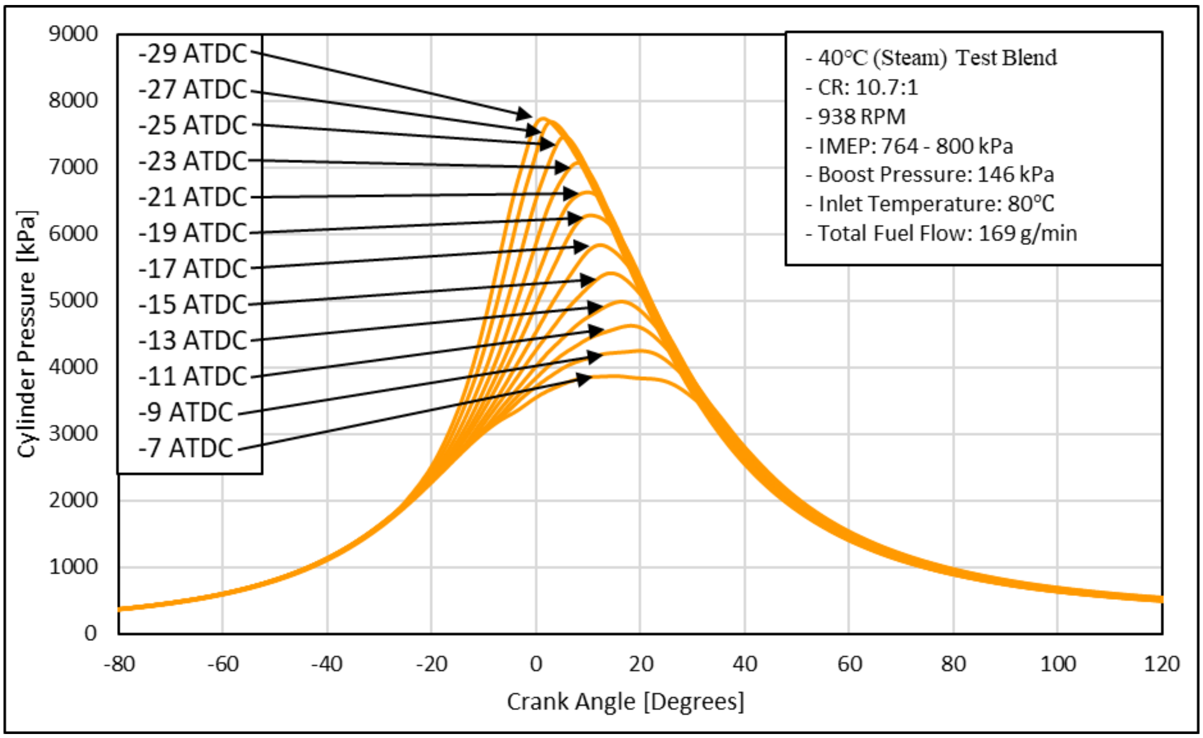

Figure 34: Cylinder pressure vs. crank angle for 40°C (Steam) test blend with a sweep of ignition timing at CR 10.7:1. The legend lists the ignition timing for each test point.

Table 7: Parameters of 40°C (Steam) test blend for changes in IMT and RPM.

Parameter	80°C IMT, 818 RPM	45°C IMT, 938 RPM	80°C IMT, 938 RPM
CR	10.7	10.7	10.7
Ignition Timing [° ATDC]	-15	-15	-15
Inlet Temperature [°C]	80	45	80
Boost Pressure [kPa]	164	137	146
Total Fuel Flow [g/min]	170	167	170
Brake Efficiency [%]	17.79	16.89	16.49
Average Peak Pressure [kPa]	6336.8	5368.0	5430.0
Peak Pressure COV [%]	3.25	3.57	3.37
Average IMEP [kPa]	922.8	814.4	800.0
IMEP COV [%]	1.09	1.10	1.18
Misfire Fraction [%]	0	0	0

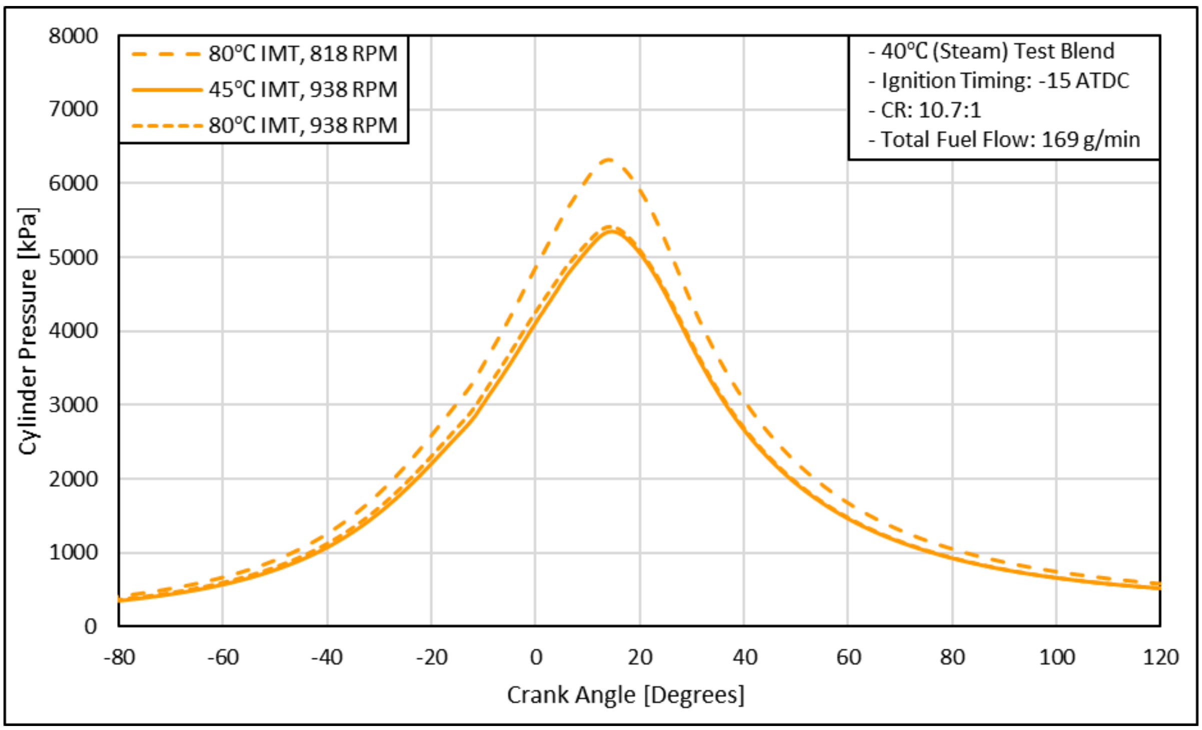

Figure 35: Cylinder pressure vs. crank angle for 40°C (Steam) test blend showing the effect of decreasing IMT and RPM independently at CR 10.7:1. Refer to Table 7 for specific testing parameters.

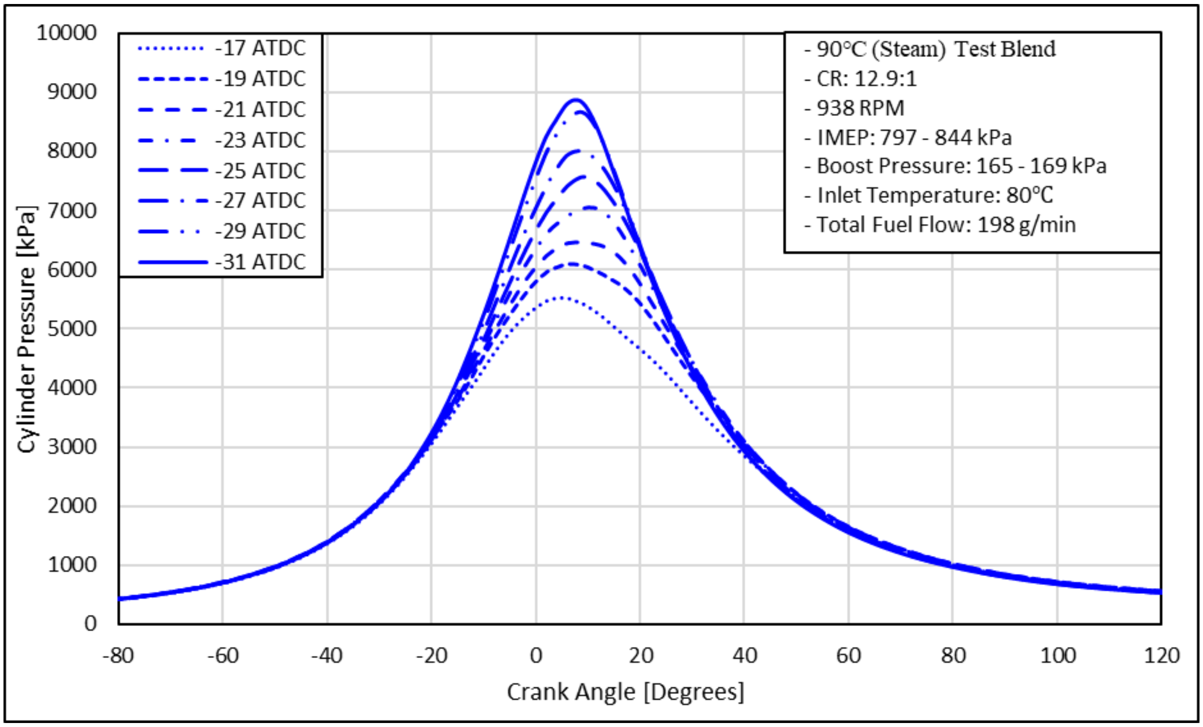

Figure 36: Cylinder pressure vs. crank angle for 90°C (Steam) test blend with a sweep of ignition timing at CR 12.9:1. The legend lists the ignition timing for each test point.

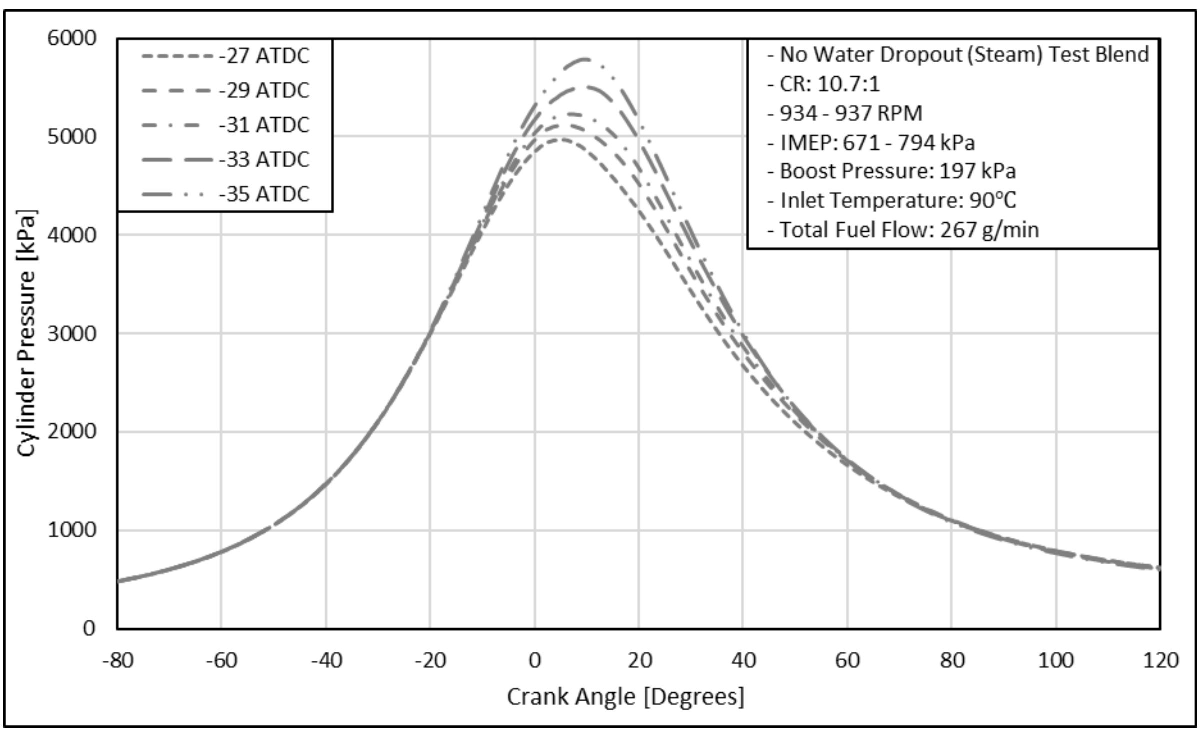

Figure 37: Cylinder pressure vs. crank angle for No Water Dropout (Steam) test blend with a sweep of ignition timing at CR 10.7:1. The legend lists the ignition timing for each test point.

Figure 38 shows the average cylinder pressure vs. crank angle for the most efficient test points for each fuel tested during steam injection blend initial combustion testing with NG for comparison. Refer to Table 8 for specific parameters for each data point. The more dilute blends required advanced timing to maintain brake efficiency. This resulted in a higher peak pressure seen for the 90°C (Steam) test blend. The most efficient data point for the No Water Dropout (Steam) test blend showed lower peak pressure than the other blends. One possible cause for this is that testing was not performed at the extreme conditions that may have been required to find the most efficient operating point. Further testing could show that the No Water Dropout (Steam) blend has the potential to operate at higher efficiencies than the other test blends but the extreme operating conditions required to reach those efficiencies, as well as the issues encountered when using a blend with such high water content, make the use of this blend undesirable.

Table 8: Parameters of most efficient data points gathered for steam injection initial combustion testing with Full Water Dropout test blend and NG for comparison.

Parameter	Full Water Dropout	40°C (Steam)	90°C (Steam)	No Water Dropout (Steam)	NG
CR	12.9:1	12.1:1	12.9:1	10.7:1	10.5:1
Ignition Timing [° ATDC]	-17	-17	-21	-35	-13
Speed [RPM]	936	939	938	937	900
Inlet Temperature [°C]	45	80	80	90	61
Boost Pressure [kPa]	130	147	169	197	104
Total Fuel Flow [g/min]	148	169	198	267	14.8
Energy Flow (LHV$\cdot\dot{m}_{fuel}$) [kW]	11.3	13.0	12.9	12.8	11.55
Electric Power [kW]	1.37	1.93	2.07	1.88	1.92
Maximum Brake Efficiency [%]	13.54	16.7	18.0	16.4	18.58
Average Peak Pressure [kPa]	4201.1	6636.1	7064.0	6188.7	5374.8
Peak Pressure COV [%]	4.59	5.03	4.12	9.25	4.92
Average IMEP [kPa]	658.7	805.9	842.4	793.7	823.9
IMEP COV [%]	4.93	1.15	3.76	3.92	0.93

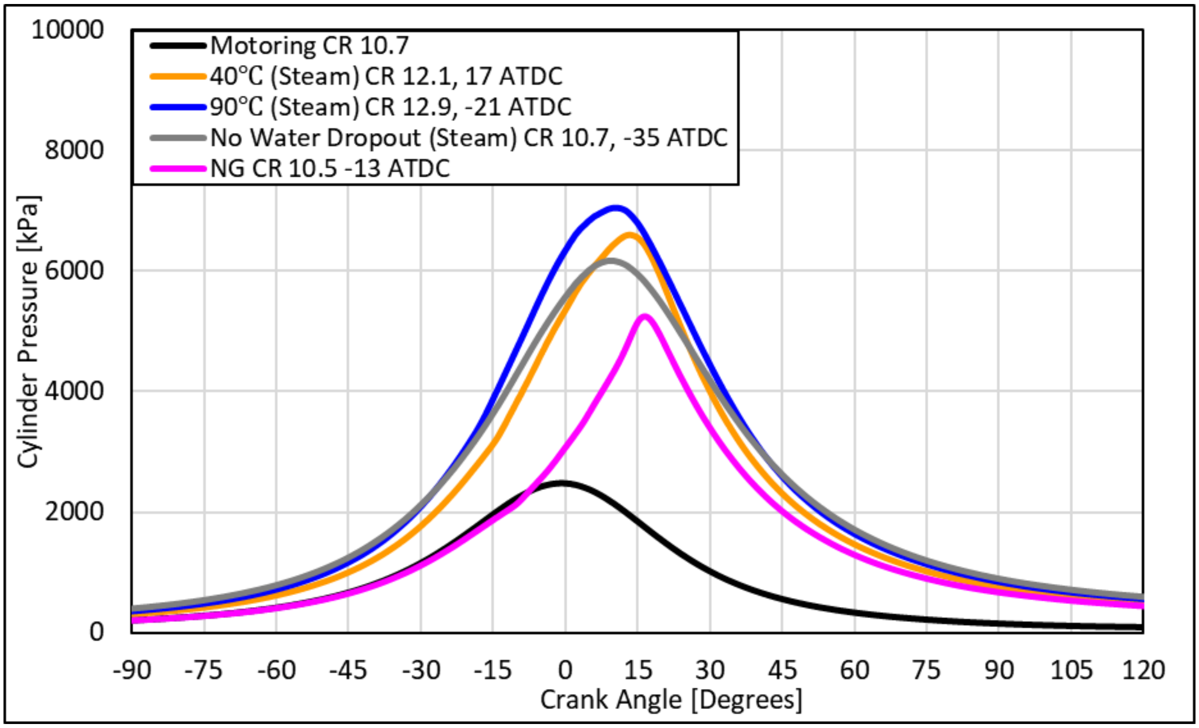

Figure 38: Cylinder pressure vs. crank angle for each test blend's most efficient data point from steam injection initial combustion testing. NG and motoring data included for comparison. Refer to Table 8 for specific testing parameters. The legend lists ignition timing and CR conditions.

Figure 39 shows the AHRR vs. crank angle for the 40°C (Steam) blend over a timing sweep with a CR of 12.1:1 and indicates that advancing timing advances the location of peak AHRR and increases the peak AHRR. This increased peak AHRR with constant fuel flow is an indication of a significant reduction in the 10-90% burn duration.

Figure 40 shows the AHRR vs. crank angle for the 40°C (Steam) test blend at a CR of 10.7:1 and ignition timing at 15° BTDC. IMT and RPM were decreased independently to show their effect. IMT has an insignificant impact on the AHRR but the decrease in RPM shows a substantial increase in peak AHRR. As mentioned, regarding Figure 35, one potential reason for this is that the slower engine speed provides the dilute fuel blend more time to achieve more complete combustion near TDC.

Figure 41 shows the AHRR vs. crank angle for the No Water Dropout (Steam) during a sweep of ignition timing from 29° BTDC to 35° BTDC at a CR of 10.7:1. As timing is advanced, the peak AHRR increases and advances towards TDC. Figure 41 also shows that as timing is advanced, the combustion is heading towards completion faster as the negative slope after peak AHRR becomes more negative.

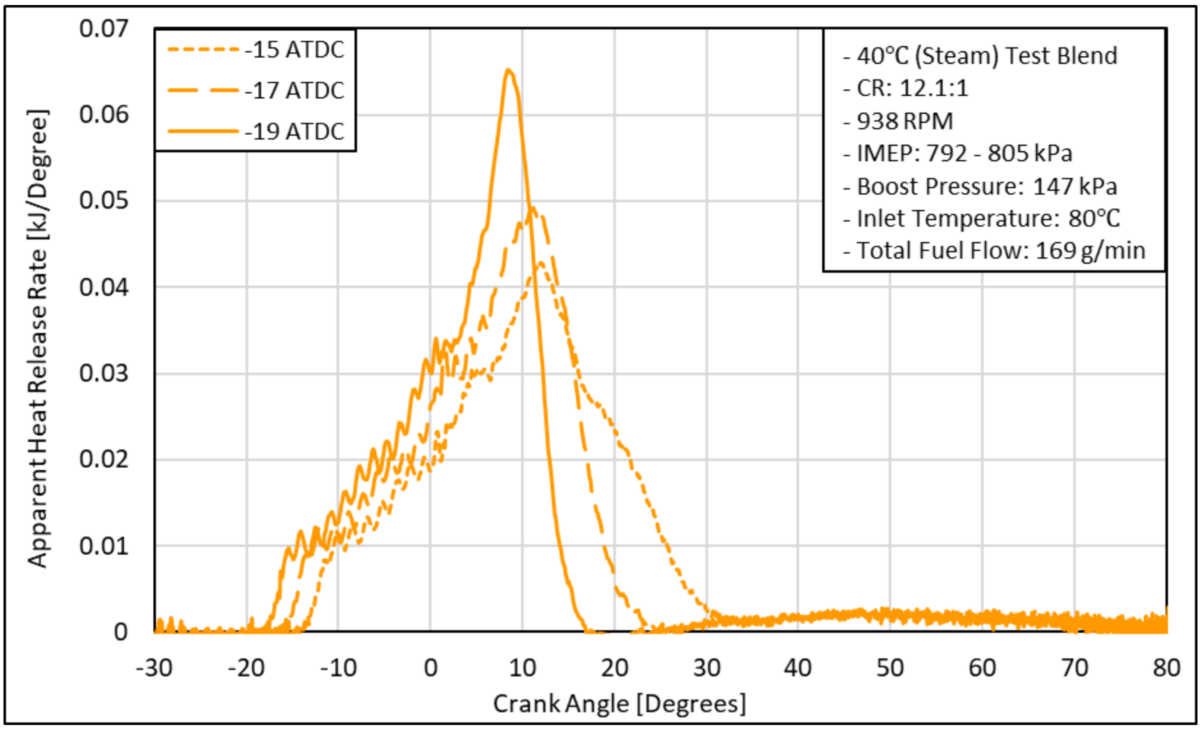

Figure 39: AHRR vs. crank angle for 40°C (Steam) test blend with a sweep of ignition timing at CR 12.1:1. The legend lists the ignition timing for each test point.

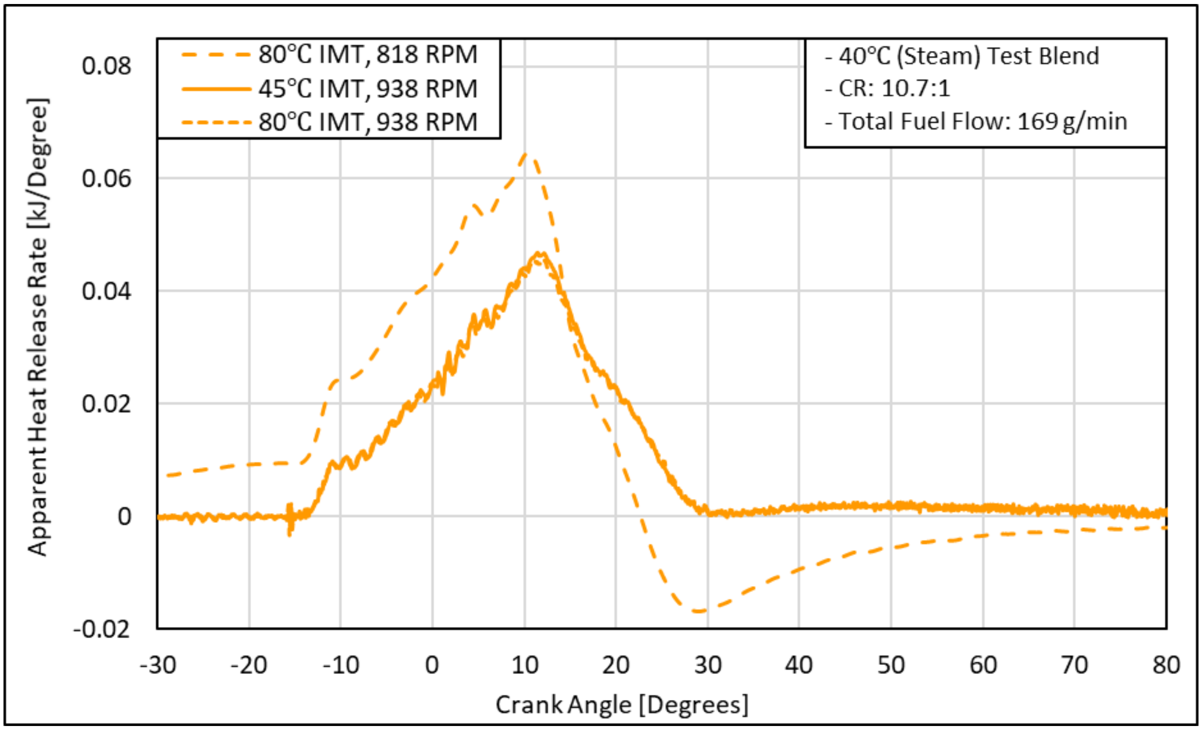

Figure 40: AHRR vs. crank angle for 40°C (Steam) test blend showing the effect of decreasing IMT and RPM independently at CR 10.7:1. Refer to Table 7 for specific testing parameters.

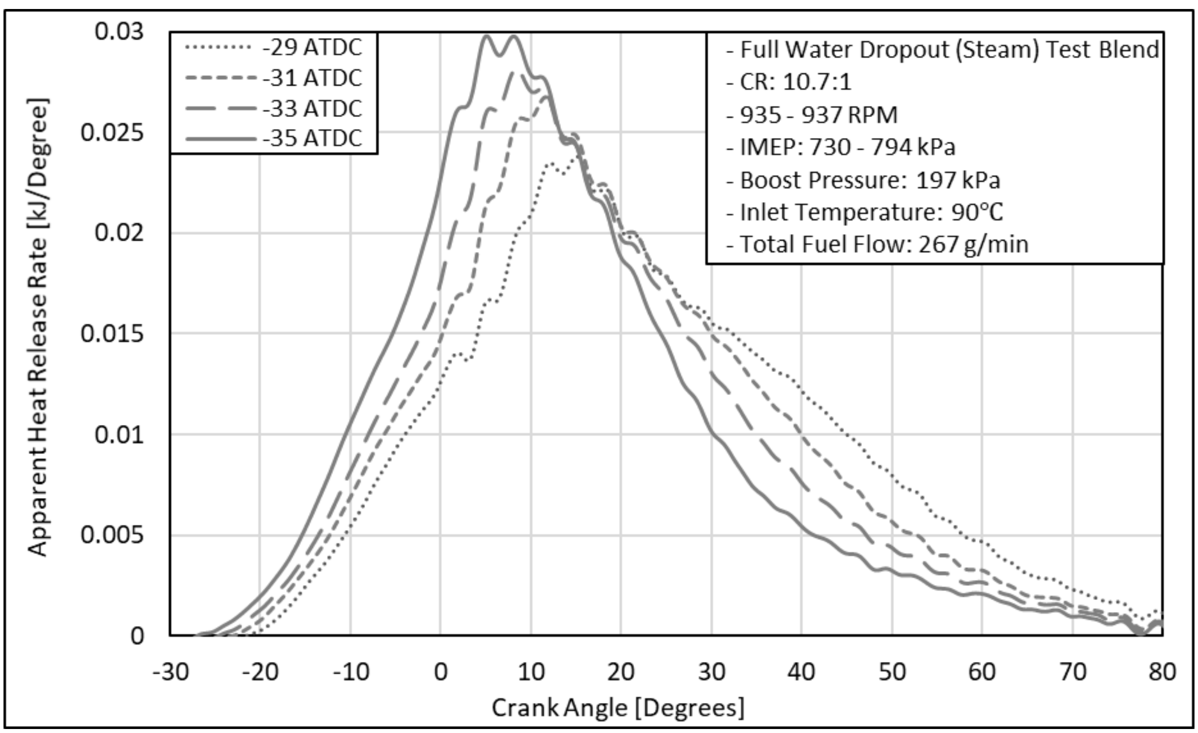

Figure 41: AHRR vs. crank angle for No Water Dropout (Steam) test blend with a sweep of ignition timing at CR 12.9:1. The legend lists the ignition timing for each test point.

Figure 42 shows the AHRR vs. crank angle for the most efficient test points for each fuel tested during steam injection blend initial combustion testing with NG for comparison. Refer to Table 8 for specific parameters for each data point. The No Water Dropout (Steam) blend shows undesirably low peak AHRR and long combustion when compared to the 40°C (Steam) and 90°C (Steam) test blends. The 40°C (Steam) blend is closest to the AHRR of NG, although the peak AHRR is still much lower.

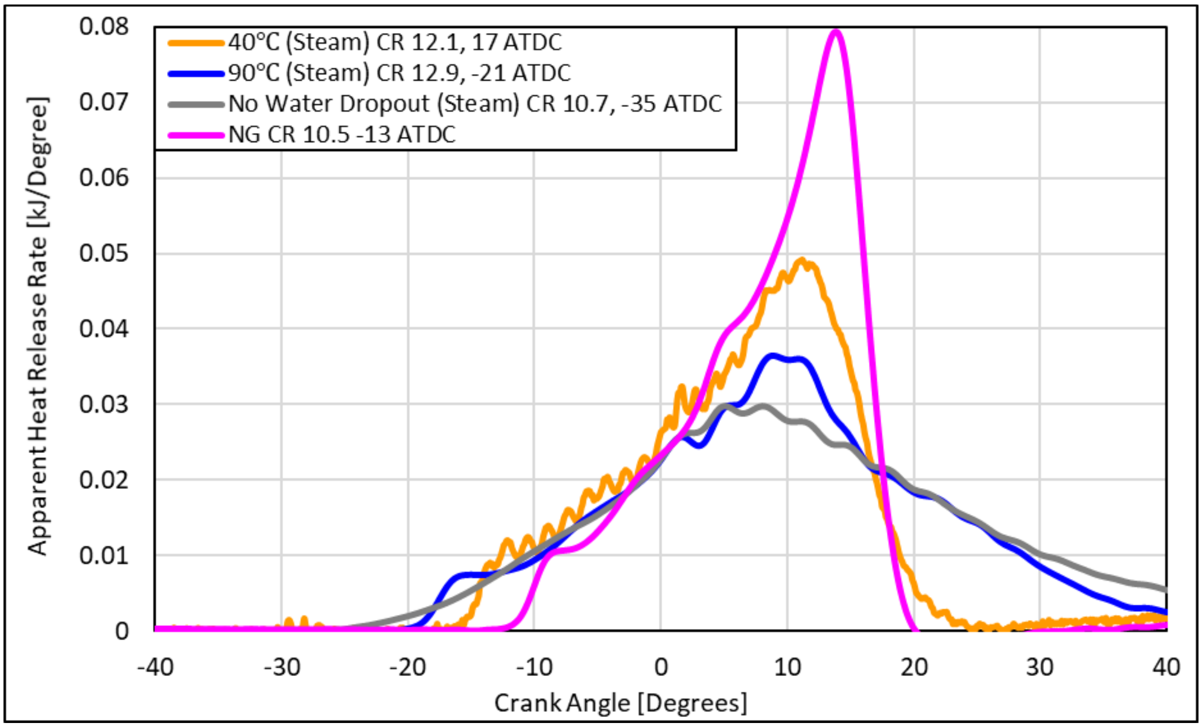

Figure 42: AHRR vs. crank angle for each test blend's most efficient data point from steam injection initial combustion testing. NG and motoring data included for comparison. Refer to Table 8 for specific testing parameters. The legend lists ignition timing and CR conditions.

Figure 43 shows the mass fraction burned vs. crank angle for the 40°C (Steam) blend at a CR of 12.1:1 for an ignition timing sweep from 15° BTDC to 19° BTDC. As ignition timing is advanced, the slope of mass fraction burned increases, and the crank angle that where 90% mass fraction burned is reached advances towards TDC. A similar but less significant trend is shown in Figure 44 for the 90°C (Steam) test blend. The No Water Dropout (Steam) blend experienced the same in Figure 45. Even with advancing timing, the No Water Dropout (Steam) blend still experienced undesirably long ignition delays and burn durations.

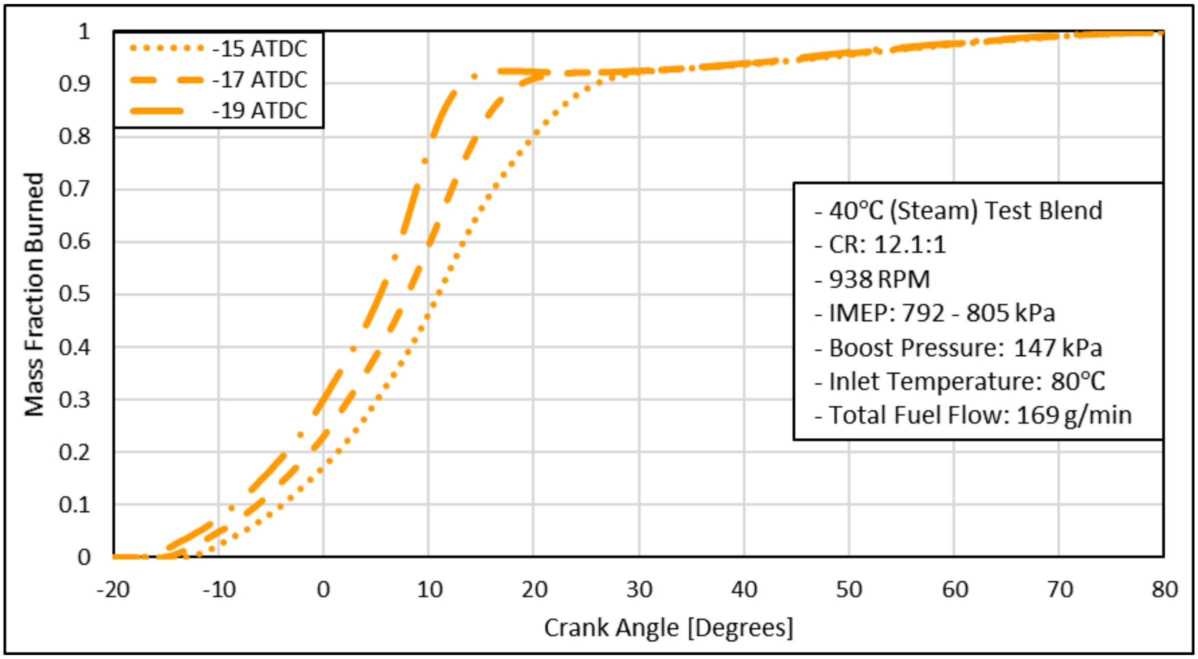

Figure 43: Mass fraction burned vs. crank angle for 40°C (Steam) test blend at CR 12.1:1. The legend lists the ignition timing for each test point.

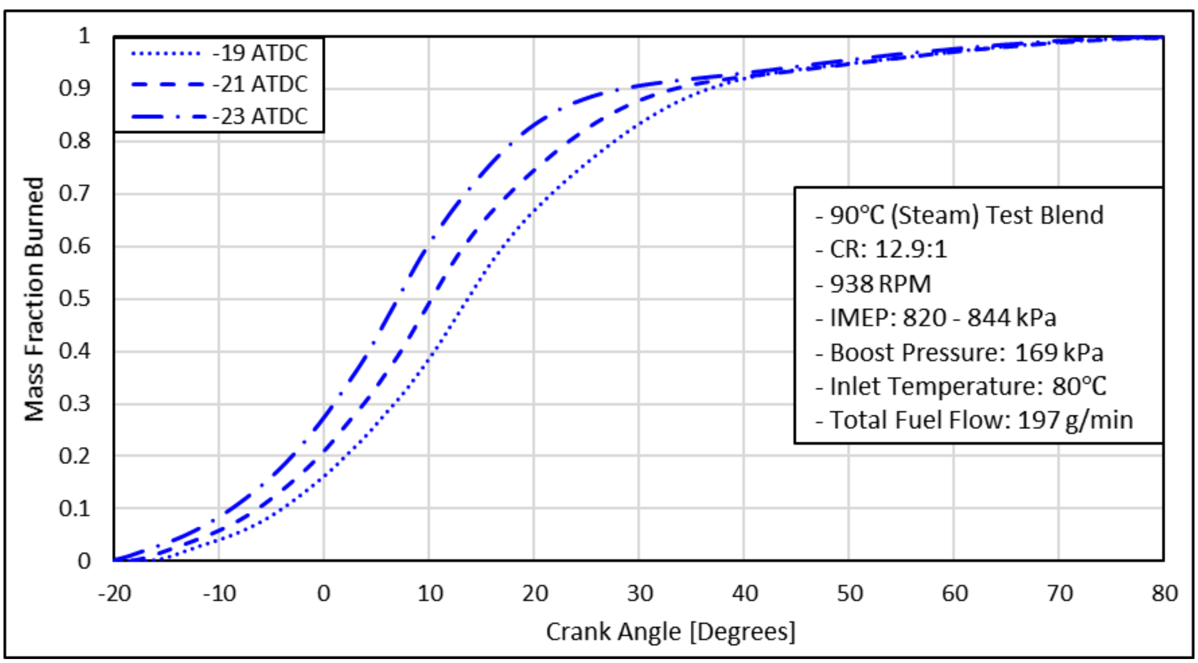

Figure 44: Mass fraction burned vs. crank angle for 90°C (Steam) test blend at CR 12.9:1. The legend lists the ignition timing for each test point.

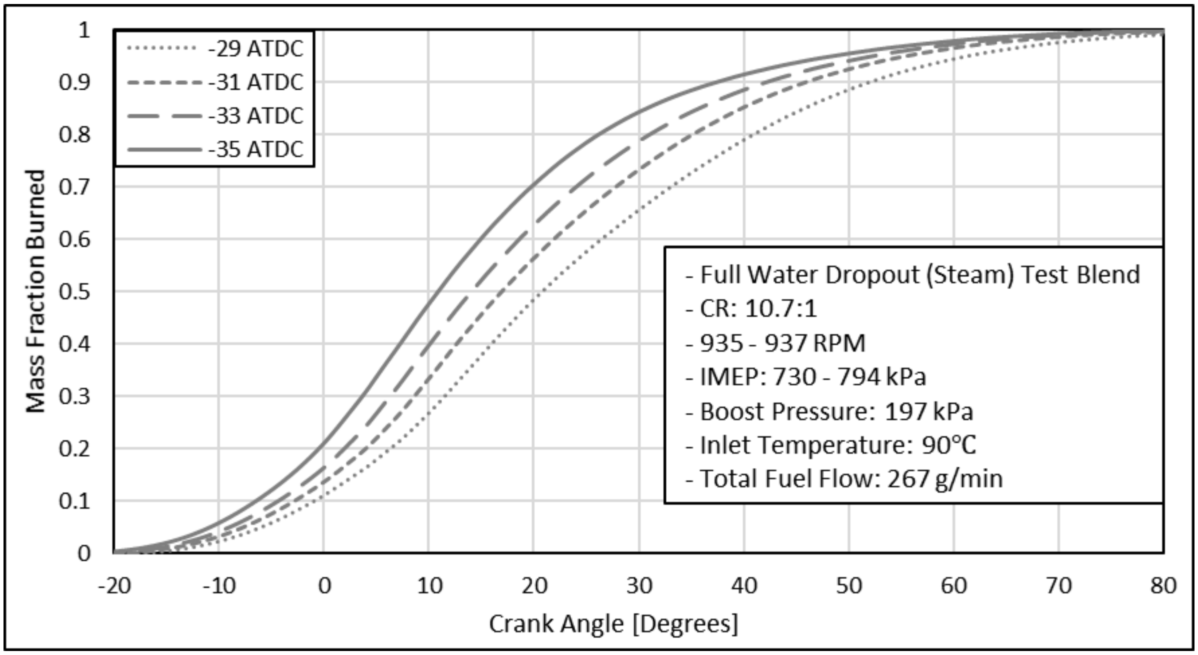

Figure 45: Mass fraction burned vs. crank angle for No Water Dropout (Steam) test blend at CR 10.7:1. The legend lists the ignition timing for each test point.

Figure 46 compares the mass fraction burned vs. crank angle for the most efficient test point for each steam injection fuel blend alongside NG. Although the 90°C (Steam) blend achieved a slightly higher brake efficiency than the 40°C (Steam) blend, the shape of the mass fraction burned graph shows that the combustion characteristics of the 40°C (Steam) blend are more desirable. Further testing is required to determine the ideal fuel blend.

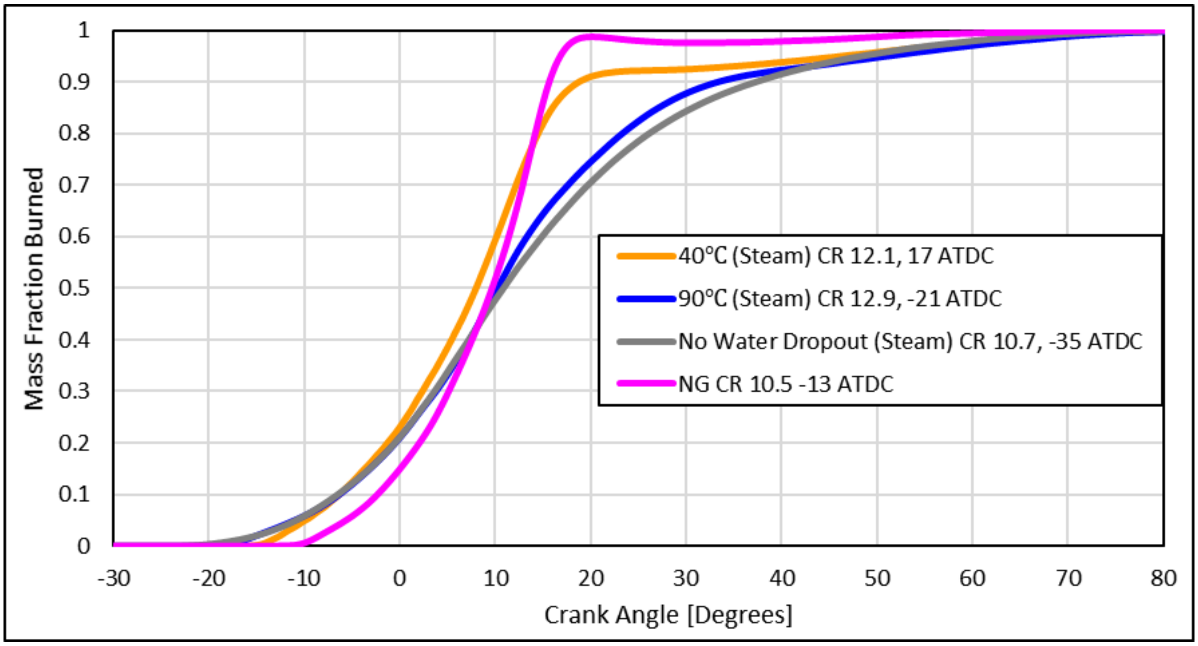

Figure 46: Mass fraction burned vs. crank angle for each test blend's most efficient data point from steam injection initial combustion testing. NG and motoring data included for comparison. Refer to Table 8 for specific testing parameters. The legend lists ignition timing and CR conditions.

Figure 47 shows the brake efficiency vs. ignition timing for several different conditions for the steam injection fuel blends. The brake efficiencies found while operating the 40°C (Steam) blend at lower engine speeds were not used when comparing to other blends so that comparisons could be made at similar operating conditions. Efficiency decreases as timing is advanced or retarded from maximum brake torque timing. We hypothesize that the No Water Dropout (Steam) blend could achieve higher brake efficiency at more advanced timing, but further testing of this blend was limited to protect the CFR test stand from damage caused by excessive water content.

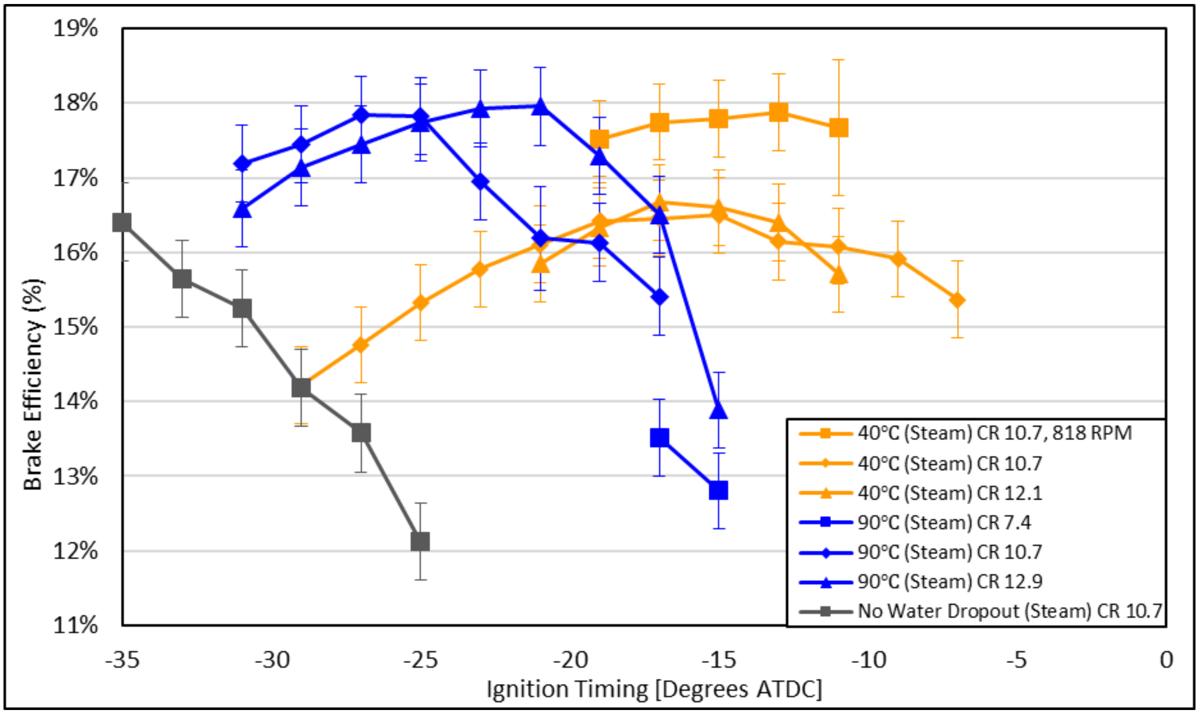

Figure 47: Brake efficiency vs. ignition timing for all test blends during steam injection initial combustion testing. Refer to Table 8 for specific testing parameters.

Figure 48 shows that IMEP COV tends to decrease as timing is advanced for each fuel blend. Low IMEP COV is associated with more stable combustion and indicates that these blends achieve steady combustion at their highest brake efficiencies. The effect of ignition timing on ignition delay is shown to be negligible in Figure 49. The impact of advancing ignition timing is much more significant with regards to burn duration (see Figure 50). Burn duration decreases as timing is advanced except for when it reaches a minimum at 23° BTDC ignition timing for the 90°C (Steam) blend at a CR of 12.9:1.

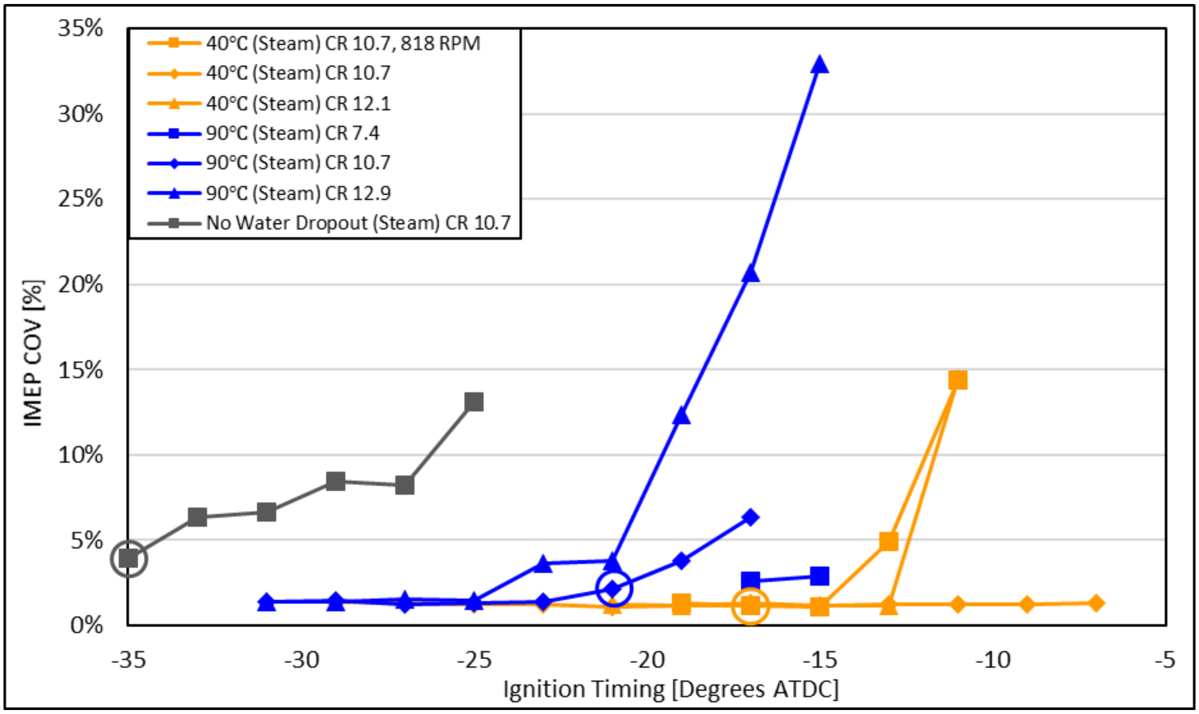

Figure 48: IMEP COV vs. ignition timing for all test blends during steam injection initial combustion testing. Most Efficient test points for each blend are circled. Refer to Table 8 for specific testing parameters.

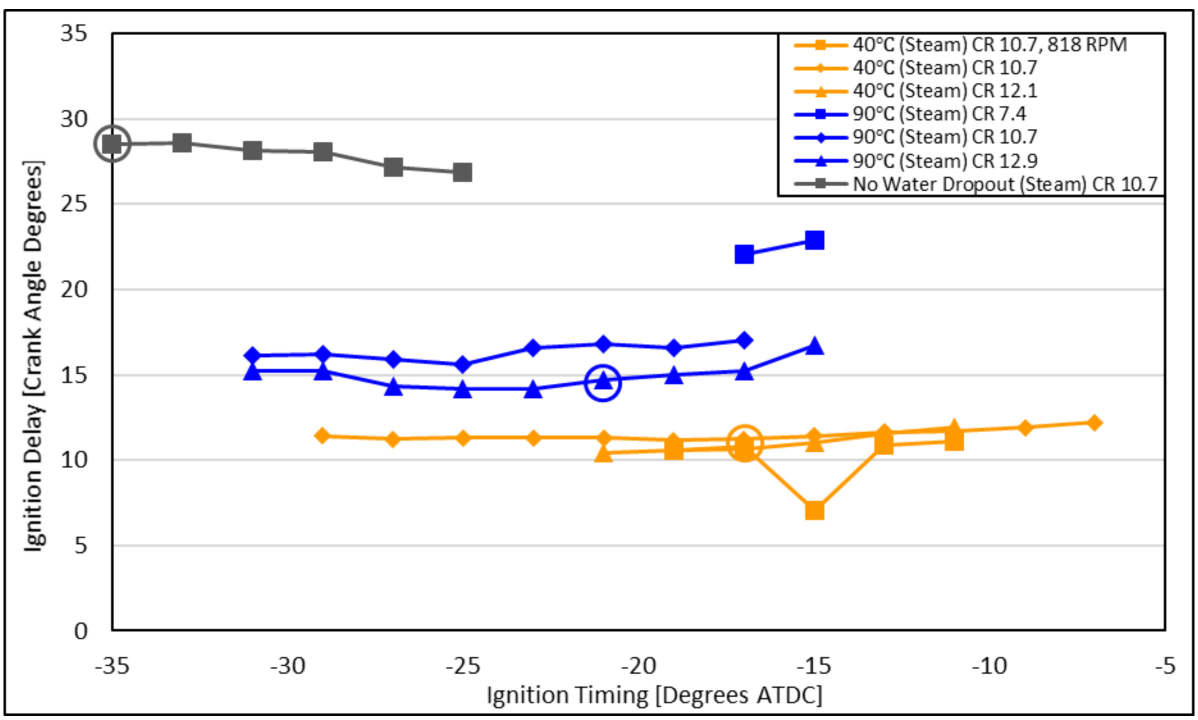

Figure 49: Ignition delay vs. ignition timing for all test blends during steam injection initial combustion testing. Most Efficient test points for each blend are circled. Refer to Table 8 for specific testing parameters.

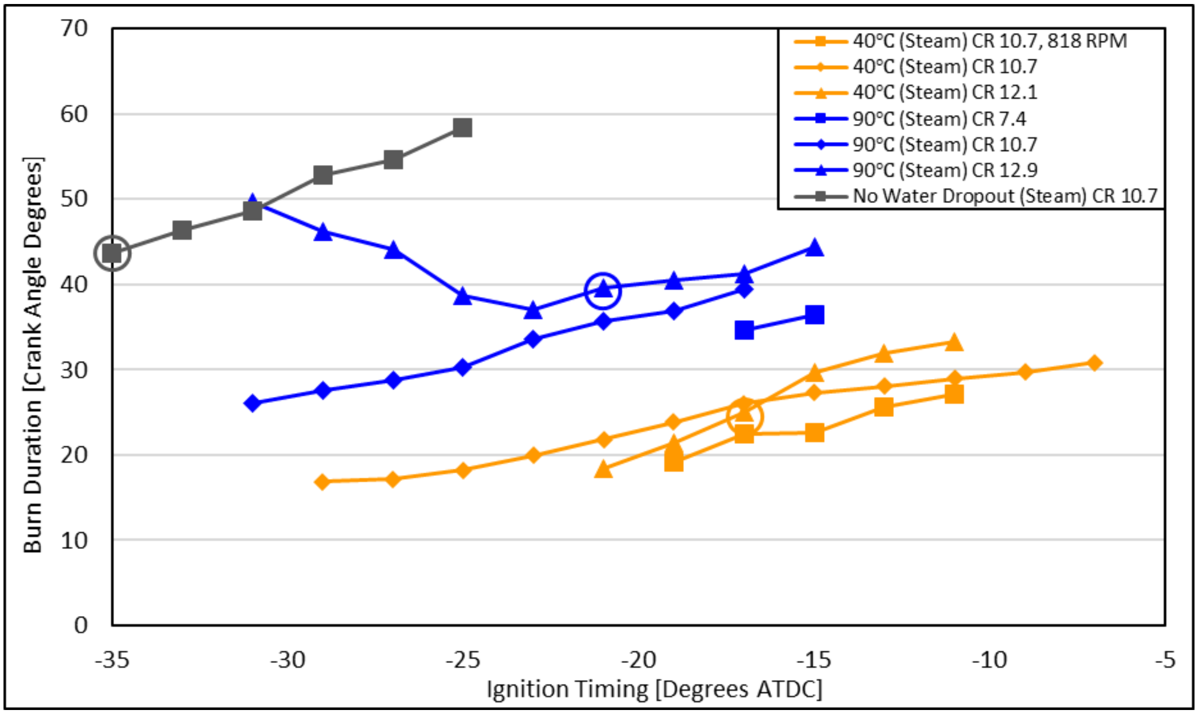

Figure 50: Burn duration vs. ignition timing for all test blends during steam injection initial combustion testing. Most Efficient test points for each blend are circled. Refer to Table 8 for specific testing parameters.

4.2. Constant IMEP Steam Injection Blend Testing

Constant IMEP testing was performed on the 40°C (Steam) and 90°C (Steam) test blends. The No Water Dropout (Steam) test blend was omitted due to its undesirable combustion characteristics and the effect of the large amount of water content on engine operation. This testing was performed to allow for a direct comparison between the two steam injection test blends of interest and to compare the operation of steam injection blends to the test blends that were simulated with direct CO_2 replacement of water content. For this testing, IMEP was maintained at 870 ±15 kPa. Test blends were operated at their maximum brake torque timing found during initial combustion testing, and a sweep of CR was performed.

The sweep of CR for each test blend showed that as CR was increased, the peak cylinder pressure would increase, and the location of peak pressure would tend to advance towards TDC.

The most efficient test point for the 40°C (Steam) test blend, seen in Figure 51, was at a CR of 12.9:1. As CR was increased above 12.9:1, the shape of the peak in the cylinder pressure curve becomes less sharp. One possible cause of this is that, at higher CRs, the clearance volume at TDC could become too small (higher surface-to-volume ratio) to support proper flame propagation for these more dilute test blends; this causes combustion to slow near TDC. Slower combustion is also made evident by increases in ignition delay and burn duration as CR is increased above 12.9:1.

The 90°C (Steam) blend operated at its highest efficiency at a CR of 10.7:1. Above a CR of 10.7:1 the burn duration increases drastically and brake efficiency decreases. Figure 52 displays the cylinder pressure vs. crank angle for the 90°C (Steam) test blend. Indications of engine knock at a CR of 13.6:1 are indicated by a small inflection point prior to a higher than expected rise in peak pressure for the change in CR.

Figure 53 shows the most efficient test points for both test blends during constant IMEP steam injection blend testing. It is interesting to note that the peak pressure curves for the 40°C (Steam) and 90°C (Steam) test blends match so closely at different engine operating conditions.

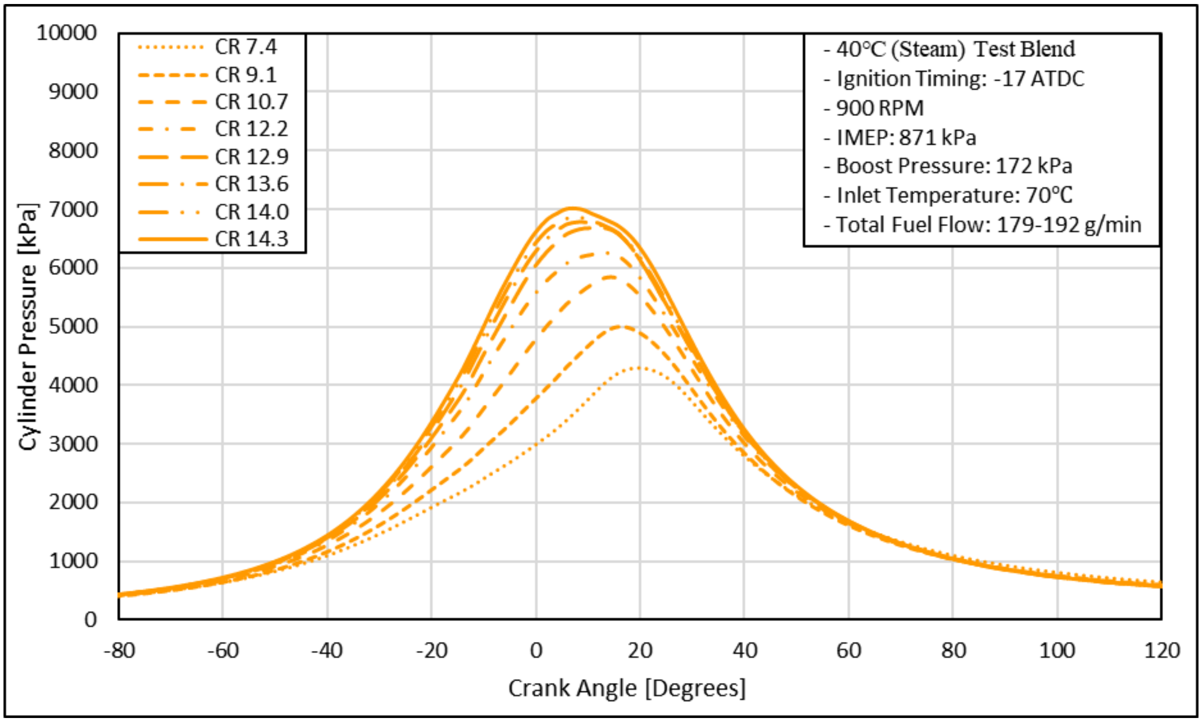

Figure 51: Cylinder pressure vs. crank angle for 40°C (Steam) test blend at maximum break torque timing of -17° ATDC with a sweep of CR from 7.4:1 – 14.3:1.

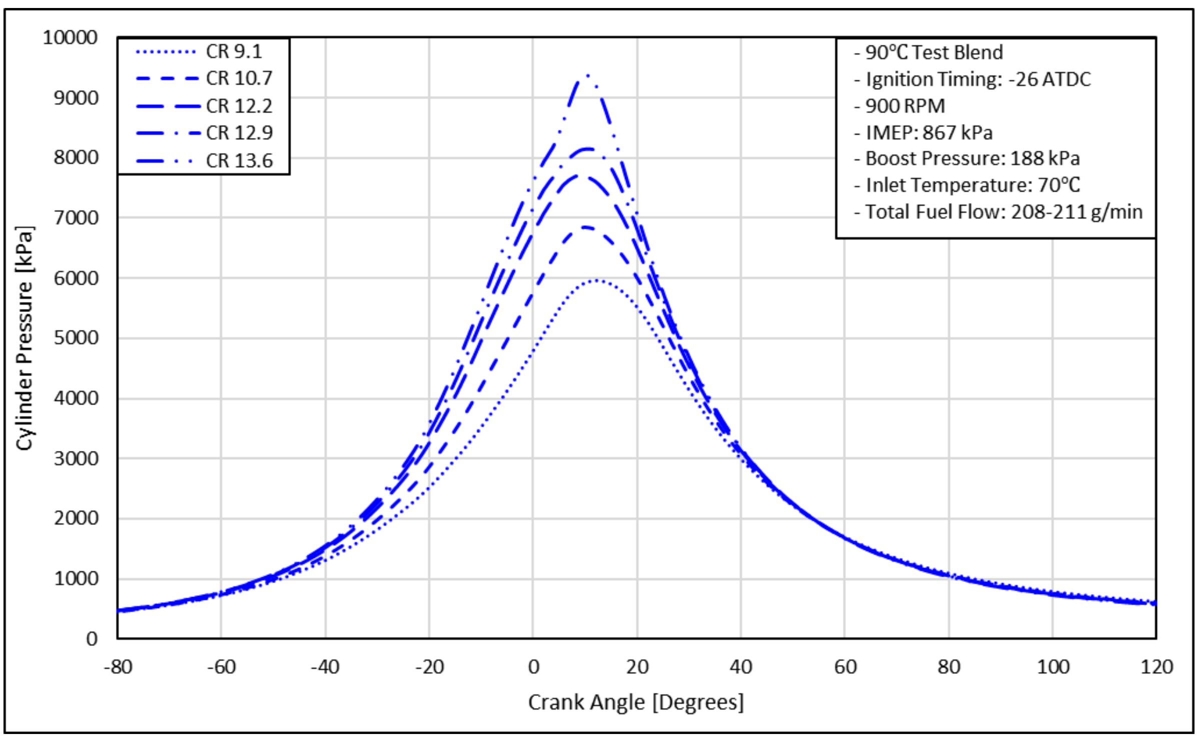

Figure 52: Cylinder pressure vs. crank angle for 90°C (Steam) test blend at maximum break torque timing of -26° ATDC with a sweep of CR from 9.1:1 – 13.6:1.

Table 9: Parameters of most efficient data points gathered for constant IMEP steam injection blend testing with Full Water Dropout, No Water Dropout (Steam) and NG data for comparison. IMEP was maintained at 870 ±15 kPa.

Parameter	Full Water Dropout	40°C (Steam)	90°C (Steam)	No Water Dropout (Steam)	NG
CR	12.9:1	12.9:1	10.7:1	10.7:1	10.5:1
Ignition Timing [° ATDC]	-17	-17	-26	-35	-13
Speed [RPM]	901	901	901	937	900
Inlet Temperature [°C]	70	70	70	90	61
Boost Pressure [kPa]	156	172	186	197	104
Total Fuel Flow [g/min]	175	180	209	267	14.8
Energy Flow (LHV·$\dot{m}_{fuel}$) [kW]	13.46	13.70	13.23	12.8	11.55
Electric Power [kW]	2.06	2.15	2.10	1.88	1.92
Maximum Brake Efficiency [%]	17.09	17.54	17.74	16.4	18.58
Average Peak Pressure [kPa]	7249.0	6721.6	6861.8	6188.7	5374.8
Peak Pressure COV [%]	5.35	3.38	3.99	9.25	4.92
Average IMEP [kPa]	861.8	886.2	873.3	793.7	823.9
IMEP COV [%]	0.98	1.35	3.58	3.92	0.93
Misfire Fraction [%]	0	0	0.1	0	0

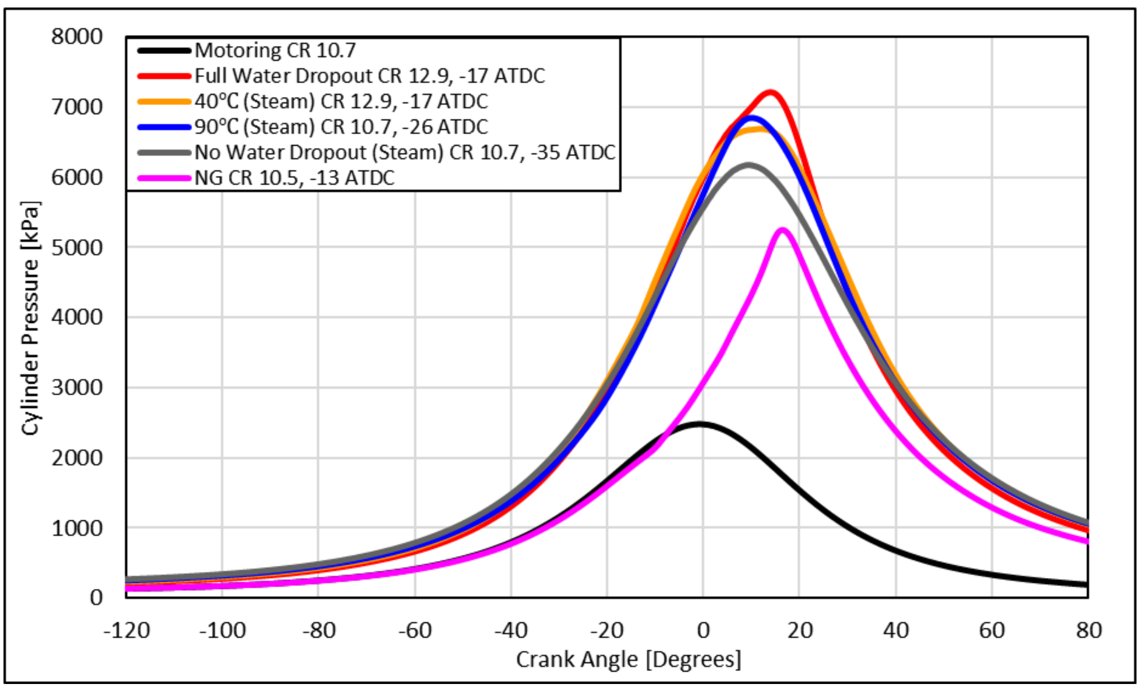

Figure 53: Cylinder pressure vs. crank angle for each test blend's most efficient data point from steam injection constant IMEP testing. No Water Dropout (Steam), NG and motoring data included for comparison. Refer to Table 9 for specific testing parameters. The legend lists ignition timing and CR conditions.

Figures 54 and 55 show the AHRR for the 40°C (Steam) and 90°C (Steam) test blends over a sweep of CR at their maximum brake torque timing. AHRR tends to decrease as CR increases. Figure 56 allows for a direct comparison between the test blends and shows that the peak AHRR for the 90°C (Steam) blend occurs much earlier than for the 40°C (Steam) blend even though each test blend has a similar cylinder pressure profile and location of peak pressure.

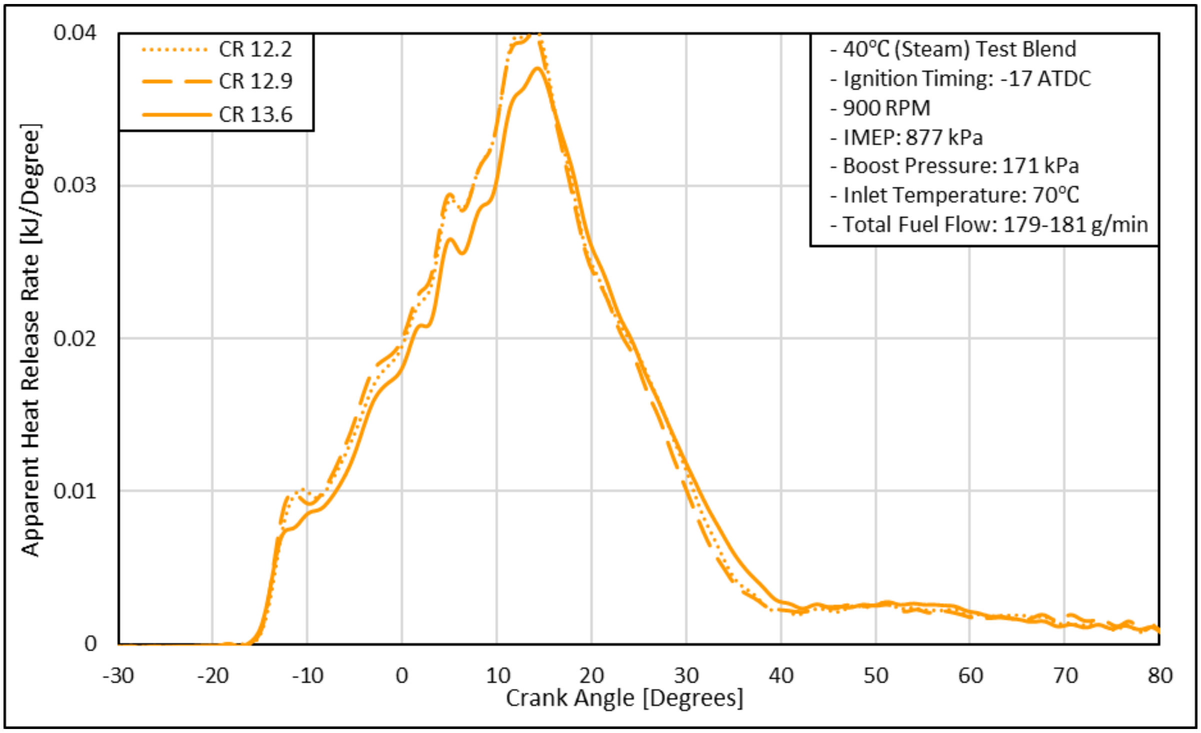

Figure 54: AHRR vs. crank angle for 40°C (Steam) test blend at maximum break torque timing of -17° ATDC with a sweep of CR from 12.2:1 - 13.6:1.

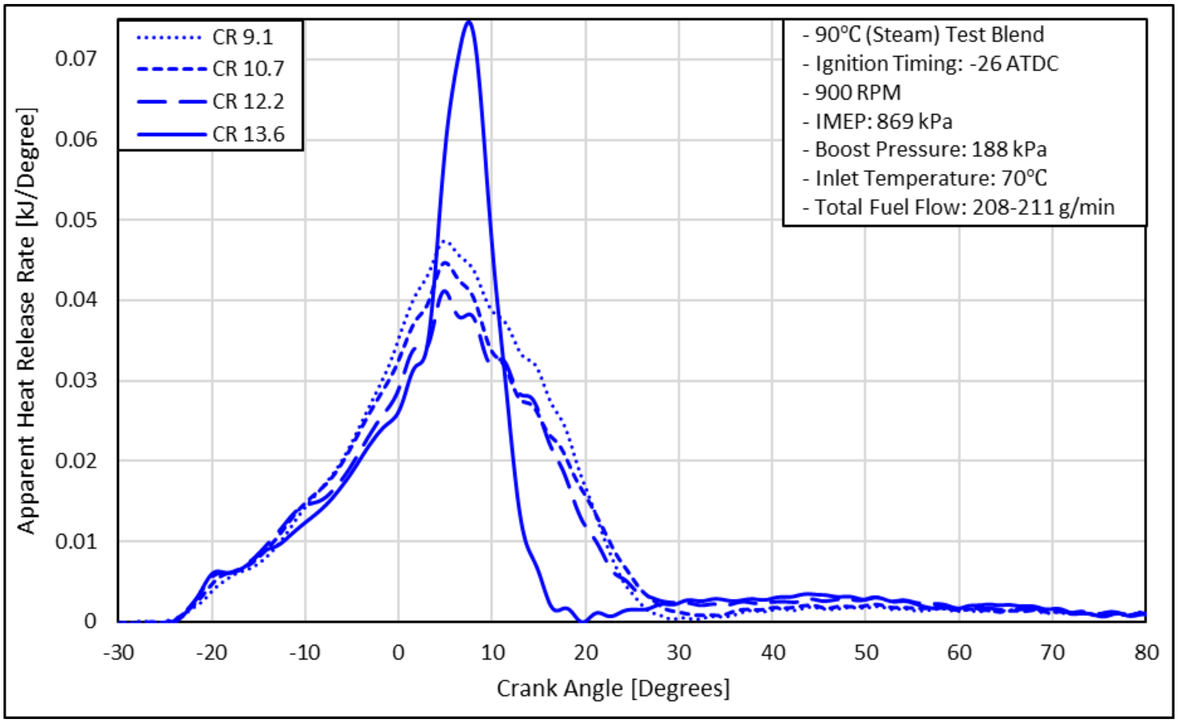

Figure 55: AHRR vs. crank angle for 90°C (Steam) test blend at maximum break torque timing of -26° ATDC with a sweep of CR from 9.1:1 - 13.6:1.

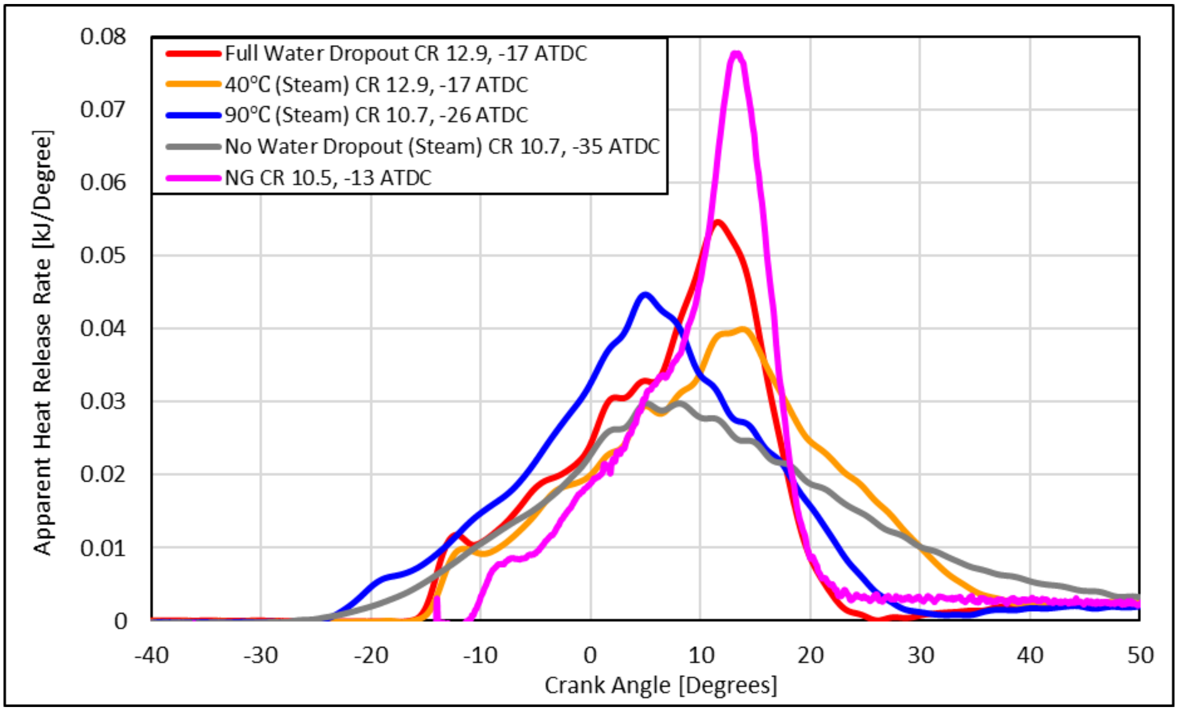

Figure 56: AHRR vs. crank angle for each test blend's most efficient data point from steam injection constant IMEP testing. No Water Dropout (Steam) and NG data included for comparison. Refer to Table 9 for specific testing parameters. The legend lists ignition timing and CR conditions.

Figures 57 and 58 show the mass fraction burned vs. crank angle for both test blends. The shape of the mass fraction burned curve is impacted little with increases in CR until an engine knock condition occurs. The onset of engine knock causes an initial increase in the mass fraction burned rate, but then the rate slows down to match that of lower CRs.

Figure 59 compares the 40°C (Steam) and 90°C (Steam) test blends against Full Water Dropout, No Water Dropout (Steam), and NG data. The 90°C (Steam) blend has a slower rate of mass fraction burned but, as the timing is more advanced for this blend, it reaches 90% mass fraction burned earlier than the NG comparison data.

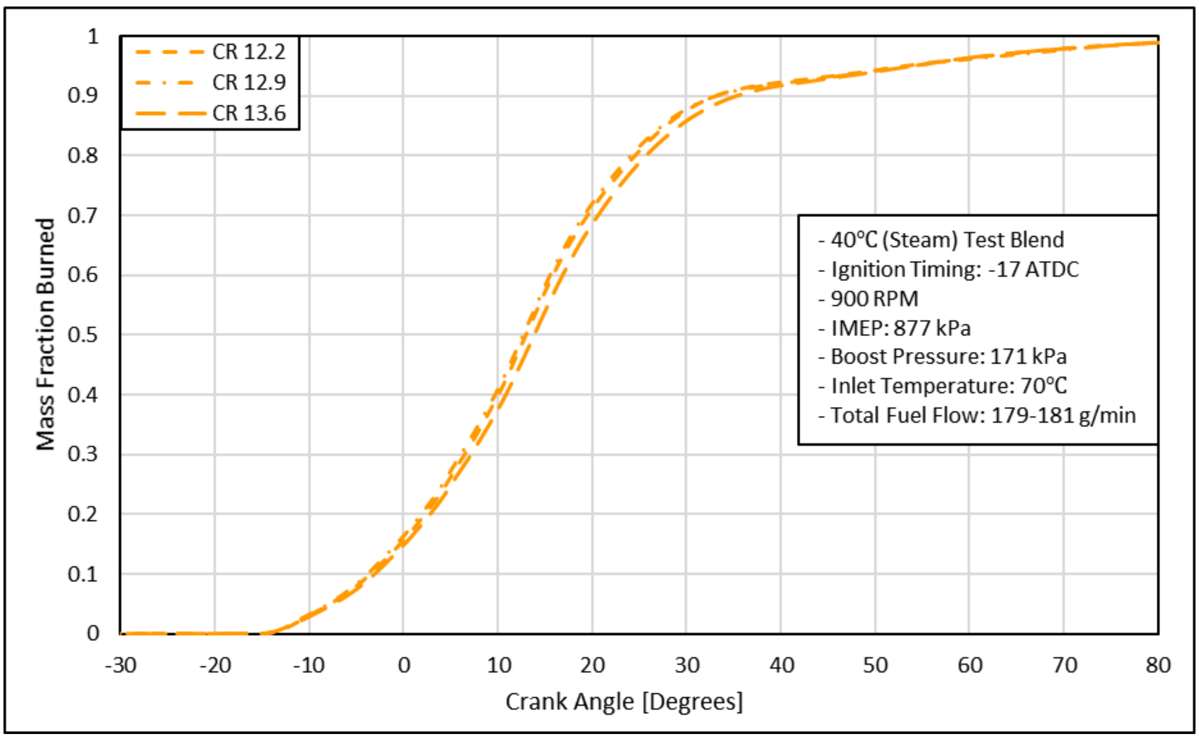

Figure 57: Mass fraction burned vs. crank angle for 40°C (Steam) test blend at maximum break torque timing of -17° ATDC with a sweep of CR from 12.2:1 - 13.6:1.

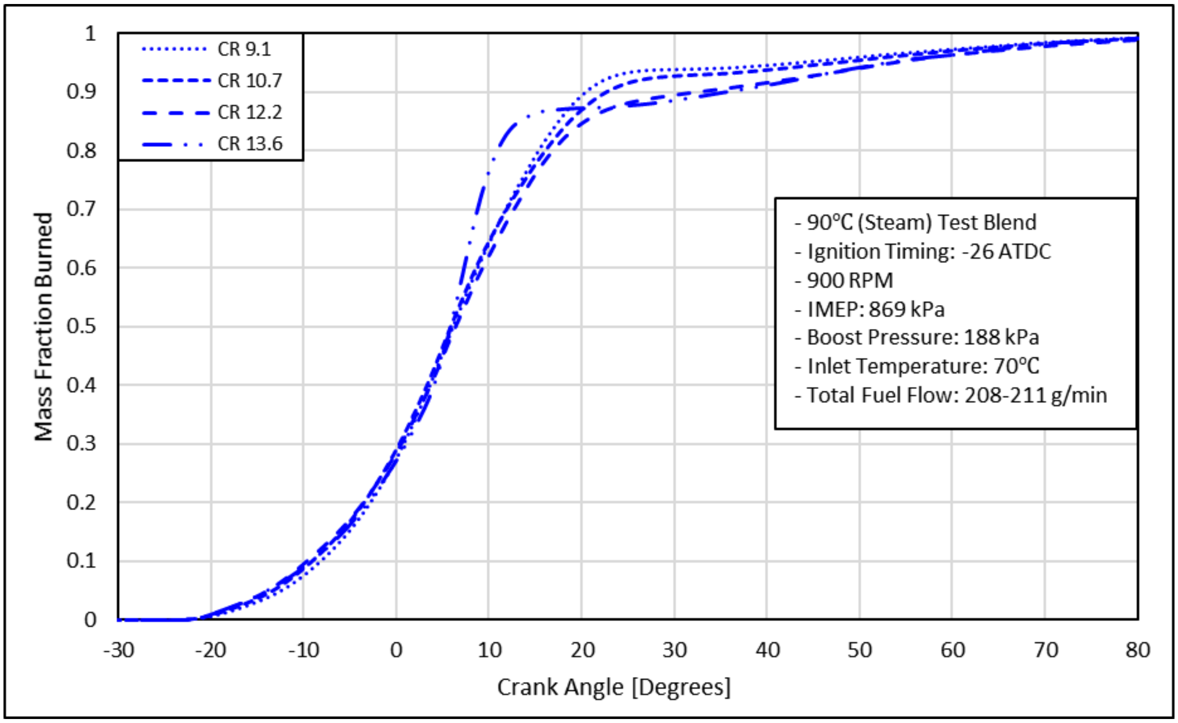

Figure 58: Mass fraction burned vs. crank angle for 90°C (Steam) test blend at maximum break torque timing of -26° ATDC with a sweep of CR from 9.1:1 - 13.6:1.

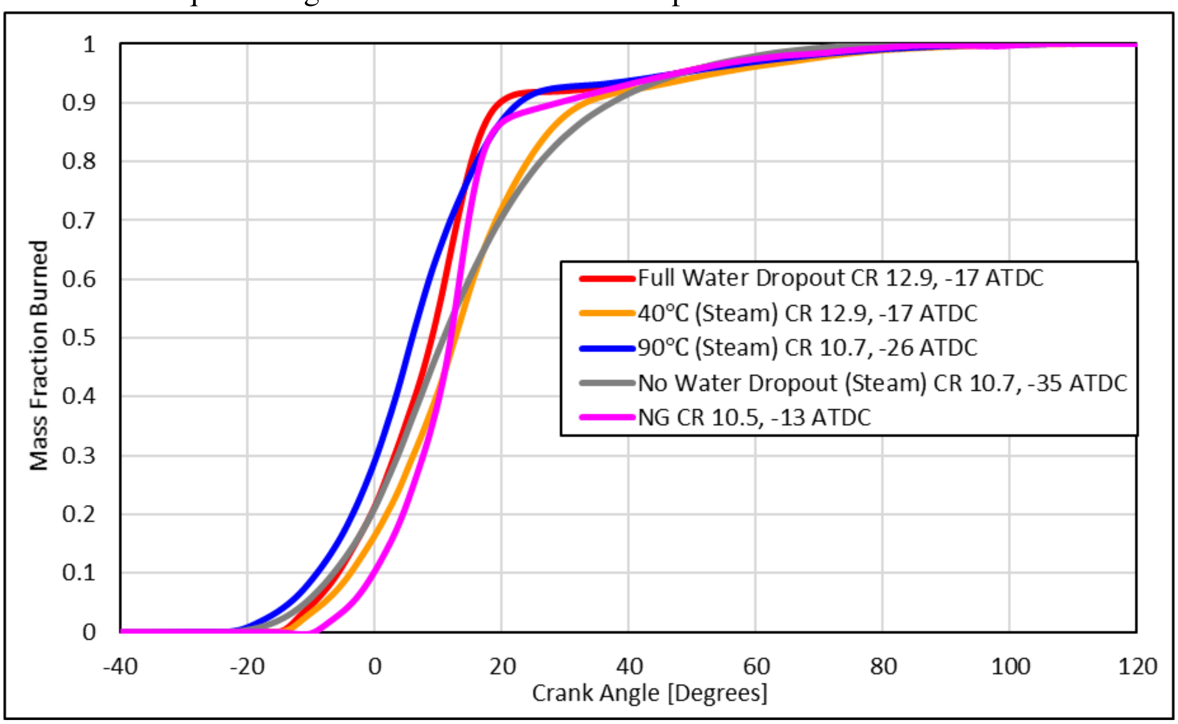

Figure 59: Mass fraction burned vs. crank angle for each test blend's most efficient data point from steam injection constant IMEP testing. No Water Dropout (Steam) and NG data included for comparison. Refer to Table 9 for specific testing parameters. The legend lists ignition timing and CR conditions.

Figure 60 displays the brake efficiency vs. CR for the 40°C (Steam) and 90°C (Steam) test blends with Full Water Dropout test blend data added for comparison. Uncertainty bars are included and were calculated as described in Section 2.7. This data shows that, at similar IMEP, the differences in test blend efficiencies are not statistically significant. Further optimization is required to determine the ideal tail-gas blend for engine operation. Both blends provide adequate engine performance, although the higher water content in the 90°C (Steam) test blend would necessitate more frequent engine maintenance.

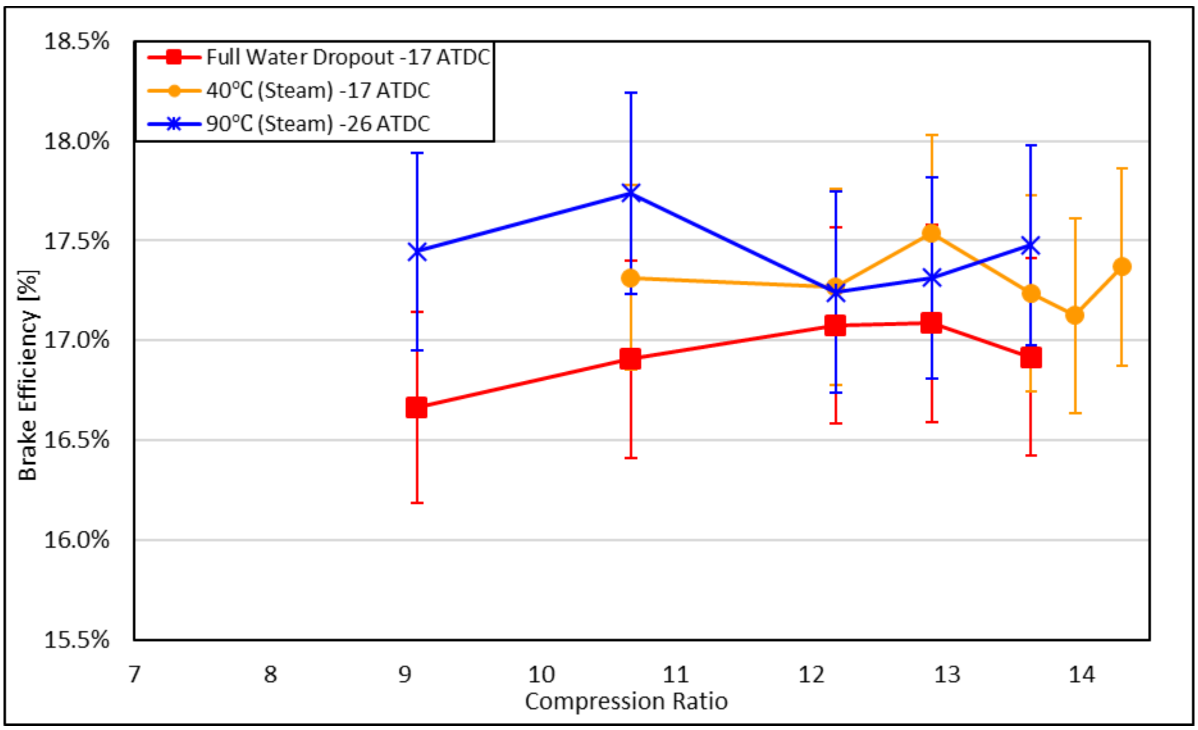

Figure 60: Brake efficiency vs. CR for all test blends at maximum brake torque timing from constant IMEP steam injection blend testing. Refer to Table 9 for specific testing parameters and No Water Dropout (Steam) blend parameters. The legend lists the ignition timing for each test point.

Figures 61 – 65 show the combustion characteristics of the 40°C (Steam) and 90°C (Steam) blends with the Full Water Dropout blend added for comparison. Each blend provided steady combustion at its most efficient test point with IMEP COV and peak pressure COV less than 6%. Figure 65 shows the increase in the location of peak pressure COV as CR is increased.

This trend is highlighted with the 40°C (Steam) blend, which shows a substantial increase in the location of peak pressure COV as CR is increased above 12.9:1.

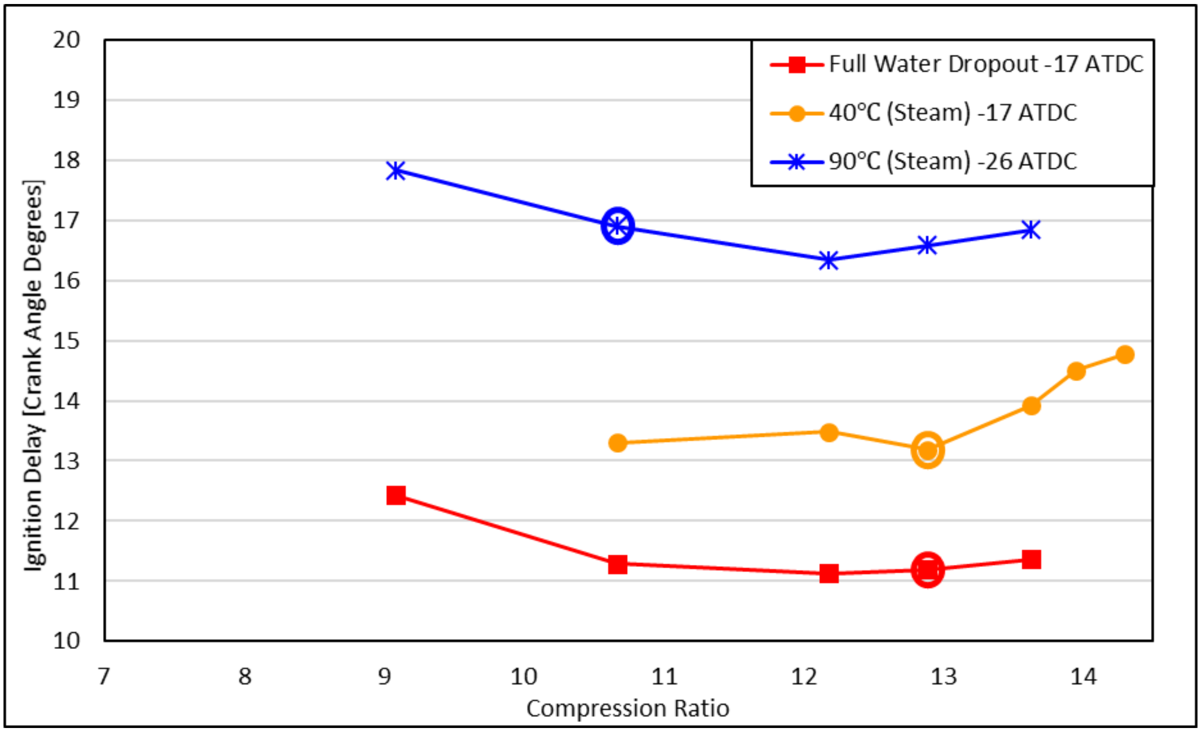

Figure 61: Ignition delay vs. CR for all test blends at maximum brake torque timing from constant IMEP steam injection blend testing with the most efficient test points circled. Refer to Table 9 for specific testing parameters and No Water Dropout (Steam) blend parameters. The legend lists the ignition timing for each test point.

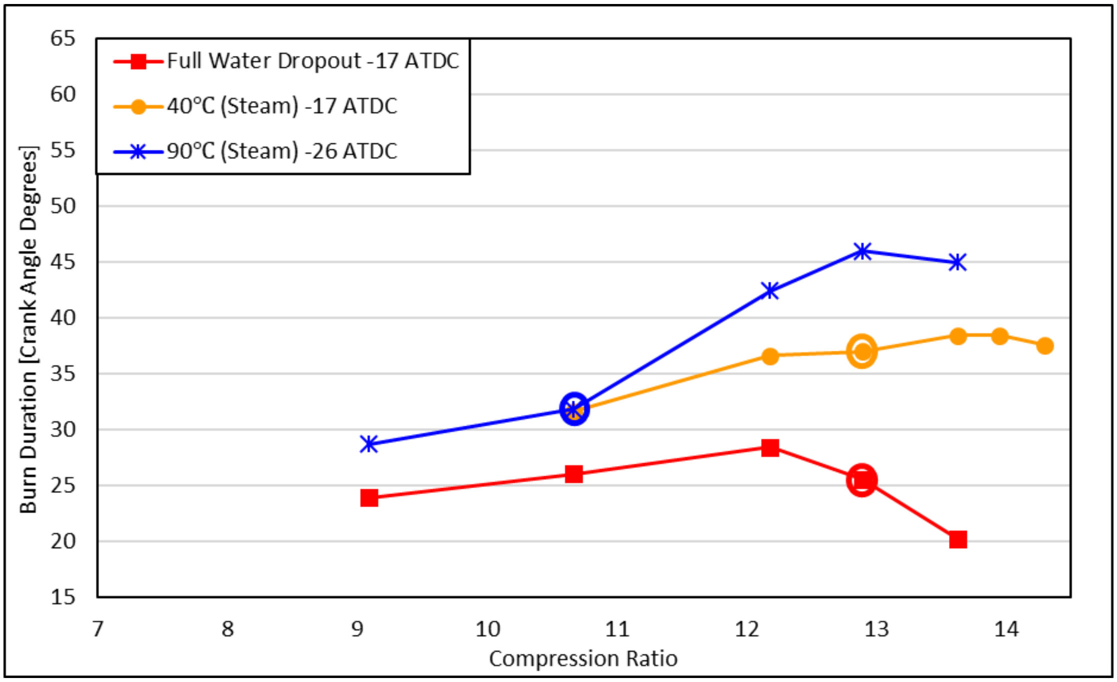

Figure 62: Burn duration vs. CR for all test blends at maximum brake torque timing from constant IMEP steam injection blend testing with the most efficient test points circled. Refer to Table 9 for specific testing parameters and No Water Dropout (Steam) blend parameters. The legend lists the ignition timing for each test point.

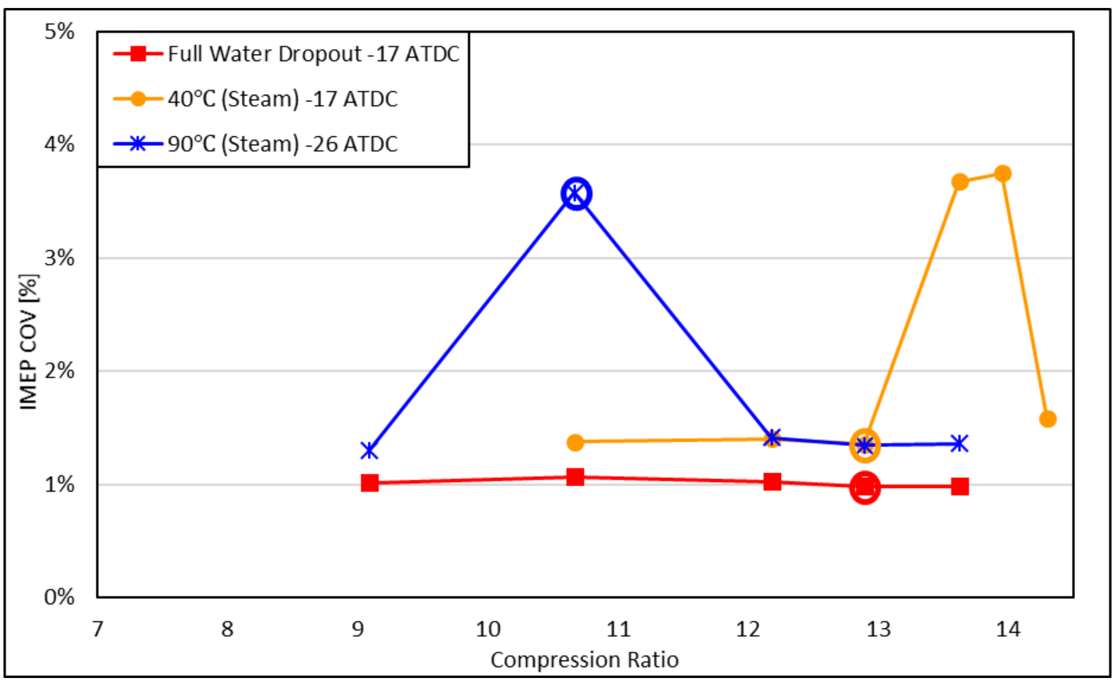

Figure 63: IMEP COV vs. CR for all test blends at maximum brake torque timing from constant IMEP steam injection blend testing with the most efficient test points circled. Refer to Table 9 for specific testing parameters and No Water Dropout (Steam) blend parameters. The legend lists the ignition timing for each test point.

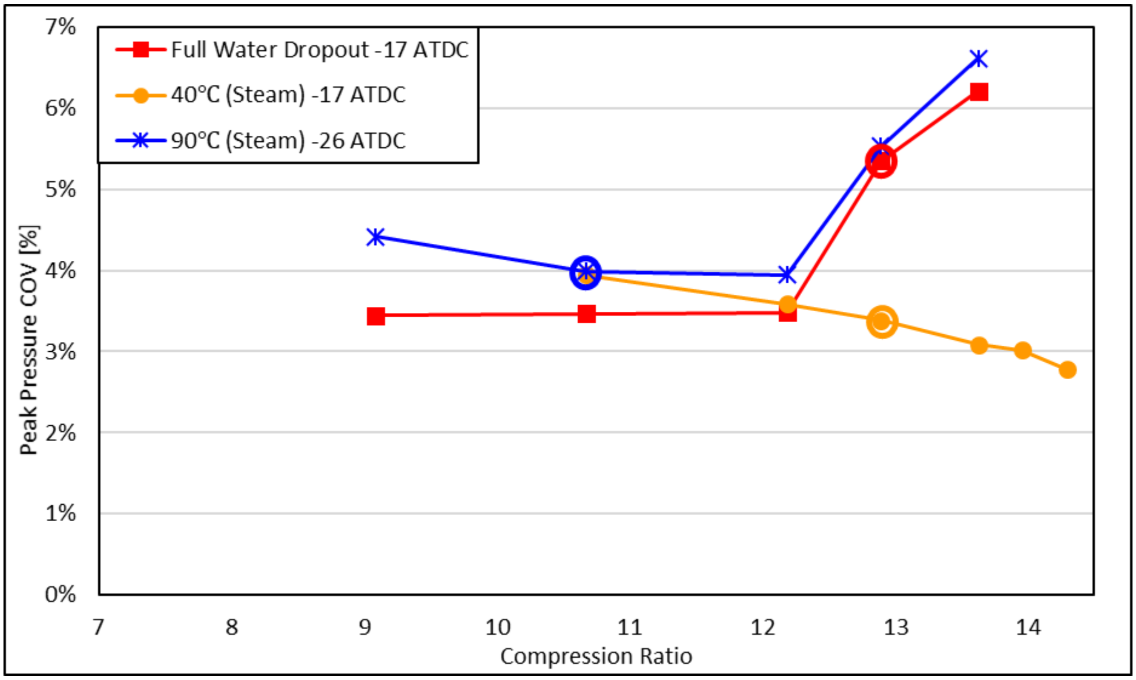

Figure 64: Peak Pressure COV vs. CR for all test blends at maximum brake torque timing from constant IMEP steam injection blend testing with the most efficient test points circled. Refer to Table 9 for specific testing parameters and No Water Dropout (Steam) blend parameters. The legend lists the ignition timing for each test point.

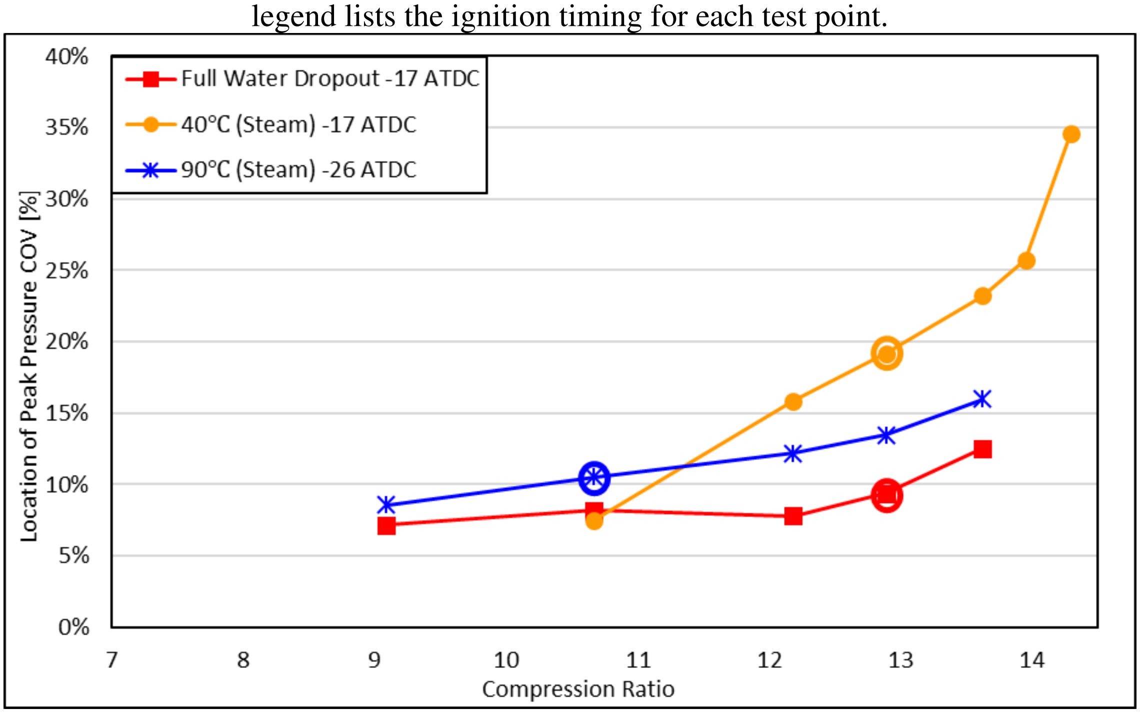

Figure 65: Location of peak pressure COV vs. CR for all test blends at maximum brake torque timing from constant IMEP steam injection blend testing with the most efficient test points circled. Refer to Table 9 for specific testing parameters and No Water Dropout (Steam) blend parameters. The legend lists the ignition timing for each test point.

4.3. Steam Injection Feasibility Testing Emissions Data

Emissions data was recorded across a sweep of ignition timing for each test blend during the steam injection blend initial combustion testing. NG and methane data are included for comparison. Data was measured and recorded using the Siemens 5-gas analyzer. A complete description of the emissions analyzers used in this testing can be found by referencing King [14] and Falloon [15]. More NG emissions baseline testing can also be found by referencing Falloon [15]. The results of this testing are displayed in Figures 66 – 68. The simulated tail-gas test blends show lower levels of BSTHC for each test point than what is measured in NG and methane, most probably due to the relatively low levels of hydrocarbons contained in the simulated tail-gas blends. Levels of BSCO are similar between the simulated tail-gas blends and NG and methane. The No Water Dropout (Steam) test blend shows increased levels of CO as ignition timing is retarded. As No Water Dropout (Steam) blend efficiency increases and combustion is more complete, the levels of BSCO are reduced close to the levels seen in the other test blends. Figure 68 shows that $BSNO_x$ measured in the simulated tail-gas blends is much lower than what is experienced with the CFR engine during the NG and methane testing. As mentioned in Section 1.2.1., the likely cause for this is reduced flame speed and combustion temperatures which limit NO_x formation. The 40°C (Steam) test blend shows increasing $BSNO_x$ levels as the ignition timing is advanced past maximum brake torque timing. Increasing $BSNO_x$ levels can be attributed to the peak heat release rate moving towards TDC as timing is advanced, which causes an increase in combustion temperature.

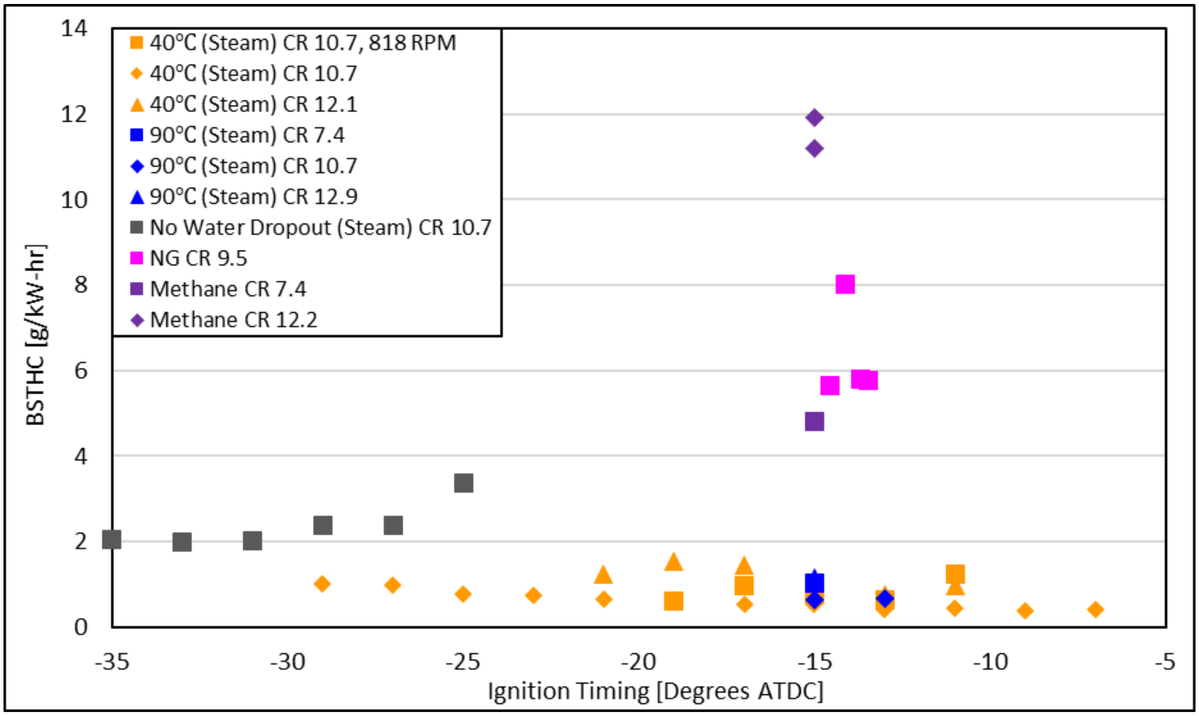

Figure 66: BSTHC vs. ignition timing for 40°C (Steam), 90°C (Steam), and No Water Dropout (Steam) test blends with NG and Methane data for comparison.

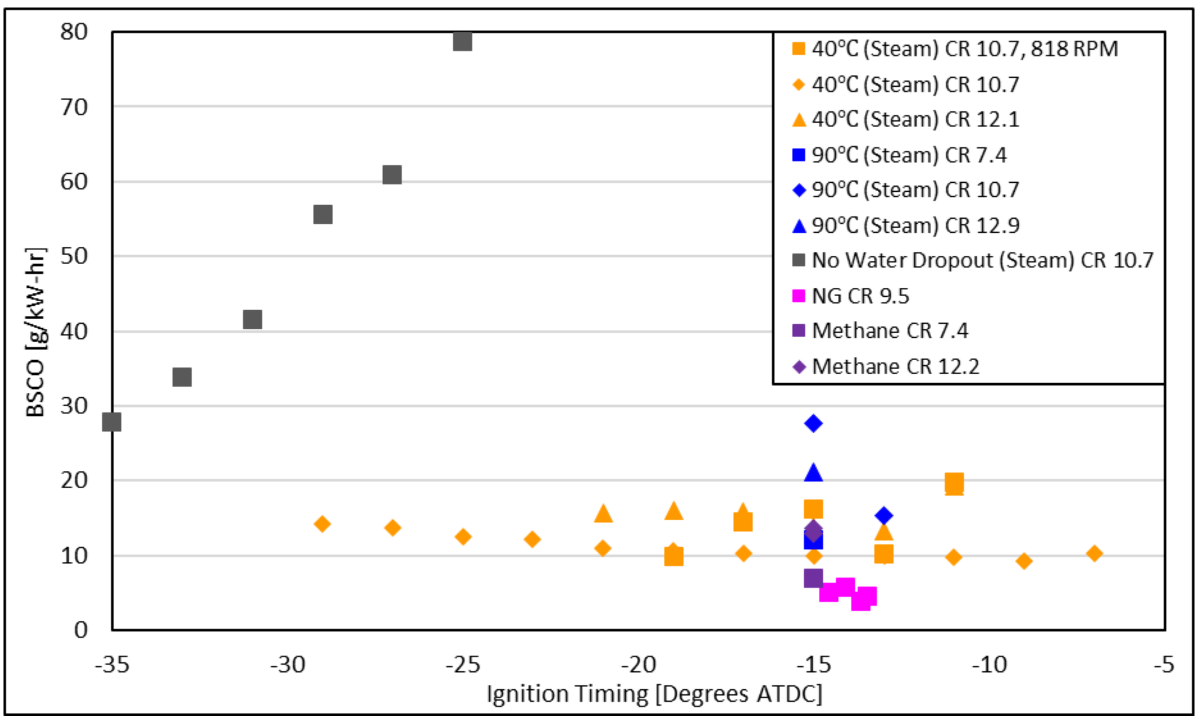

Figure 67: BSCO vs. ignition timing for 40°C (Steam), 90°C (Steam), and No Water Dropout (Steam) test blends with NG and Methane data for comparison.

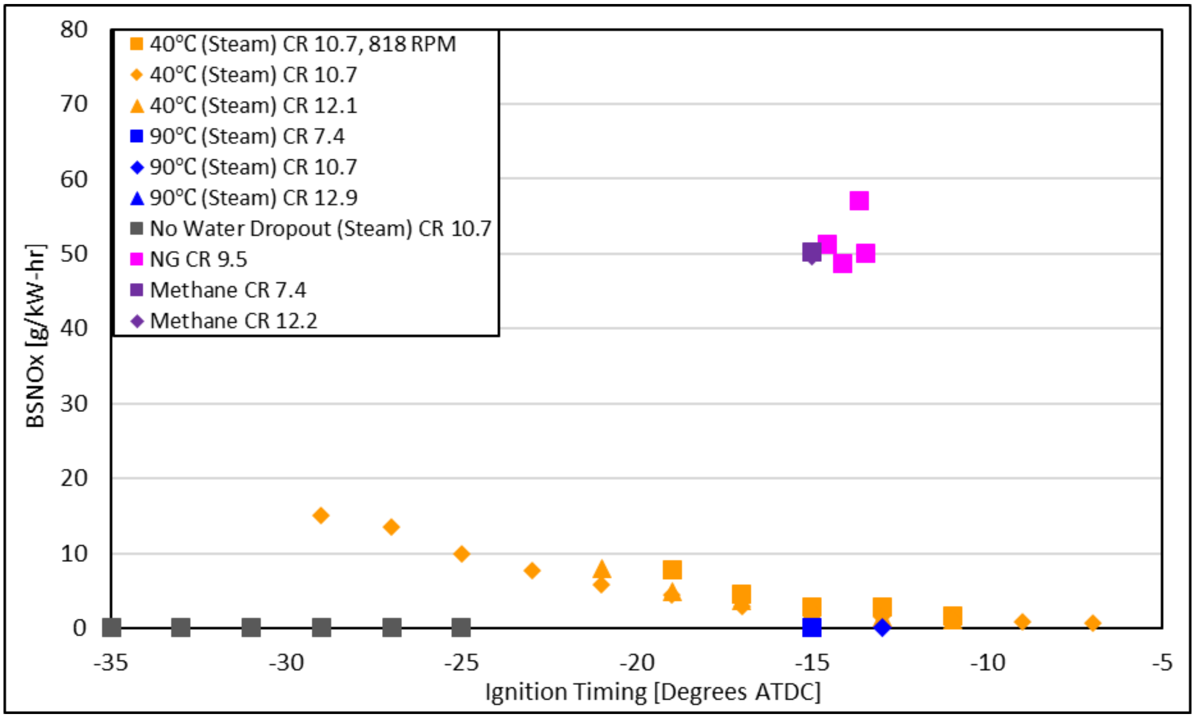

Figure 68: $BSNO_x$ vs. ignition timing for 40°C (Steam), 90°C (Steam), and No Water Dropout (Steam) test blends with NG and Methane data for comparison.

4.4. Steam Injection Constant IMEP Emissions Data

Emissions data recorded during steam injection constant IMEP testing is shown in Figures 69 – 71 with NG and methane data for comparison. This data was recorded at an IMEP of 870±15 kPa for the simulated tail-gas blends but not the NG and methane data. Each simulated tail-gas blend is operating at or near maximum brake torque timing. Each figure, besides Figure 70, shows that the emissions levels are only slightly affected by increasing CR. Increases in BSCO for the 40°C (Steam) test blend are seen in Figure 70 as CR is increased, most likely due to the presence of unburnt fuel in the exhaust gas as flame quenching occurs with decreased squish volume. Similar trends are seen in Figures 69 – 71 that have been discussed before. Simulated tail-gas blends show decreased BSTHC and $BSNO_x$ when compared to NG and methane but exhibit similar or higher levels of BSCO.

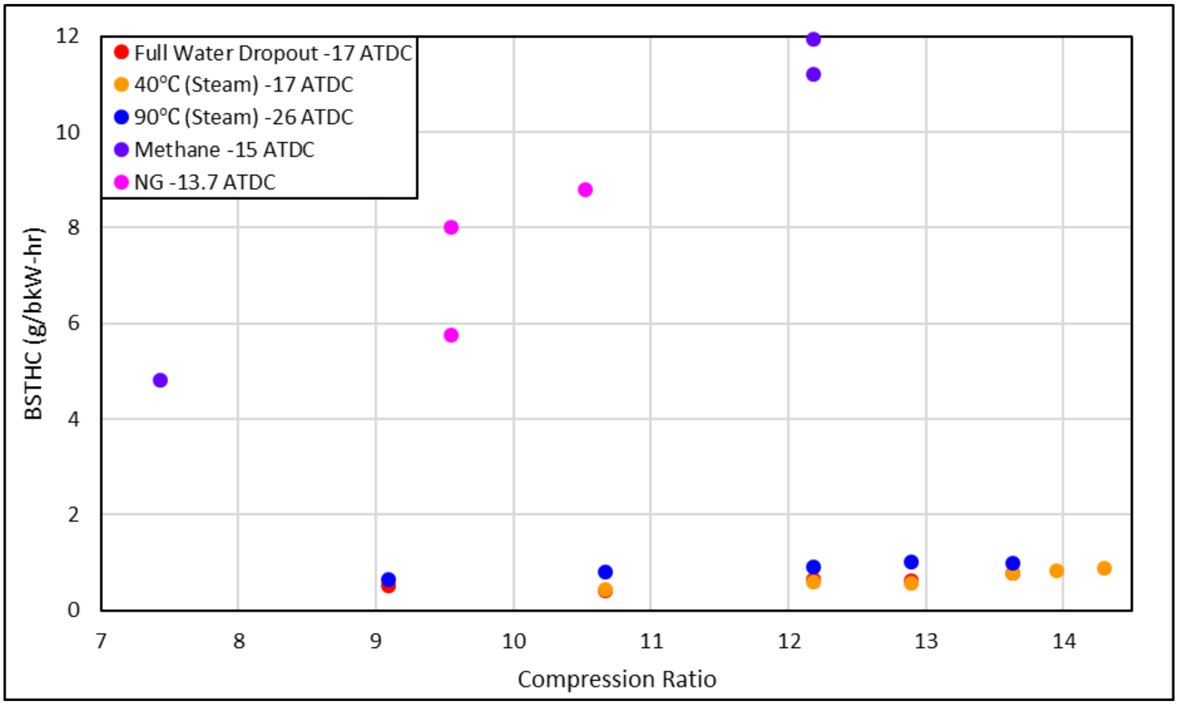

Figure 69: BSTHC vs. CR at maximum brake torque timing for Full Water Dropout, 40°C (Steam), and 90°C (Steam) test blends with NG and Methane data for comparison. The legend lists the ignition timing for each test point.

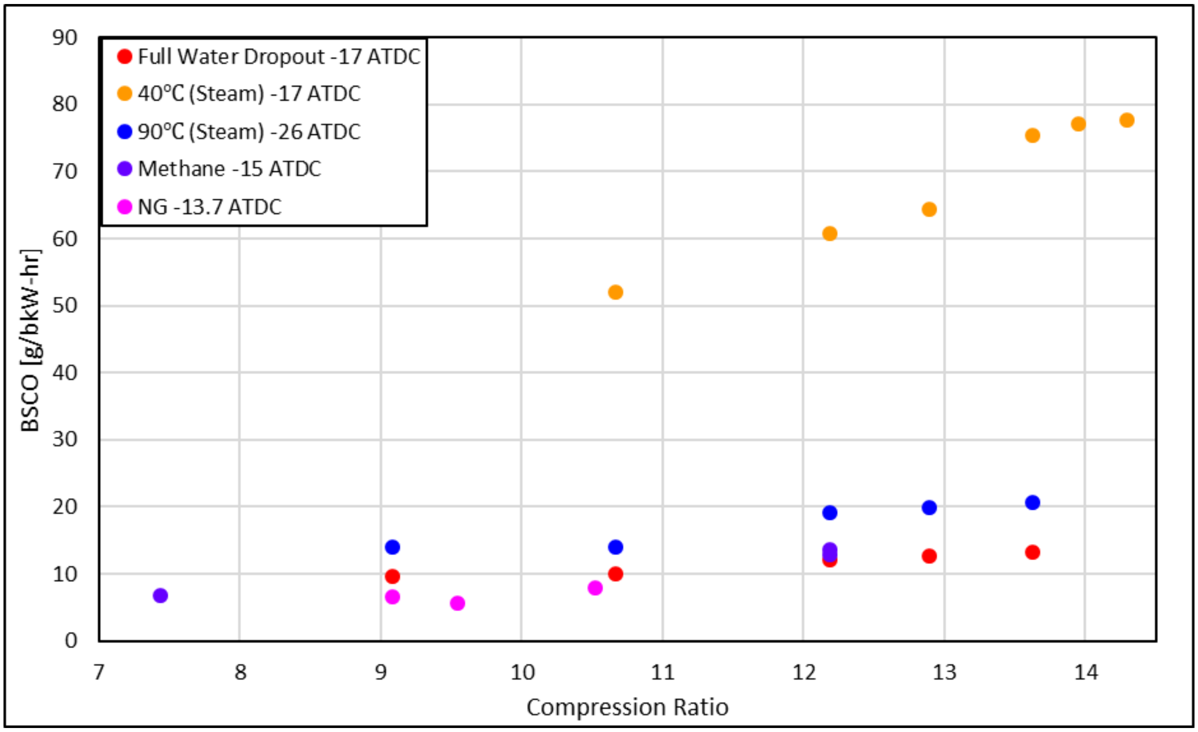

Figure 70: BSCO vs. CR at maximum brake torque timing for Full Water Dropout, 40°C (Steam), and 90°C (Steam) test blends with NG and Methane data for comparison. The legend lists the ignition timing for each test point.

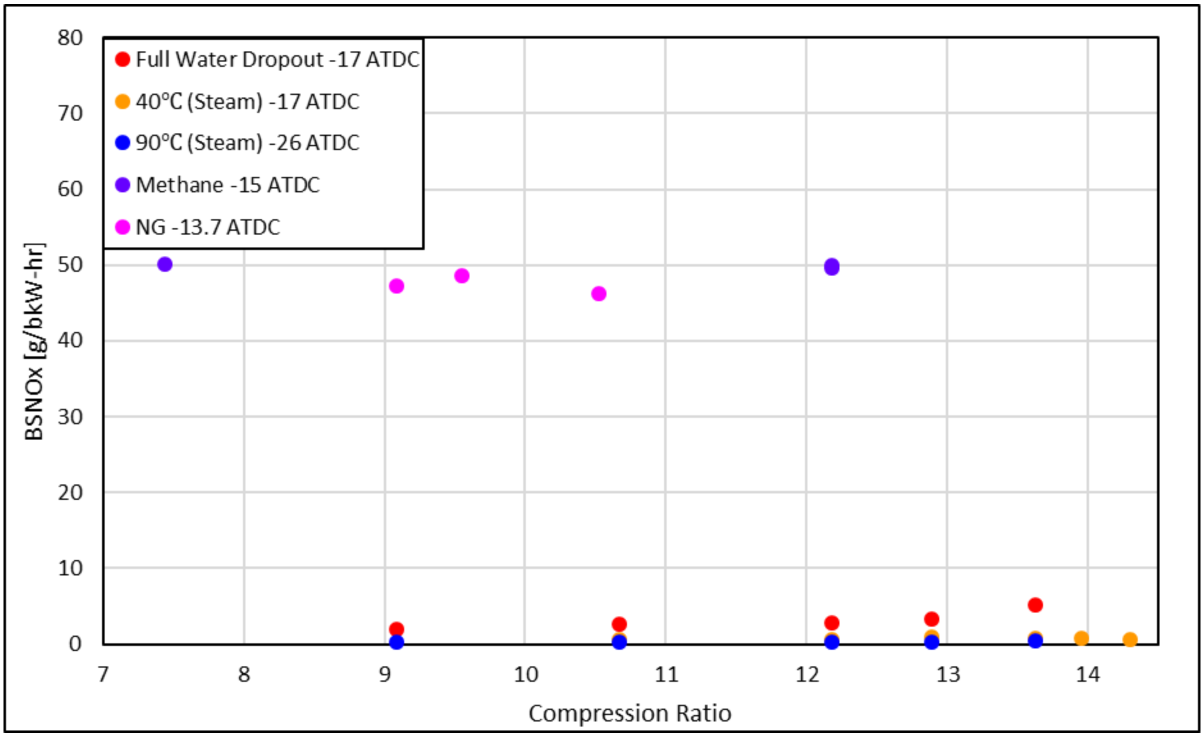

Figure 71: $BSNO_x$ vs. CR at maximum brake torque timing for Full Water Dropout, 40°C (Steam), and 90°C (Steam) test blends with NG and Methane data for comparison.

CHAPTER 5: RESPONSE SURFACE METHOD OPTIMIZATION

5.1. 40°C (Steam) Blend Optimization

RSM optimization was performed for the 40°C (Steam) test blend. Earlier testing of the 90°C (Steam) test blend showed that brake efficiency was insensitive to changes in IMT at the elevated temperatures required to prevent condensation of water in the engine intake. 90°C (Steam) blend testing also showed that IMEP was always maximized to provide the highest efficiency rise. Because of this, 40°C (Steam) blend RSM optimization omitted IMT and IMEP from the optimization variables. IMT was held at 48°C for all testing, and IMEP was set to 1000±10 kPa at initial testing points. Fuel flow was maintained constant until a maximum IMEP of 1100 kPa was reached as brake efficiency increased. Fuel flow was decreased to maintain a maximum IMEP of 1100 kPa for the remainder of testing. IMEP was increased to 1145 kPa for a final data point to see the potential change in engine efficiency with a broader engine operating envelope.

Table 10 is included to show the process used to create one of the efficiency optimization vectors. This table shows the steps required to create vector 1 for the 40°C (Steam) test blend. The increment/decrement step size is at the top of the table and is used to calculate target parameters at each corner of the modified Box-Behnken shape. Table 10 then lists the two measurements taken at the center points followed by each corner. Eight corners are required for three optimization variables. The parameters of each center and corner test point and the brake efficiency measured at those points are included in the final column of Table 10. The final rows of Table 10 show the calculated final efficiency vector, followed by vector steps one through four. Vector steps one through four are calculated by multiplying the final efficiency vector by the step number, 1, 2, 3 and 4, to calculate the target parameters for each step.

Table 10: RSM Optimization 40°C (Steam) Blend Vector 1. Center point parameters have green backgrounds, incremented parameters have yellow, and decremented parameters are highlighted in red.

Parameter	Speed [RPM]	CA50 [°ATDC]	CR	Measured Brake Efficiency
Increment/Decrement	50	3° Advance	2.5	N/A
Center 1	1050	10	10	18.17
Center 2	1050	10	10	18.12
Corner 1	1100	13	12.5	18.39
Corner 2	1100	13	7.5	16.84
Corner 3	1100	7	12.5	18.62
Corner 4	1100	7	7.5	16.92
Corner 5	1000	13	12.5	18.1
Corner 6	1000	13	7.5	16.82
Corner 7	1000	7	12.5	17.7
Corner 8	1000	7	7.5	16.93
Final Efficiency Vector	0.083	-0.001	0.361	N/A
Vector Step 1 (Center Point)	1050	10.00	10.00	18.05
Vector Step 2	1054.16	10.00	10.90	18.25
Vector Step 3	1058.31	9.99	11.81	18.65
Vector Step 4	1062.47	9.99	12.71	18.44

Figures 72 – 74 show the cylinder pressure vs. crank angle for each step of each efficiency vector followed during 40°C (Steam) blend RSM optimization. The data point with the highest efficiency for each vector is shown with a solid line. The energy flow is listed in each figure for each test point. Figure 73 and 73 show that the energy flow, and total fuel flow, was reduced to maintain IMEP below 1100 kPa as efficiency increased during testing. Figure 72 shows the most drastic changes in the shape of the cylinder pressure trace because the magnitude of the CR component of the efficiency vector was larger in vector 1 than it was in vectors 2 and 3. The CR component of vector 1 was 0.181, vector 2 was 0.072, and vector 3 was -0.012. The data set with the highest efficiency in Figure 74 displays a lower peak pressure than the initial steps of efficiency vector 3 because the CR component of efficiency vector 3 was negative.

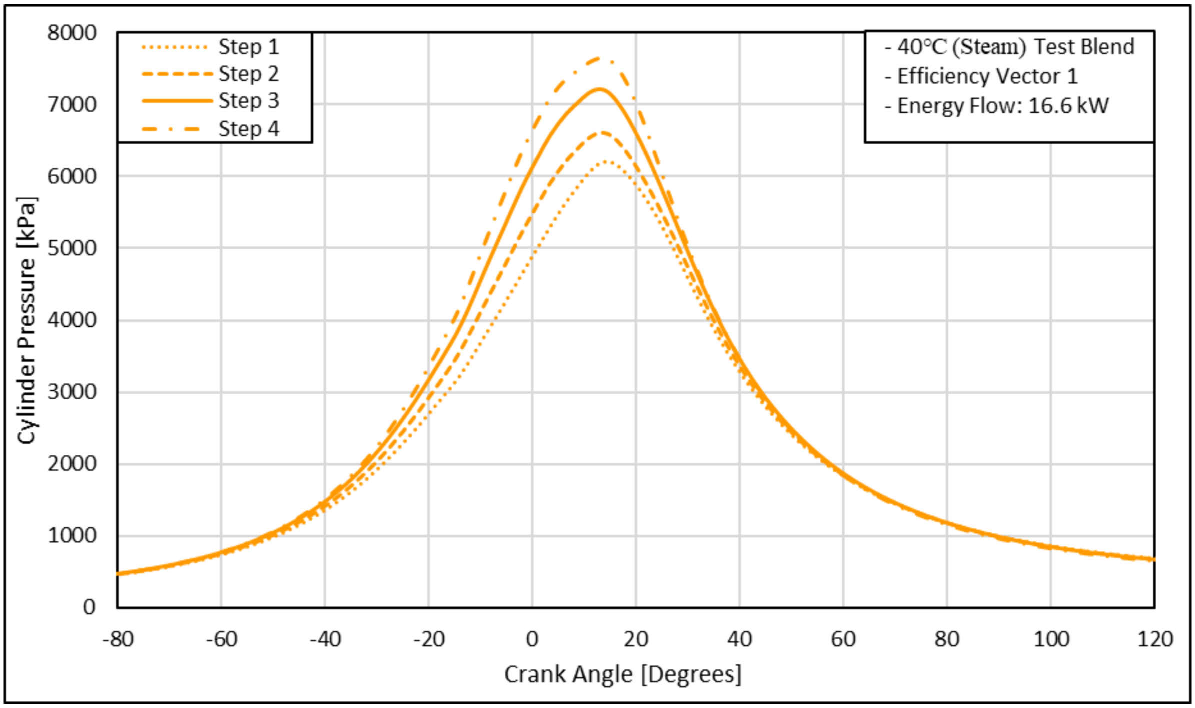

Figure 72: Cylinder pressure vs. crank angle for the 40°C (Steam) test blend at each step along vector 1. Energy flow (LHV·$\dot{m}_{fuel}$) for each data point is included in the figure. A solid line indicates the most efficient data point.

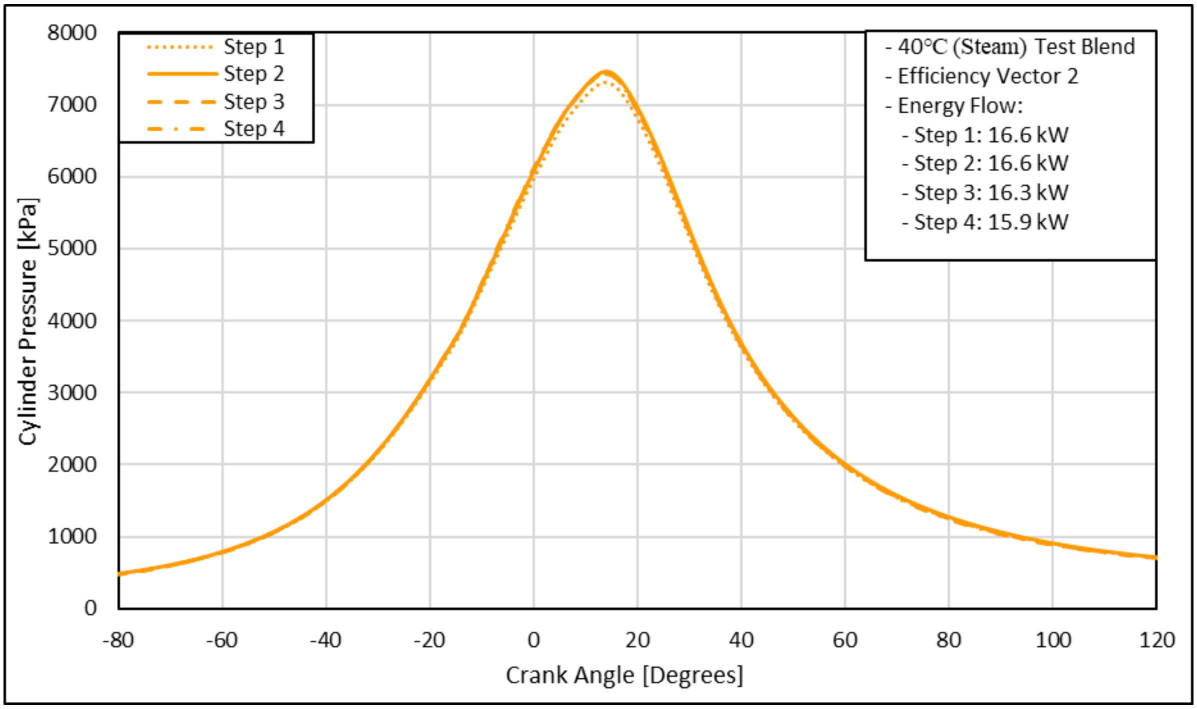

Figure 73: Cylinder pressure vs. crank angle for the 40°C (Steam) test blend at each step along vector 2. Energy flow (LHV$\cdot\dot{m}_{fuel}$) for each data point is included in the figure. A solid line indicates the most efficient data point.

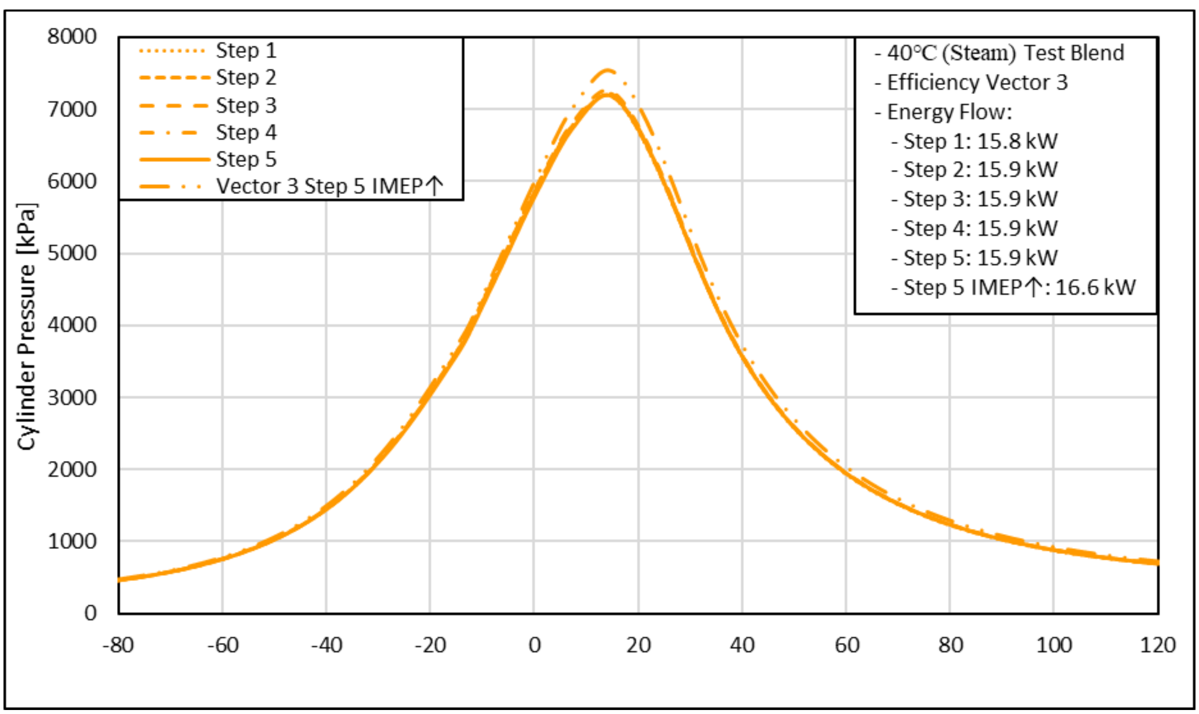

Figure 74: Cylinder pressure vs. crank angle for the 40°C (Steam) test blend at each step along the vector 3. Energy flow (LHV$\cdot\dot{m}_{fuel}$) for each data point is included in the figure. A solid line indicates the most efficient data point.

Figure 75 shows the brake efficiency of each step of each efficiency vector for the 40°C (Steam) test blend. Each vector is followed as efficiency increases. Once a decrease in efficiency is seen, the highest efficiency point becomes the center of a new modified Box-Behnken shape, and a new efficiency vector is calculated.

Figures 76 and 77 show the peak pressure and IMEP COV for each step of each efficiency vector. These figures make it clear that steady engine operation on the 40°C (Steam) test blend is possible. Any COV value below 5-10% is considered steady combustion for the CFR test stand.

The ignition delay and burn duration vs. efficiency vector step can be seen in Figures 78 and 79 for each step of each vector. As efficiency increases, both ignition delay and burn duration tend to decrease, meaning that the fuel is igniting more readily and is burning faster as the optimal data point is reached.

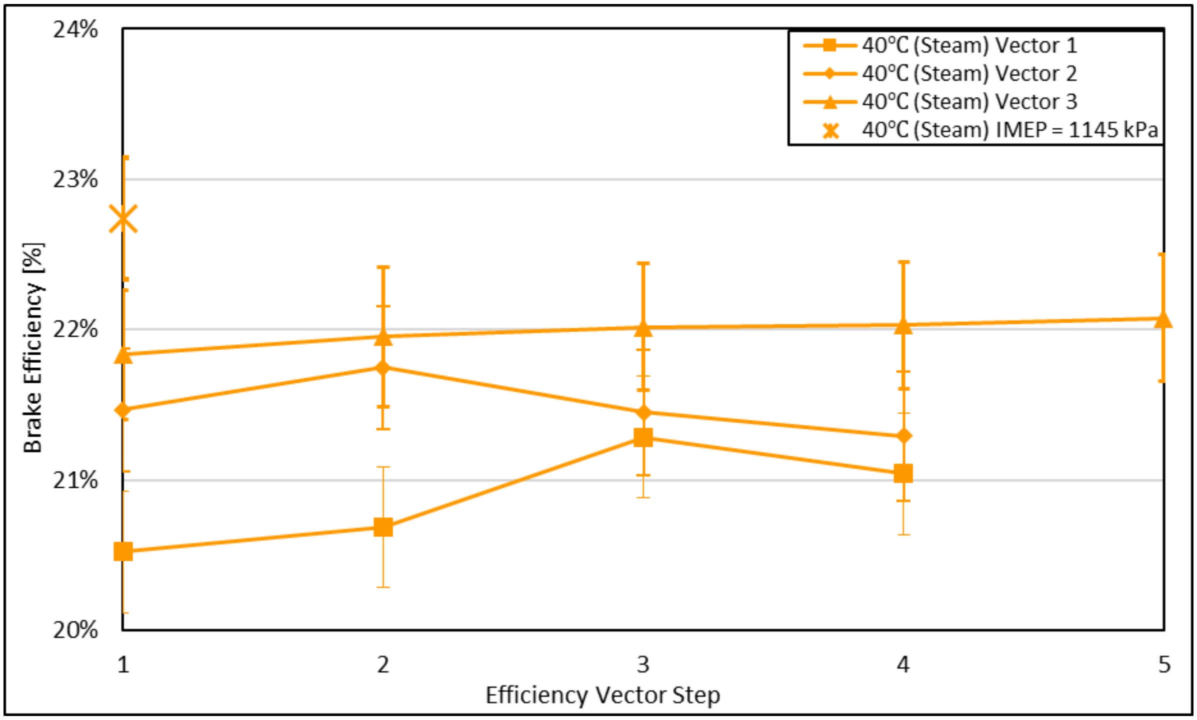

Figure 75: Brake efficiency vs. efficiency vector step for the 40°C (Steam) test blend. Vectors 1, 2, and 3 are shown with an extra data set added for vector 3 step 5 with increased IMEP.

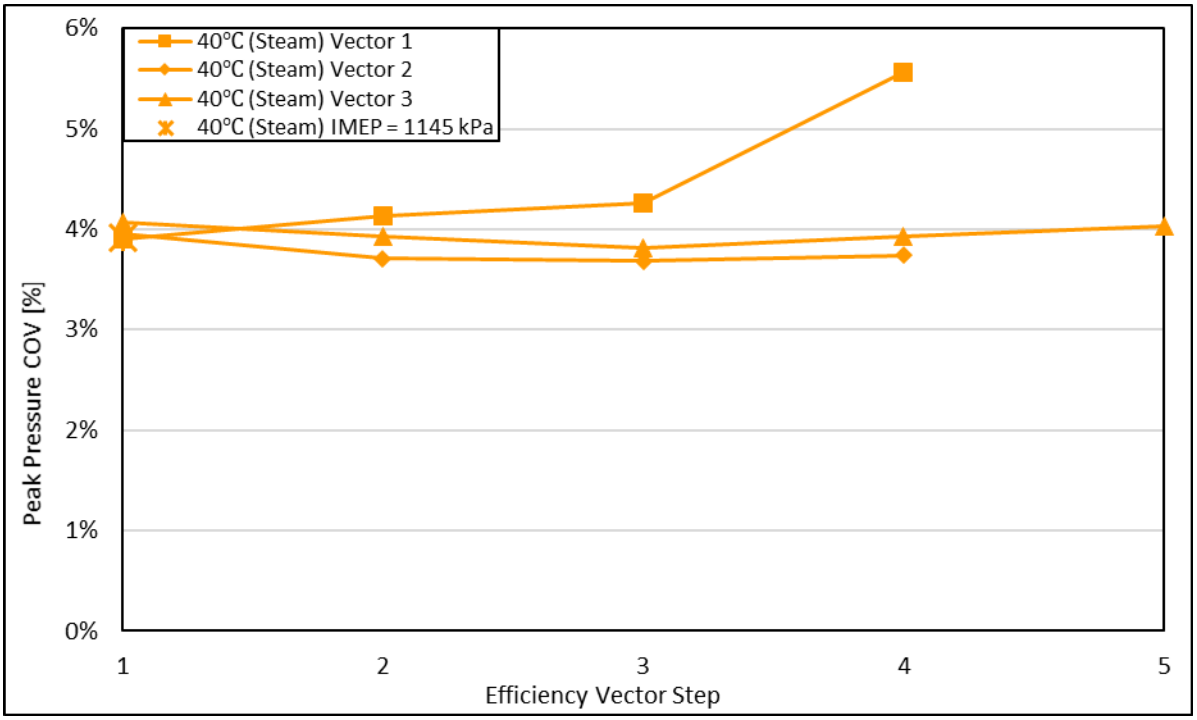

Figure 76: Peak pressure COV vs. efficiency vector step for the 40°C (Steam) test blend. Vectors 1, 2, and 3 are shown with an extra data set added for vector 3 step 5 with increased IMEP.

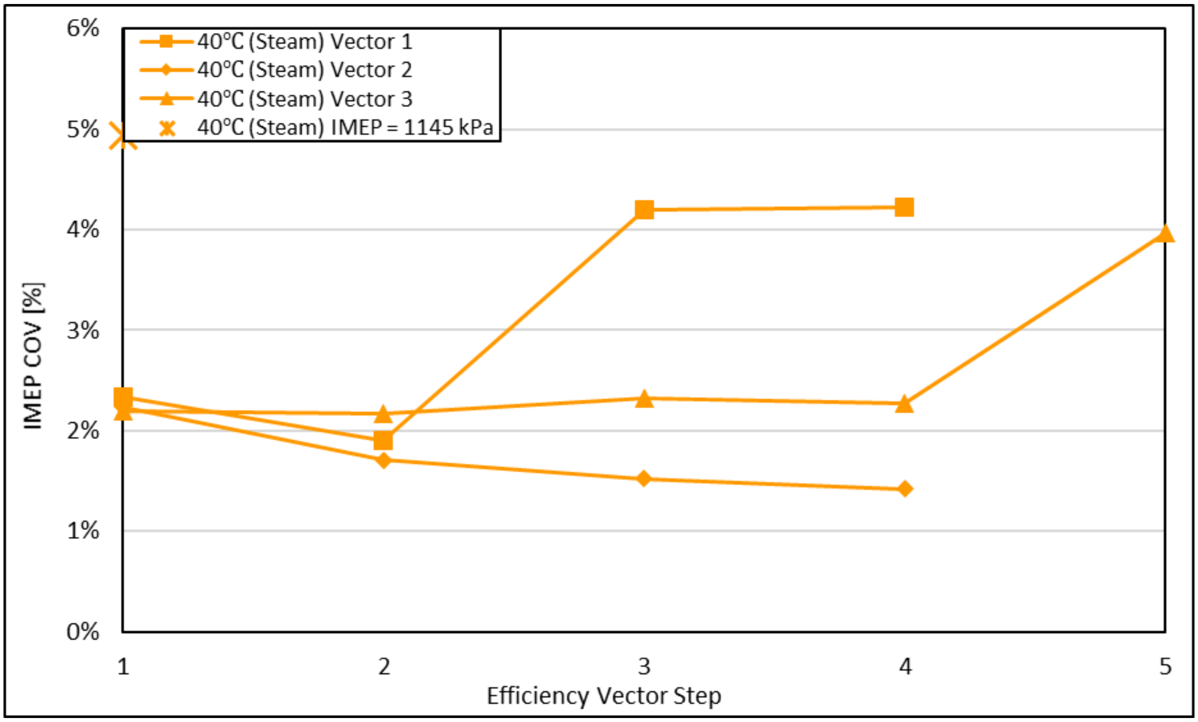

Figure 77: IMEP COV vs. efficiency vector step for the 40°C (Steam) test blend. Vectors 1, 2, and 3 are shown with an extra data set added for vector 3 step 5 with increased IMEP.

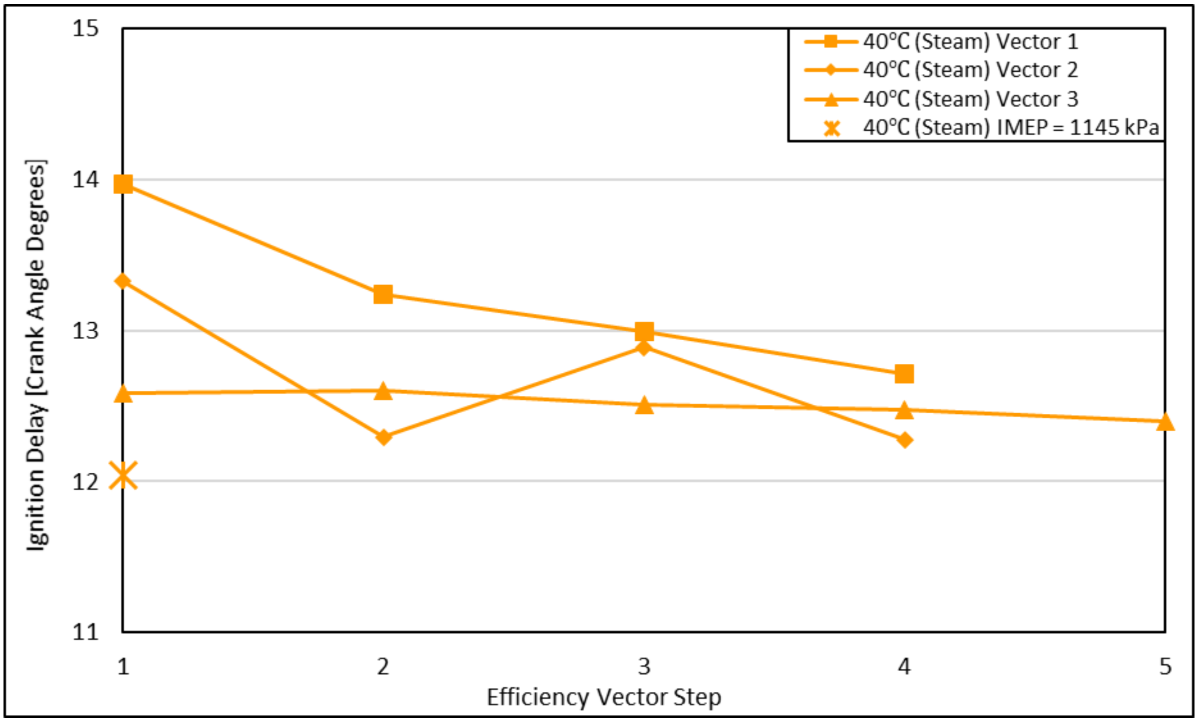

Figure 78: Ignition delay vs. efficiency vector step for the 40°C (Steam) test blend. Vectors 1, 2, and 3 are shown with an extra data set added for vector 3 step 5 with increased IMEP.

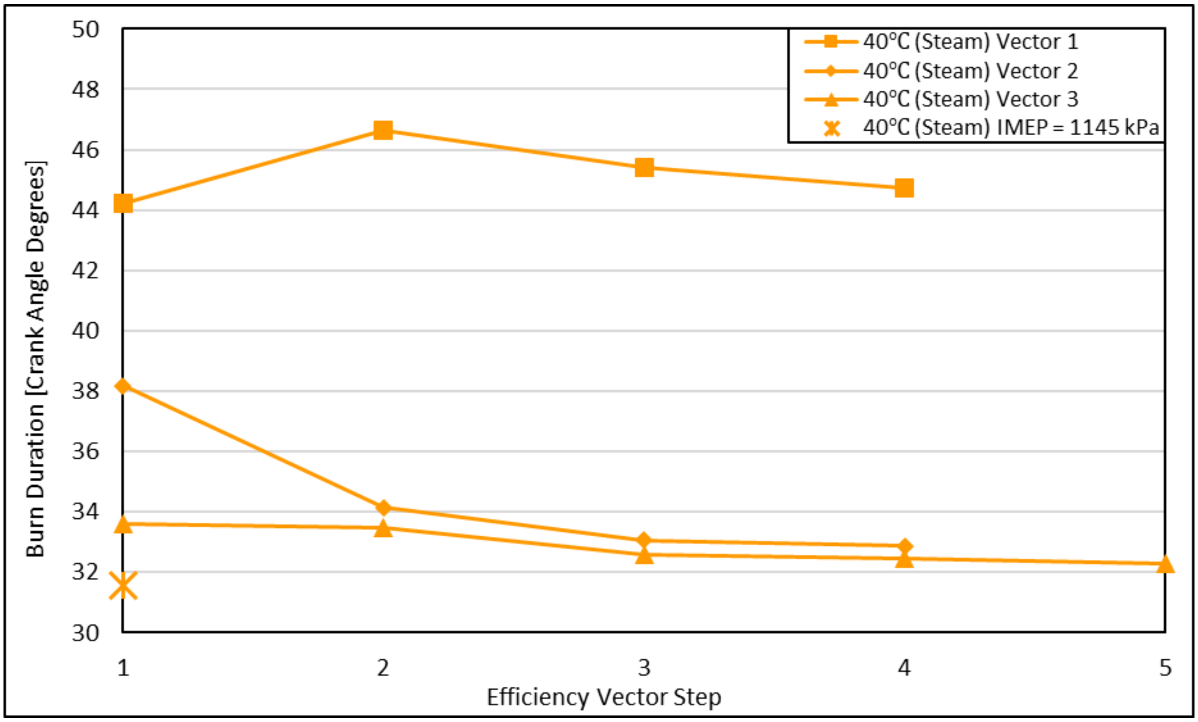

Figure 79: Burn duration vs. efficiency vector step for the 40°C (Steam) test blend. Vectors 1, 2, and 3 are shown with an extra data set added for vector 3 step 5 with increased IMEP.

5.2. 90°C (Steam) Blend Optimization

RSM optimization was performed for the 90°C (Steam) test blend. All five optimization variables, IMT, Speed, CA50, IMEP, and CR, were included in the first optimization vector for this test blend. The use of 5 optimization variables required that the modified Box-Behnken shape consisted of 32 data points. The resulting magnitude of the IMT component of the final vector was only -0.013°C. The negative value is expected as a decrease in IMT increases the density of the air-fuel mixture, creating a more energy-dense and easier to burn substance. The small magnitude of the IMT component shows that a much larger step size would be required to see the benefit of a decrease in IMT. A substantial decrease in IMT is not possible as this would cause condensation in the engine intake as the dewpoint of the air-fuel mixture is reached. IMT was omitted from future RSM optimization due to its lack of effect on engine brake efficiency.

IMEP was also omitted from future RSM optimization because it was clear that each optimization would cause IMEP to be maximized to maximize measured brake efficiency. IMEP could not be maintained at the target value for all optimization steps as the CFR test stand was limited to a maximum of 6.6 g/min of H_2 flow. As increasing fuel flow above this amount was not possible, IMEP targets were not met after vector 1 step 5. The maximum target IMEP was eventually reached at vector 2 step 4 once engine efficiency increased. A maximum speed limit of 1200 RPM was also reached at vector 1 step 7. The engine speed was not allowed to increase past 1200 RPM during testing.

Figures 80 and 81 show the cylinder pressure vs. crank angle for the 90°C (Steam) test blend as efficiency vectors 1 and 2 are followed. Figure 80 shows only steps 1, 4 and 7 of vector 1 to increase the clarity of the figure.

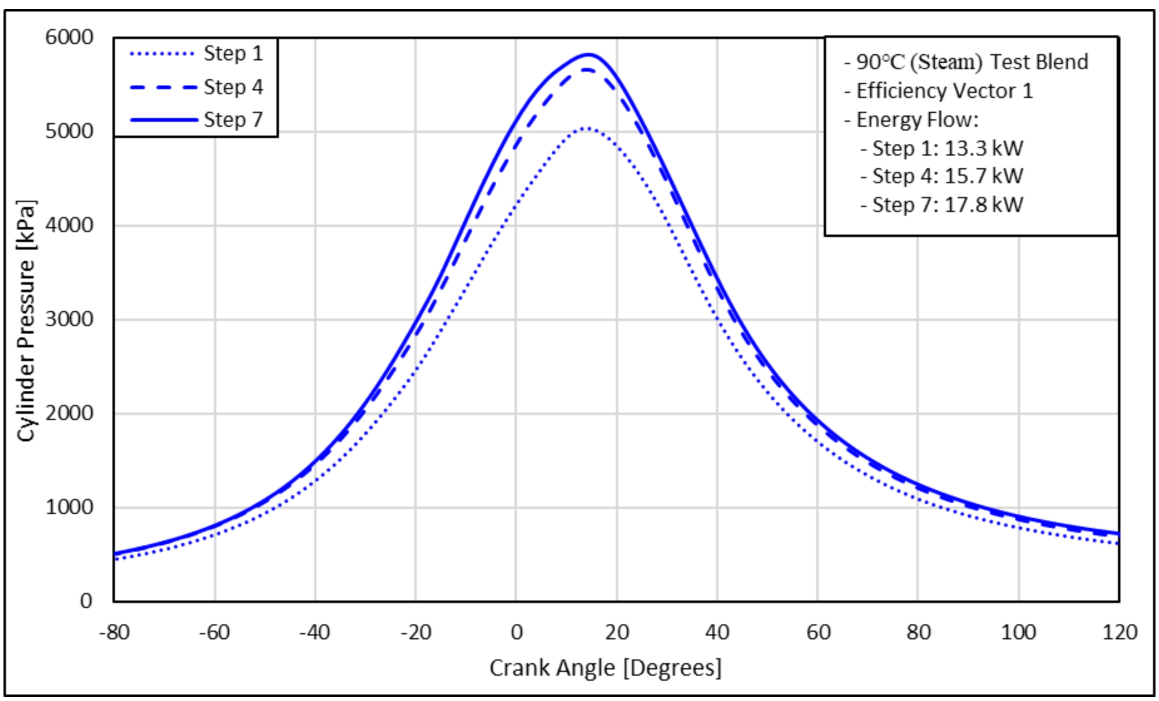

Figure 80: Cylinder pressure vs. crank angle for the 90°C (Steam) test blend at steps 1, 4, and, the highest efficiency, step 7 along vector 1. Some steps along the efficiency vector are omitted to increase visibility. Energy flow (LHV$\cdot\dot{m}_{fuel}$) for each data point is included in the figure. A solid line indicates the most efficient data point.

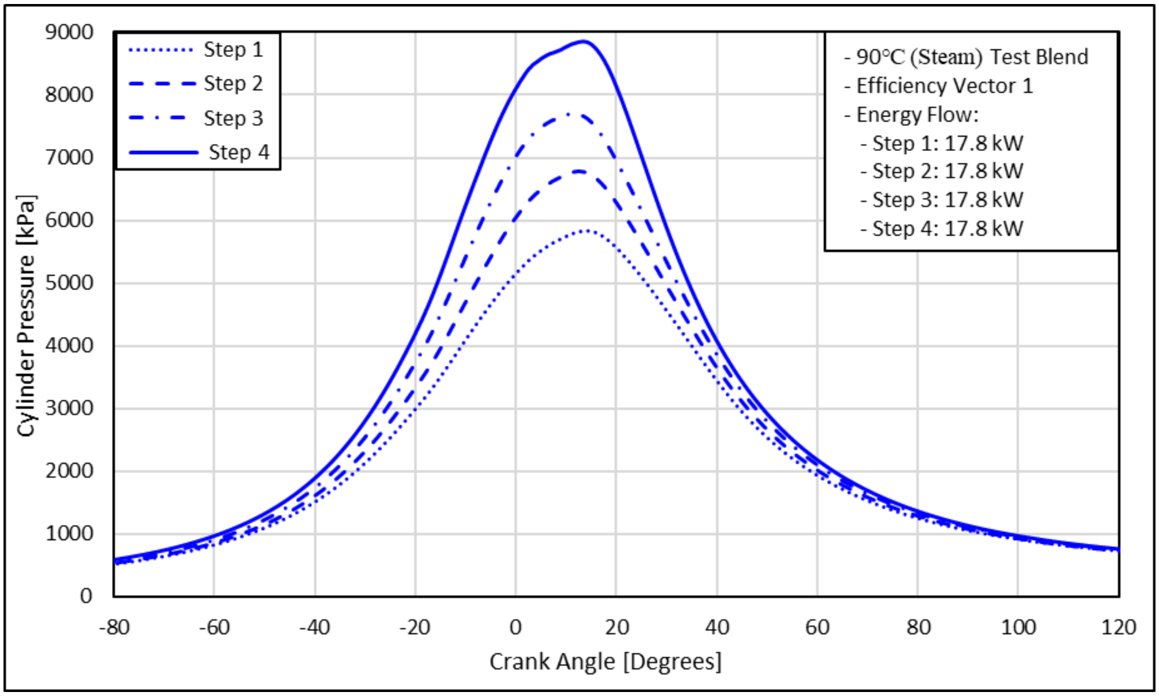

Figure 81: Cylinder pressure vs. crank angle for the 90°C (Steam) test blend at steps 1 through 4 of efficiency vector 2. Energy flow (LHV$\cdot\dot{m}_{fuel}$) for each data point. A solid line indicates the most efficient data point.

The brake efficiency vs. efficiency vector step for vectors 1 and 2 are shown in Figure 82. Much larger increases in efficiency are seen for the 90°C (Steam) blend than what is shown for the 40°C (Steam) blend in Figure 75. This is because the initial conditions for the 90°C (Steam) blend were much less favorable than those used in the RSM optimization of the 40°C (Steam) test blend. The final efficiency values between the two test blends were very comparable. The effectiveness of RSM optimization is evident when looking at the efficiency increase seen as each efficiency vector step is followed.

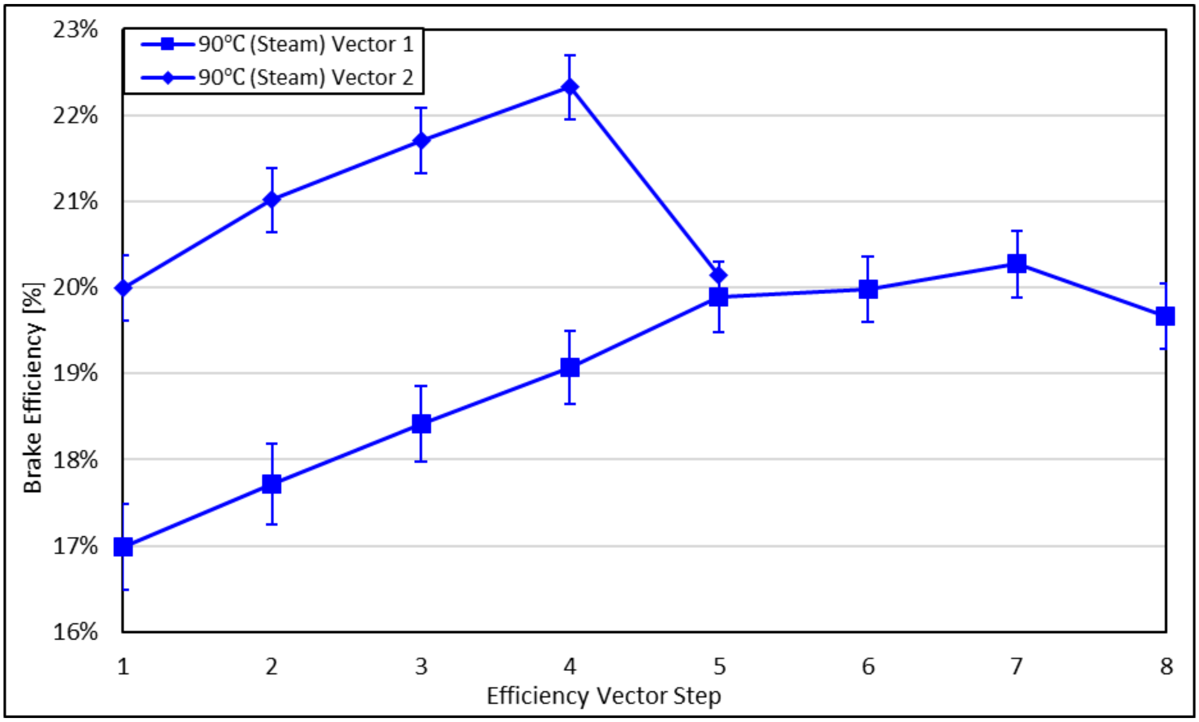

Figure 82: Brake efficiency vs. efficiency vector step for the 90°C (Steam) test blend. Vectors 1 and 2 are shown.

Steady combustion was also achieved throughout RSM optimization for the 90°C (Steam) test blend. Peak pressure and IMEP COV values are shown in Figures 83 and 84. These values are only slightly higher than those seen in RSM optimization of the 40°C (Steam) blend, but all are below 10%.

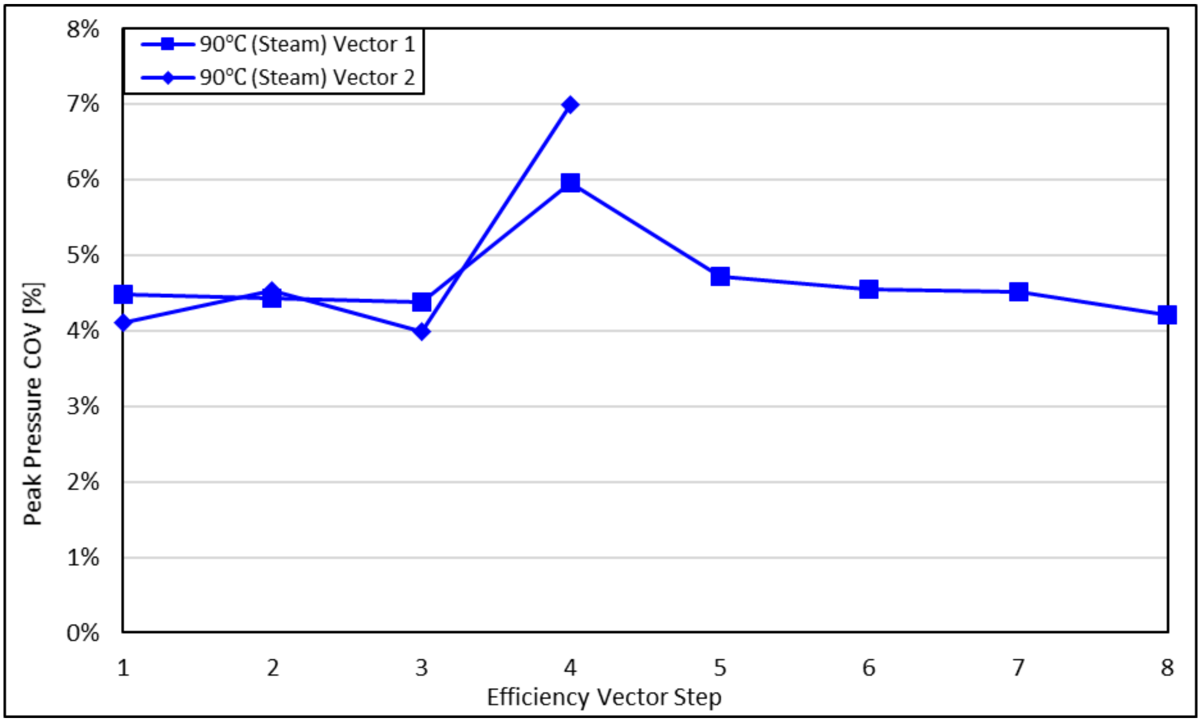

Figure 83: Peak Pressure COV vs. efficiency vector step for the 90°C (Steam) test blend. Vectors 1 and 2 are shown.

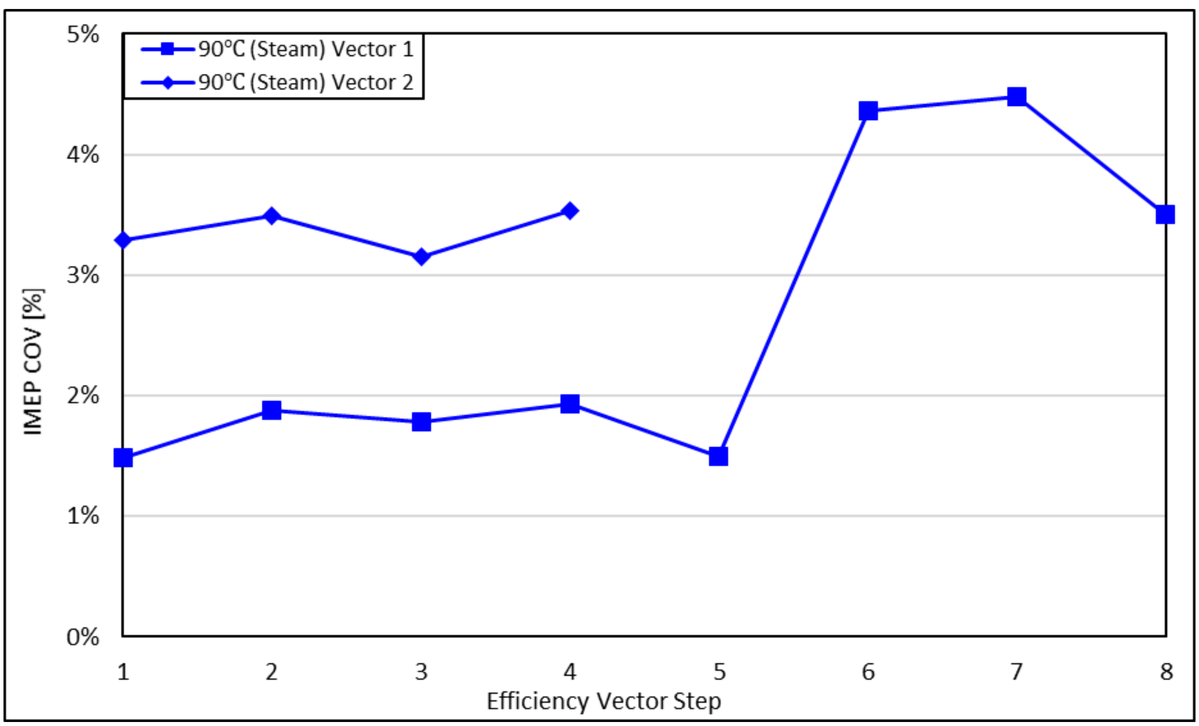

Figure 84: IMEP COV vs. efficiency vector step for the 90°C (Steam) test blend. Vectors 1 and 2 are shown.

Burn duration for this fuel blend is shown to increase as the efficiency vectors are followed in Figure 85. One possible cause for this is that the fuel flow during this testing is relatively high when compared to the 40°C (Steam) blend. At the lower efficiency test points early in RSM optimization, this large amount of fuel takes longer to combust fully than the less dilute 40°C (Steam) fuel. As efficiency increases, less unburnt fuel exits the cylinder. Since more fuel is being consumed, the measured burn duration increases even as brake efficiency increases.

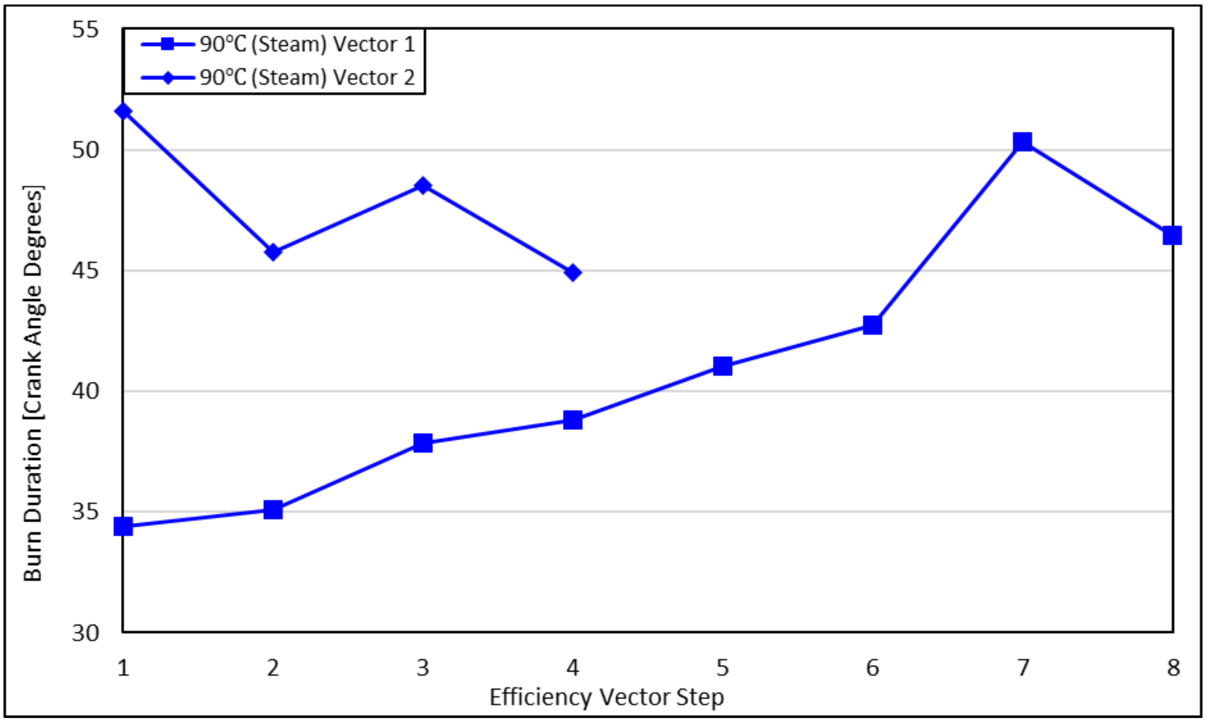

Figure 85: Burn duration vs. efficiency vector step for the 90°C (Steam) test blend. Vectors 1 and 2 are shown.

5.3. 40°C and 90°C (Steam) Comparison

After RSM optimization testing for the 40°C (Steam) and 90°C (Steam) test blends, it is clear that both blends are viable fuels for an ICE. Both test blends achieved similar brake efficiencies and exhibited stable combustion at high power levels for the CFR test stand. Table 11 shows the parameters for each fuel blend at the test points that had the highest brake efficiencies. While either test blend is suitable for ICE operation based on testing parameters, the

90°C (Steam) blend could cause increased engine wear due to high water content. The 40°C (Steam) blend was also able to achieve a similar brake efficiency at lower engine power levels than the 90°C (Steam) blend. A more robust and better-tuned engine could show a larger benefit to using the 40°C (Steam) blend than what could be measured using the CFR test stand.

The following direct comparisons can be made by referencing Figures 86 – 88. The 90°C (Steam) test blend requires a higher CR and operates at a higher peak pressure than the 40°C (Steam) blend when both are optimized. Figures 87 and 88 make it clear that the 90°C (Steam) blend does not match the combustion rate or combustion efficiency that the 40°C (Steam) blend does. The 90°C (Steam) blend exhibits a much longer burn duration and ignition delay than what is seen in the 40°C (Steam) blend.

Table 11: Parameters for the 40°C (Steam) and 90°C (Steam) test blends at the highest measured brake efficiencies achieved during RSM optimization.

Parameter	40°C (Steam)	90°C (Steam)
CR	9.53	12.75
Ignition Timing [° ATDC]	-15.9	-21.4
CA50 [° ATDC]	11.04	11.61
Speed [RPM]	952	1075
Inlet Temperature [°C]	47	70
Boost Pressure [kPa]	192	234
Total Fuel Flow [g/min]	219	275
Energy Flow (LHV$\cdot\dot{m}_{fuel}$) [kW]	16.61	17.78
Electric Power [kW]	3.31	3.55
Maximum Brake Efficiency [%]	22.24	22.33
Average Peak Pressure [kPa]	7563.8	8955.0
Peak Pressure COV [%]	3.91	6.99
Average IMEP [kPa]	1145.3	1105.2
IMEP COV [%]	4.93	3.53

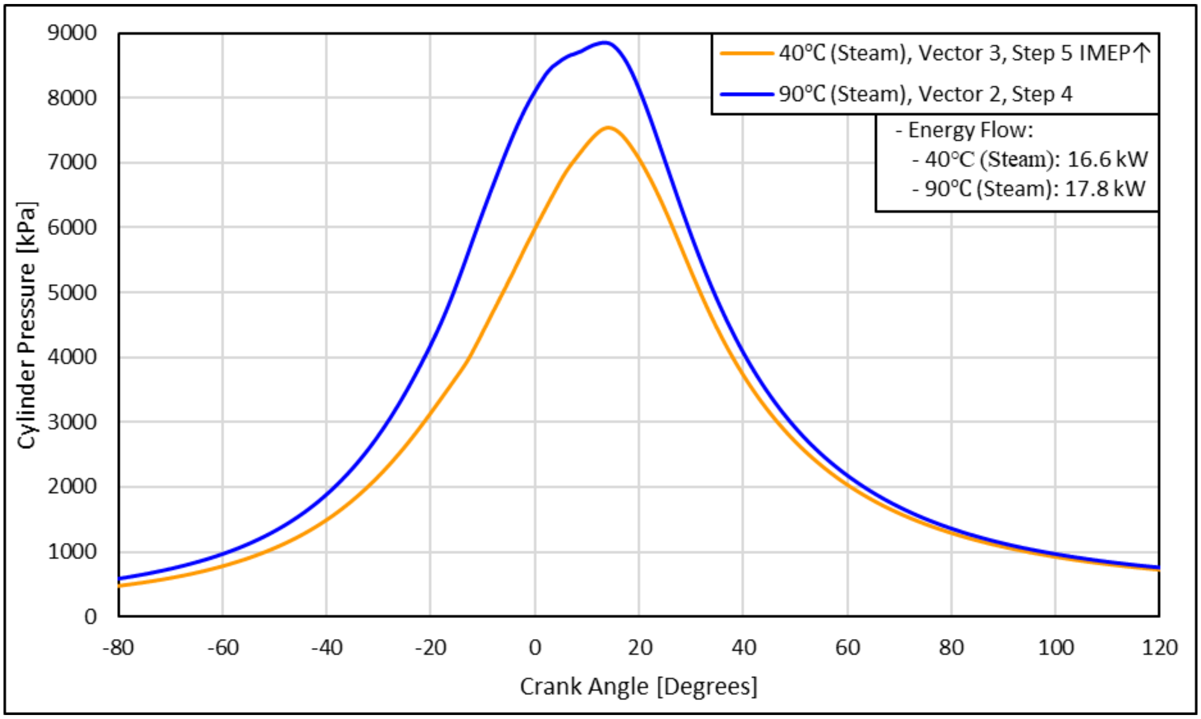

Figure 86: Cylinder pressure vs. crank angle at the most efficient datapoints for the 40°C (Steam) and 90°C (Steam) test blends. Energy flow (LHV$\cdot\dot{m}_{fuel}$) for each data point.

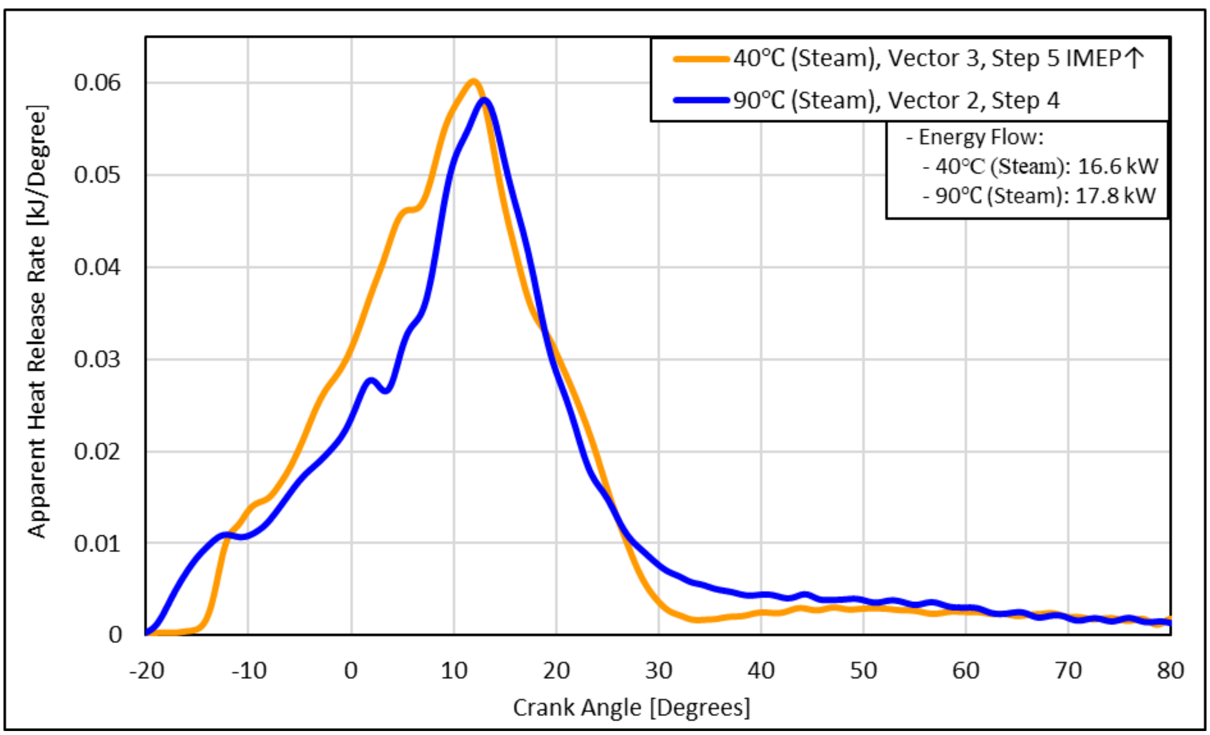

Figure 87: AHRR vs. crank angle at the most efficient datapoints for the 40°C (Steam) and 90°C (Steam) test blends. Energy flow (LHV$\cdot\dot{m}_{fuel}$) for each data point.

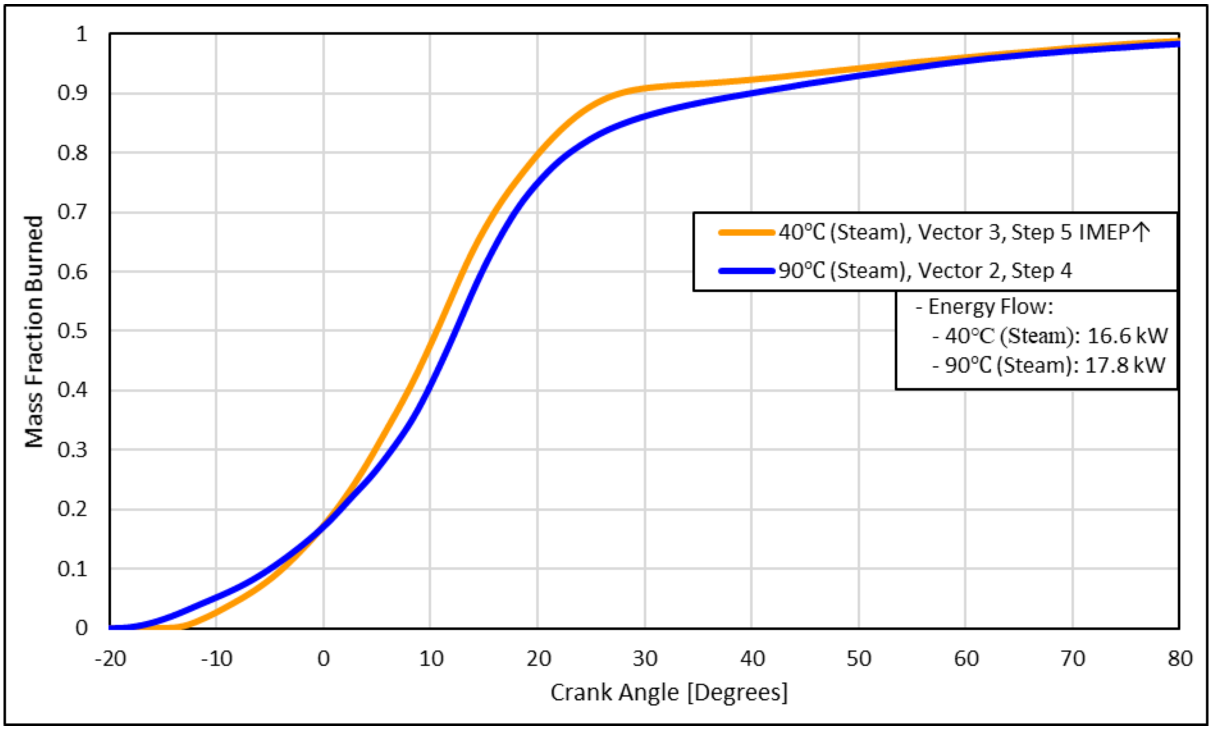

Figure 88: Mass fraction burned vs. crank angle at the most efficient datapoints for the 40°C (Steam) and 90°C (Steam) test blends. Energy flow (LHV·$\dot{m}_{fuel}$) for each data point.

CHAPTER 6: CONCLUSIONS AND FUTURE WORK

6.1. Conclusions

The purpose of this work was to determine the feasibility of utilizing the exhaust anode tail-gas from a MS-SOFC to fuel an ICE. Figure 89 shows the steps taken to complete this research. Initial feasibility testing involved direct mole % replacement of the expected water content in the tail-gas with excess CO_2. Fully simulated anode tail-gas was then tested using a steam generator to blend the water into the fuel. Seven different test blends were used in the course of this study, one with all the water content removed, three blends with CO_2 replacement of water content, and three blends with steam injection to fully simulate the expected anode tail-gas blend. Testing was performed first to determine the combustibility of each blend, and then testing was performed for each blend, except the No Water Dropout blends, at constant IMEP to allow a more direct comparison between test blends. The ideal test blend could not be determined by the previous testing alone. For this reason, RSM optimization was performed on two steam injection test blends. Specific conclusions and observations from all trials are listed below:

1) CO_2 replacement blend testing determined that ICE operation on dilute anode tail-gas was possible.
2) Steam injection blend testing confirmed the feasibility of using dilute anode tail-gas to fuel an ICE by fully simulating the expected tail-gas composition and producing steady engine power with all test blends.
3) Engine operation on simulated anode tail-gas is expected to produce engine out NO_x about 99% lower and THC about 90% lower than NG. The 40°C (Steam) test blend is expected to produce about 900% more engine-out CO than NG based on data points gathered before RSM optimization. Although this is a large increase, operation at higher engine brake efficiency tended to decrease engine-out CO emissions. Similarly, the 90°C (Steam) blend is expected to produce about 300% more engine-out CO than NG. Emissions regulations vary with application and location, but exhaust aftertreatment will likely be required for CO reduction. Further emissions analysis is required at higher engine brake efficiencies to determine

4) RSM optimization of the 40°C (Steam) and 90°C (Steam) test blends was extremely successful. The 40°C (Steam) blend showed a two-percentage point increase in brake efficiency to 22.24% while the 90°C (Steam) blend showed five percentage point increase to a total of 22.33%. For comparison, although RSM optimization was not performed for NG and methane fuel, the highest brake efficiency achieved during baseline testing of NG and methane was 18.51%.
5) It is unclear which test blend, 40°C (Steam) or 90°C (Steam), is the ideal blend. The 40°C (Steam) blend seems to have more ideal combustion characteristics, but similar brake efficiencies can be achieved using the 90°C (Steam) blend. The 24% by volume water content of the 90°C (Steam) blend is still cause for concern when compared with the 2.5% by volume water content of the 40°C (Steam) blend. Further testing will be required to determine the long-term effects of ICE operation using the 90°C (Steam) blend. These effects will need to be assessed and compared to the difficulty of producing an intercooler capable of dropping out enough water to reach a fuel dewpoint temperature of 40°C.

6.2. Future Work

Future work for this project is already underway. A 12kW 3-cylinder prototype engine has been developed by Kohler Engines in collaboration with CSU. This engine will be fueled by a fuel cell simulator capable of producing simulated anode tail-gas at about seven times the maximum fuel flow rate provided by the CFR engine test stand. Testing will involve further characterization of the anode tail-gas combustion properties and determination of an ideal fuel blend. This testing will lead to the production of the next larger prototype engine designed to run on actual anode tail-gas from a prototype MS-SOFC. A key challenge to produce a hybrid SOFC/ICE system will be the system integration required for ICE load control to match the incoming fuel flow rate to the engine with the rate of anode tail-gas from the fuel cell.

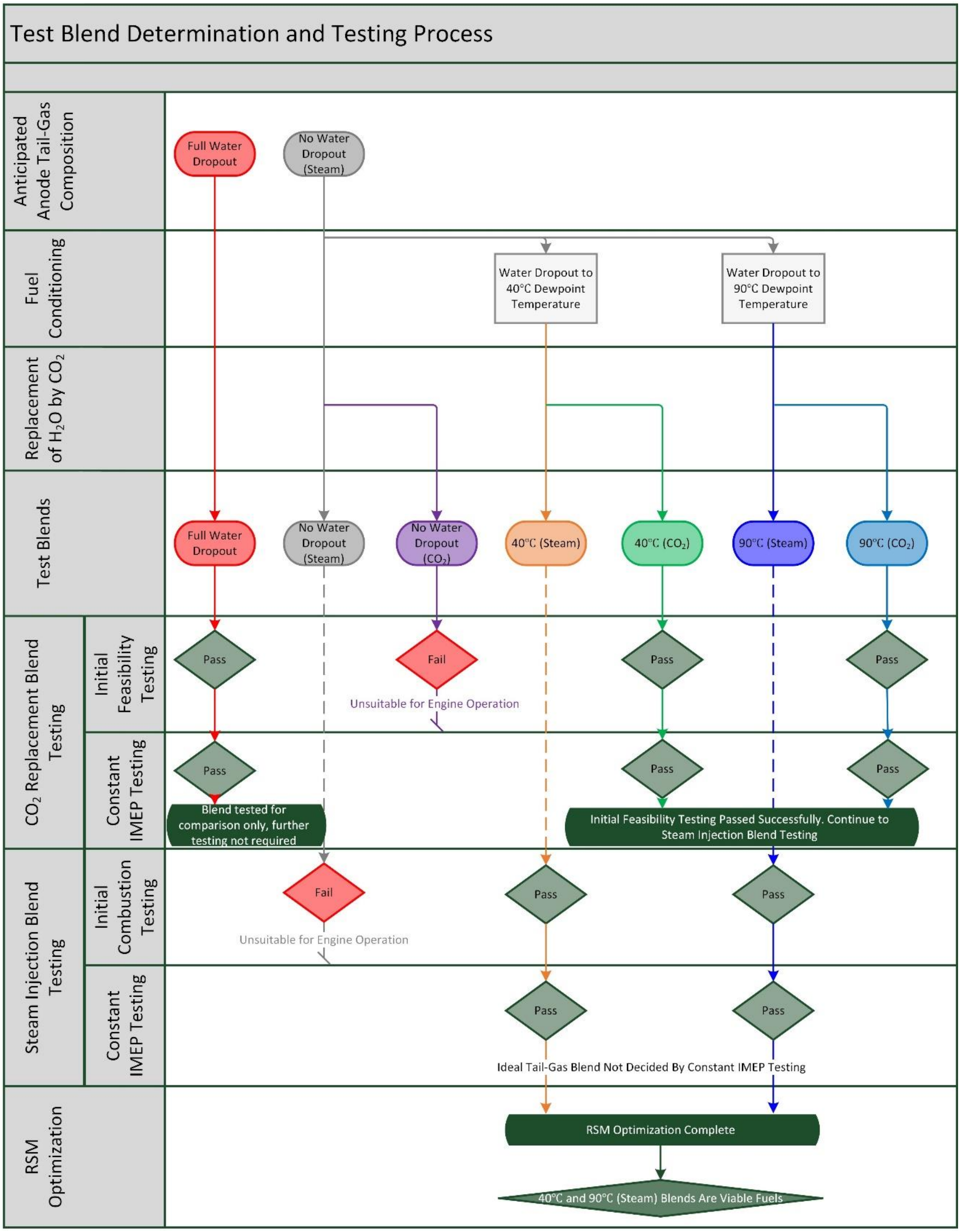

Figure 89: Final flowchart representing test blend determination, selection and testing sequence.

REFERENCES

[1] V. V. Krishnan, "Recent Developments in metal-supported solid oxide fuel cells: Metal-supported solid oxide fuel cells," *Wiley Interdisciplinary Reviews: Energy and Environment,* vol. e246, no. 10.1002/wene.246, 2017.

[2] R. Braun, N. Sullivan, T. Vincent, R. Danforth, T. Bandhauer, D. Olsen, D. Windom and B. Schaffer, "Development of a novel high efficiency, low cost hybrid SOFC/internal combustion engine power generator," *Symp. (Int.) SOFCs 16,* 2019.

[3] D. Wise, "Investigation into producer gas utilization in high performance natural gas engines," *Colorado State University,* 2013.

[4] G. R. Sridhar, H. Sridhar, S. Dasappa, P. J. Paul, N. Rajan and H. Mukunda, "Development of producer gas engines," *Proceedings of The Institution of Mechanical Engineers Part D-journal of Automobile Engineering - PROC INST MECH ENG D-J AUTO,* vol. 219, pp. 423-438, 2005.

[5] U. Babu and L. Kumararaja, "A Research on Producer Gas in Internal Combustion Engines," *International Journal of Recent Technology and Engineering,* vol. 8, no. 1S4, pp. 2277-3878, 2019.

[6] S. B. Shrestha and G. Narayanan, "Landfill Gas With Hydrogen Addition - A Fuel for SI Engines," *Fuel,* vol. 87, pp. 3616-3626, 2008.

[7] H. S. D.J. Picken, "The Use of Anaerobic Digester Gas as an Engine Fuel," *Journal of Agriculutural Engineering Research,* vol. 26, no. 1, pp. 1-7, 1981.

[8] D. Singh, T. Nishiie, S. Tanvir and L. Qiao, "An Experimental and Kinetic Study of Syngas/Air Combustion at Elevated Temperatures and the Effect of Water Addition," *Fuel,* vol. 94, pp. 448-456, 2012.

[9] H. e. Arruga, "Effect of Intake Manifold Water Injection on a Natural Gas," *IOP Conference Series: Materials Science and Engineering,* pp. 1-14, 2017.

[10] I. e. a. Cesur, "The Effects of Electronic Controlled Steam Injection on Spark Ignition Engine," *Applied Thermal Engineering,* pp. 61-68, 2013.

[11] Swagelok, "Valve Sizing Technical Bulletin," 2007.

[12] B. Lian, T. Sun and Y. Song, "Parameter Sensitivity Analysis of a 5-DoF Parallel Manipulator," *Robotics and Computer-Integrated Manufacturing,* vol. 46, pp. 1-14, 2017.

[13] R. J. Moffat, "Describing the Uncertainties in Experimental Results," *Experimental Thermal and Fluid Science,* vol. 1, no. 1, pp. 3-17, 2003.

[14] B. A. King, "Experimental Evaluation of Stack Testing Methods for Accurate VOC Measurement," *Colorado State University,* 2019.

[15] T. Falloon, "The Effect of Fuel Additives in a Natural Gas and Gasoline Engine," *Colorado State University,* 2016.

[16] S. a. G. W. Neyeloff, "Performance of a CFR Engine Burning Simulated Anaerobic Digester's Gas," *ASAE Publ.; (United States),* Vols. 4-81, 1981.

[17] A. Witek-Krowiak, K. Chojnacka, D. Podstawczyk, A. Dawiec and K. Pokomeda, "Application of Response Surface Methodology and Artificial Neural Network Methods in Modelling and Optimization of Biosorption Process," *Bioresource Technology,* vol. 160, pp. 150-160, 2014.

[18] S. J. Kline and F. A. McClintock, "Describing Uncertainties in Single-Sample Experiments," *Mechanical Engineering,* pp. 3-8, 1953.